A COMPUTATIONAL INVESTIGATION OF IMPULSIVE AND PULSED STARTING ANNULAR JETS

by

EMAD MOHAMED REFAAT ABDEL-RAOUF

A DISSERTATION

Submitted in partial fulfillment of the requirements
for the degree of Doctor of Philosophy
in the Department of Mechanical Engineering
in the Graduate School of
The University of Alabama

TUSCALOOSA, ALABAMA

2011

ABSTRACT

A computational study is carried out on low Reynolds number impulsive and pulsating annular jets. This work is inspired by the biological flow of marine life that uses jet propulsion for self maneuver. Marine life such as squids and jellyfish propel themselves by discharging a water jet followed by a refilling phase. The discharging portion is a starting jet, i.e. the releasing of a moving fluid into a quiescent fluid, while the refilling phase can be viewed as an inflow jet. The combined jets will be called fully oscillating jets. Although fully oscillating jets have been indirectly examined experimentally, they have never been studied computationally.

This dissertation is divided into three investigations that examine the starting jet, inflow jet, and fully oscillating jet based on the resultant force (i.e. either thrust or suction force) at the annulus exit plane, jet efficiency, and vortex dynamics. Furthermore, each of the following three performance criterion is examined under various velocity imposed boundaries (i.e. impulsive, unit pulsed, and sinusoidal pulsed jets), ambient pressure, and blocking ratios.

An axisymmetric, incompressible and unsteady Navier Stokes numerical model was used to implement the analysis. The model was validated against theoretical and experimental results, where both result types bounded the computational results of this endeavor. In addition, numerical verification was carried out on each of the three investigations ensuring grid and time independent results.

Several substantial outcomes were drawn from the results of the three investigations. The numerical results confirmed previously published experimental data regarding the universal

dimensionless time scale (i.e. vortex formation number) of optimal vortex ring development triggered by starting jets. Moreover, the computational results showed evidence that the vortex formation number was not affected by ambient pressure nor blocking ratio. The computational results also confirmed earlier experimental findings that pulsed jet inflows trigger a standing vortex ring. Furthermore, the current study showed that impulsive jet inflows do not trigger vortex ring formation. In addition, unlike the expected net thrust of zero due to mass flux, fully oscillating jets showed evidence of thrust augmentation due to the enhanced entrainment caused by the vortex formation.

DEDICATION

I praise Allah for amongst which He blessed me with a family that has always stood by my side. I dedicate this research to my parents for instilling in me the value of knowledge, to my brother for his moral support, and to my beloved wife Aida for her patience with me over the past two hectic years.

LIST OF ABBREVIATIONS AND SYMBOLS

A	annulus cross sectional area, m^2
BR	blocking ratio
D	hydraulic diameter, m
f	force, N
F	dimensionless force
I	impulse, N-s
ke	kinetic energy, J
l	boundary length, m
L	length of annulus, m
N	dimensionless cycle period
p	pressure, N/m^2
P	dimensionless pressure
r	radial coordinate, m
R	dimensionless radial coordinate
Re	Reynolds number
s	integration variable for cross section area, m^2
St	Strouhal number
t	time, s

T dimensionless time

U dimensionless velocity

V velocity, m/s

$\forall$ volume, m^3

x axial coordinate, m

X dimensionless axial coordinate

α tip angle of annulus

η propulsive efficiency

Γ vortex circulation, m^2/s

ν kinematic viscosity, m^2/s

ρ density, kg/m^3

σ dimensionless shear stress

τ integration variable for time, s

ω cycle frequency, 1/s

Ω vorticity, 1/s

Subscript

avg average value

gage gage pressure value

mom momentum force component

pres pressure force component

o initial value

R radial direction

V vortex value

X axial direction

θ transverse direction

Superscript

* dimensionless value

ACKNOWLEDGEMENTS

I would like to acknowledge my family, colleagues, and faculty for their help and support with this research. I am most appreciative to my dissertation committee: Dr. John Baker, Dr. Clark Midkiff, Dr. Muhammad Sharif, Dr. Robert Taylor, and Dr. Keith Williams. In particular, I am very grateful to the committee chairman Dr. Baker for his support over the years. With his care, sincerity, and guidance, Dr. Baker has set a standard for me as to what a teacher and a researcher should be like. I would like to thank Dr. Sharif for always giving me sound advice.

I would also like to acknowledge the United States Department of Education for its help in funding this research through the Graduate Assistance in Areas of National Need (GAANN) Fellowship. I would also like to acknowledge The University of Alabama for its funding through the Graduate Council Fellowship (GCF).

CONTENTS

ABSTRACT ii

DEDICATION iv

LIST OF ABBREVIATIONS AND SYMBOLS v

ACKNOWLEDGEMENTS viii

LIST OF TABLES xii

LIST OF FIGURES xiii

1. INTRODUCTION 1

a. Overview 1

b. Starting Jet 2

c. Inflow Jets 8

d. Fully Oscillating Jets 9

e. Research Motivation 9

f. Specific Objectives 10

g. Important Terminology 11

2. COMPUTATIONAL INVESTIGATION OF LOW REYNOLDS NUMBER STARTING ANNULAR JETS 12

a. Abstract 12

b. Introduction 13

c. Problem Description 16

d. Numerical Model 17

e. Results and Discussion.....21

f. Conclusion.....37

g. Acknowledgements.....39

h. References.....39

3. IMPULSIVELY STARTED AND PULSATED ANNULAR JETS 42

a. Abstract 42

b. Introduction.....43

c. Problem Description.....44

d. Numerical Model 46

e. Results and Discussion.....48

f. Conclusion.....61

g. Acknowledgements.....63

h. References.....63

4. COMPUTATIONAL INVESTIGATION INTO THE STRUCTURE OF FULLY OSCILLATING ANNULAR JETS.....65

a. Abstract 65

b. Introduction.....66

c. Problem Description.....67

d. Numerical Model 69

e. Results and Discussion.....71

f. Conclusion.....84

g. Acknowledgements.....86

h. References.....86

5. CONCLUSION.....88

REFERENCES 91

LIST OF TABLES

2.1 Dimensionless Circulation, Γ^*, of Leading Vortices 23

LIST OF FIGURES

1.1 Squid Propulsion Schematic 1

1.2 Vortex Ring Development 6

2.1 Annulus Schematic 16

2.2 Outer Boundaries of Numerical Model.....19

2.3 Grid Convergence Plot.....20

2.4 Numerical Results Validation 21

2.5 Vorticity Contour Plots of Vortex Development at $St = 0.18$ 22

2.6 Unit Pulsed Starting Jet Vortex Distribution at $St = 0.18$ 25

2.7 Sinusoidal Pulsed Starting Jet Vortex Distribution at $St = 0.18$ 25

2.8 Impulsively Started Jet Vortex Distribution at $T = 5.52$ 26

2.9 Vortex Leapfrogging.....27

2.10 Thrust Output of Impulsively Started Jets 28

2.11 Thrust Components of Impulsively Started Jets 29

2.12 Thrust Output of Pulsating Starting Jets 30

2.13 Thrust Components of Unit Pulsation.....32

2.14 Thrust Components of Sinusoidal Pulsation.....33

2.15 Propulsive Efficiency of Impulsively Started Jets 35

2.16 Propulsive Efficiency of Pulsed Jets at Various Blocking Ratios 36

2.17 Propulsive Efficiency of Pulsed Jets at Various Pressures 37

3.1 Annulus Schematic 45

3.2 Outer Contour of Mesh 46

3.3 Vorticity Contours of Impulsive Inflow Jets for a) BR=0 & 101 kPa, b) BR=0 & 0.670 kPa, and c) BR=0.75 & 0.670 kPa 49

3.4 Circulation of Impulsive Inflow Jets.....50

3.5 Vorticity Contours of Unit Pulsed Inflow Jets.....51

3.6 Vorticity Contours of Sinusoidal Pulsed Inflow Jets.....52

3.7 Circulation of Pulsed Inflow Jets.....53

3.8 Net Force of Impulsive Inflow Jets.....55

3.9 Force Components of Impulsive Inflow Jets 56

3.10 Net Force of Sinusoidal Pulsed Inflow Jets 57

3.11 Force Components of Sinusoidal Pulsed Inflow Jets.....59

3.12 Efficiency of Pulsed Inflow Jets 61

4.1 Annulus Schematic 69

4.2 Outer Contour of Numerical Mesh 70

4.3 Numerical Results Validation.....72

4.4 Vortex Circulation of Fully Oscillating Unit Pulsed Jets 74

4.5 Vortex Circulation of Fully Oscillating Sinusoidal Pulsed Jets.....74

4.6 Vorticity Contours of Fully Oscillating Unit Pulsed Jets 75

4.7 Vorticity Contours of Fully Oscillating Sinusoidal Pulsed Jets.....76

4.8 Vorticity Distribution of Fully Oscillating Jets 78

4.9 Thrust Output of Fully Oscillating Jets.....79

4.10 Thrust Components of Fully Oscillating Jets.....81

4.11 Percentage of The Pressure Thrust Component.....81

4.12 Propulsive Efficiency of Fully Oscillating Jets 83

4.13 Propulsive Efficiency Cycle Patterns.....84

CHAPTER 1

INTRODUCTION

Overview

Certain marine life, the likes of squids and jellyfish, propel themselves by means of periodically releasing jets, i.e. an active fluid discharged via a nozzle or an orifice into a latent fluid. According to Anderson and DeMont (2000), squids fill their mantel cavities with the surrounding water by means of muscular relaxation and then release a jet through a funnel (shown in Figure 1.1) by means of muscular contraction. Hence, such propulsion mechanism can be modeled by two components: an inflow jet and a starting jet.

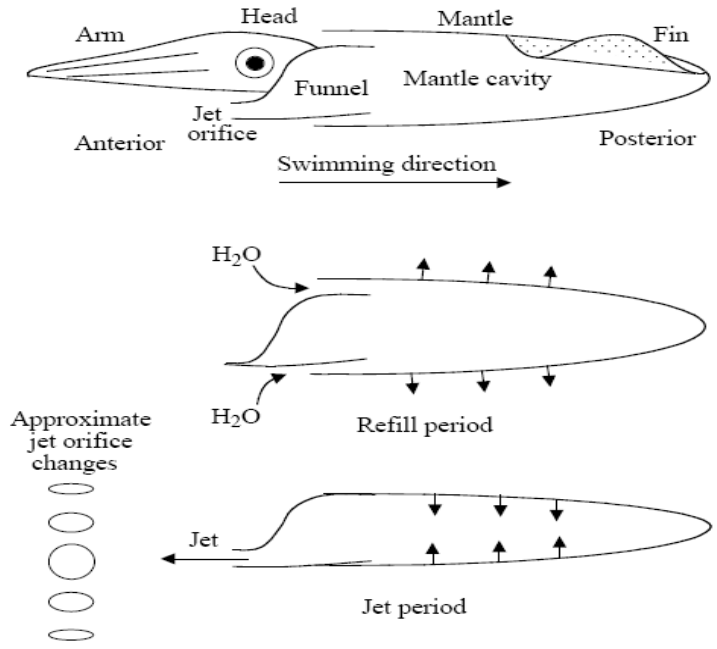

Figure 1.1. Squid propulsion schematic (Reproduced with permission of Anderson and DeMont, 2000).

The starting and inflow jets will be isolated and investigated separately in chapters 2 and 3, respectively, in general terms (i.e. not specific to marine life). Furthermore, both outflow and inflow jets will be combined into a single jet that will be referred to as a fully oscillating jet and investigated in chapter 4. The remainder of the introduction will highlight relevant research relating to the three jet types (i.e. starting, inflow, and fully oscillating), as well as highlight the areas that need to be researched in the last section.

Starting Jet

The starting jet example of the squid is part of a larger fluid flow category described by the term starting jets, where an active fluid is discharged via a nozzle or an orifice into a latent fluid. According to Pawlak et al. (2007), starting jets are common in many applications including fuel and oxidizer jets in combustion chambers, pressured vessel breaches, tidal jets, and animal propulsion. Such class of jet problems is associated with high fluid entrainment that is enhanced by the formation of vortices. Most of the literature on this topic has been focused on studying both the jet (i.e. annular jets, round jets, etc.) structure and the vortex formation.

Velocity Profile

The investigation of the structure of starting jets has typically been undertaken by examining the velocity profiles and studying the associated vortex rings. It has been customary to divide the velocity profile region near the jet annulus entry into three zones: initial, intermediate, and fully developed (Ko & Lam, 1985). Circulation takes place in the initial zone, while reattachment takes place in the intermediate zone. In the fully developed zone, the dimensionless velocity profile as a function of the radial direction remains near constant along the axial direction.

The effects of the annulus entry geometry on the velocity profiles of a starting jet have also been investigated. For example, Uyttendaele and Shambaugh (1989) studied annular jets with sharp-edged inlets to simulate the melt blowing process for producing microfibers. They found out that the lengths of the three zones and the velocity profiles in fully developed zone are independent of the Reynolds number and the length to stroke ratio of the orifice.

In another study, Ko and Chan (1978) studied annular configuration effects on the velocity profile examining a basic annulus (without a central bullet) along with conical and elliptical bullet-centered annuli. Regardless of the annulus configuration, their results shows that the initial zone was located within two hydraulic diameters from the annulus; the intermediate zone took place within two and five hydraulic diameters; and the fully developed zone took place at axial distances larger than five hydraulic diameters from the annulus.

Vortex Ring Structure

The vortex ring structures triggered by starting jets have also been studied extensively. Some studies like the classical one done by Norbury (1973) are based on theoretical derivations and aimed at determining vortex ring properties such as circulation and kinetic energy at the core of the ring. Other studies produced significant results based on both theoretical and experimental analysis. For example, Didden (1979) determined a relation for the vortex ring circulation as a function of the outlet flow conditions of a starting jet initiated by a hydraulic piston drive that forced water through a nozzle and into a water tank.

In addition, a significant number of experiments has been conducted on vortex ring structures. For example, the stability of the vortex rings was addressed by Maxworthy (1972), where he generated vortices using a hypodermic syringe that expelled fluid (via a submerged manifold in a fish tank) through a drilled hole in a thin sheet of brass. He determined that the

vortex ring is stable throughout its motion for Reynolds number less than 600. He also noted that out of the disorganized flow of the unstable vortex rings at Reynolds numbers greater than 1000, stable vortex rings were formed.

Sallet and Widmayer (1974) addressed vortex ring turbulence by analyzing the vortices of a vortex generator that transformed the motion of a pneumatic actuator to a piston/cylinder device via a groove-cam linkage. Two types of clams were used that allowed for a steady piston velocity and a steady piston acceleration in order to form laminar and turbulent vortex rings, respectively. Their results showed that the development of both laminar and turbulent vortex rings was completed within three hydraulic diameters from the orifice using several Reynolds numbers ranging from 8010 to 12250.

The effects of the annulus geometry on vortex rings were also investigated. For example, Syed and Song (2009) studied the effects of orifice and nozzle shaped annulus exit geometry on the vortices generated from air jets with Reynolds numbers in the range of 450 to 4580. Their experiment showed that relative to the nozzle geometry, the orifice geometry enhanced the vortex formation by producing vortices with higher vorticity, faster downstream propagation, and lesser entrainment of the surrounding fluid.

Although not as numerous as the experimental investigations, computational studies on vortex rings were also undertaken. For instance, Riley and Stevens (1993) numerically determined that the motion of two identical viscous vortex rings moving around the same axis of symmetry would move around each other in a leapfrogging motion until they eventually become a single ring, where the leapfrogging motion increases with increasing Reynolds number. Note that such finding was confirmed experimentally by Maxworthy (1972).

Vortex Formation Number

Instead of concentrating on the vortex ring structures as had traditionally been done, Gharib et al. (1998) focused on the experimental parameters involved in producing starting jets in order to maximize the circulation of the triggered vortices. Using a piston and cylinder setup, they varied the entry diameter, Reynolds number, and boundary wall angle (to simulate nozzle and orifice effects). They also experimented with several piston stroke to diameter ratios, as well as various piston velocity programs that incorporated impulsive and non-impulsive piston movements.

After significant parametric variations, Gharib et al. (1998) found that the maximum circulation of the generated vortex rings happened within a limited dimensionless time range of 3.6 to 4.5. This observation led them to conclude that optimal vortex development occurs at universal time scale of approximately 4, which they called the 'formation number.' At the formation number, the vortex is said to 'pinch-off', i.e. to no longer entrain additional circulation (or energy) by forcing a trailing jet from which the vortex eventually detaches. Figure 1.2 shows vortex ring development at various dimensionless times, where vortex pinch-off can be noted by time $T = 8$.

The presence of a universal time scale for vortex development was also confirmed computationally by Rosenfeld et al. (1998) using a finite element package to model the axisymmetric time-dependent incompressible Navier Stokes equations. Their results showed vortex formation numbers of approximately 4 by varying the same parameter types as Gharib et al. (1998). In addition, Rosenfeld et al. (1998) varied the velocity profile of the starting jet. The formation number of 4 that was obtained by Gharib et al. (1998) and Rosenfeld et al. (1998) had assumed a uniform velocity profile. However, for a parabolic velocity, Rosenfeld et al. (1998)

obtained a formation number of approximately 0.9. As a result, they concluded that the variations to the uniform velocity profile that would occur due to changes of the flow parameters caused the previously noted slight differences of the vortex formation number (i.e. 3.6 to 4.5).

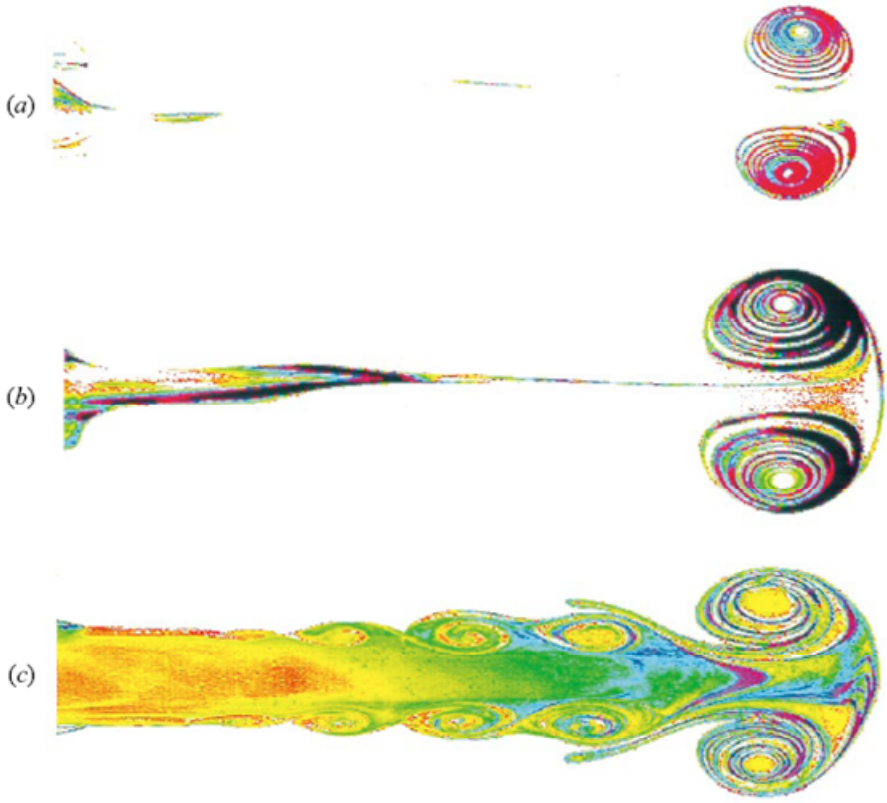

Figure 1.2. Vortex ring development at a) $T = 2$, b) $T = 3.8$, and c) $T = 8$ (Reproduced with permission of Gharib et al., 1998).

It is important to note that both Gharib et al. (1998) and Rosenfeld et al. (1998) had attributed the existence of a universal time scale in vortex ring development to the Kelvin-Benjamin variational principle. As described by Dabiri (2009), this principle states that a "steady, symmetry-axis-touching vortex ring possesses maximum energy relative to the equivalent rearrangements of its vorticity that maintain the same total impulse." In other words, the vortex will continue to entrain more mass as long as the incoming energy is greater than the

energy of the vortex. Once the energy of the vortex is greater than the incoming fluid, vortex 'pinch-off' will occurs. For further verification, Shusser and Gharib (2000) showed by derivation that the assumption that at pinch-off, the translational velocity of the vortex ring was the same as the jet velocity near the ring, which was used by a model by Shusser and Gharib (1999), was in fact equivalent to the Kelvin-Benjamin variational principle.

Vortices and Jet Performance

Experiments have also shown that vortex ring formation and development are directly related to the overall thrust/impulse performance of the starting jet. For example, Krueger and Gharib (2003) noted that the pressure component of impulse, which they called the "nozzle-exit overpressure," was a major contributor to the total impulse prior to the vortex pinch-off and had negligible effects after pinch-off. Hence, the impulse due to pressure was greatest at the beginning of the vortex formation and then decreased until reaching an insignificant value by the time of vortex pinch-off.

Furthermore, Krueger and Gharib (2005) calculated the momentum component of thrust at the nozzle exit by measuring the jet outflow velocity. They noted that the thrust at the starting jet outflow was greater than the expected thrust from the supplied mass flux, which they called "thrust augmentation" and attributed it to the vortex formation. In addition, Krueger and Gharib (2005) experimented with several starting jet frequencies and noted that the thrust augmentation decreased with decreasing frequency.

Vortices and Biological Flow

Several studies have tried to associate optimal vortex formation with biological flow. Linden and Turner (2004), for example, were among the earliest to suggest that the jets produced by certain marine life such as squids, salps, and jellyfish trigger optimal vortices that

corresponded with ideal jet performance. However, both Linden and Turner (2004) and Dabiri and Gharib (2005) pointed out a discrepancy in that claim by the fact that large squids trigger inefficient jets while small squids trigger efficient jets. Both groups explained this inconsistency by the fact that large squids need to escape predators, and thus, they have to sacrifice efficiency for acceleration and overall thrust output.

Gharib et al. (2006) investigated the vortex formation that occurs when the blood flows from the cardiac left atrium to the left ventricle through the mitral valve. Echocardiograms of 110 randomly selected people of various ages showed vortex formation numbers in the range of 3.5 to 5.5 (i.e. in the proximity of the previously determined universal dimensionless time scale of 4) for people with healthy hearts and smaller vortex formation numbers with people with dilated cardiomyopathy (DCM). These results led Gharib et al. (2006) to conclude that the optimal vortex formation can be an indicator of cardiac health.

Inflow Jets

Unlike the literature-rich starting jet (i.e. jet outflow) research, research on jet inflows has been limited due to its narrow practical applications. One such application is suction feeding, where according to Bishop et al. (2008), a fish captures its prey by rapidly opening its mouth creating a suction that causes the inflow of the water along with the prey into the mouth. Another application is the recovery stroke or refilling phase of the jet propulsion of certain marine life. Dabiri et al. (2005), for example, examined the recovery stroke of jellyfish during which they noted formation of a stopping vortex. In fact, the research done by Dabiri et al. (2005) is the only one that the author of this dissertation is aware of that deals with vortex formation for jet inflow.

Fully Oscillating Jets

As previously mentioned, the term ‘fully oscillating’ in this dissertation will be used to refer to a combined jet outflow followed by a jet inflow. The author of this dissertation is not aware of any experimental or computational studies that addressed fully oscillating jets. Note that the term ‘fully pulsed’ jet, which was used previously by (for example) Krueger and Gharib (2005), is not to be confused with the term ‘fully oscillating’ jet of this dissertation. Fully pulsed jets are pulsed jets that alternate between a period of jet outflow and a period of no flow, while fully oscillating jets are pulsed jets that alternate between a period of jet inflow and a period of jet outflow.

Research Motivation

A general survey of the research pertaining to starting jets, inflow jets, and fully oscillating jets was presented in the previous sections. The importance of fully oscillating jets, which are pertinent to marine life that rely on jet propulsion for self-movement, was shown. The target of this research will be to computationally study and compare the performance of fully oscillating jets with its constituent jets (i.e. the starting jet and the inflow jet) based on the analysis of vortex formation, thrust, and efficiency.

This research is unique in several ways. This will be the first-ever study of fully oscillating jets, and it will enhance the understanding of jet inflows, which have not been extensively studied. In addition, this research will study the effects of pressure variations on jet performance, which was never addressed in vortex ring research. With much of the current vortex formation research being inspired by biological flow including marine life that swim at various depths, it will be advantageous to investigate whether or not the vortex formation number is affected by pressure variations.

Furthermore, the effects of the entry geometry on the jet performance have not been totally addressed in past research. Although the effects of entry diameter and boundary wall angle have been addressed, the effect of blockage on vortex formation has not been investigated. Note that the previous starting jet studies that incorporated blockage analyzed the results based on the velocity profiles and not vortex formation. Hence, this research also aims at enhancing the entry geometry studies on the overall jet performance (particularly vortex formation) by varying the blocking ratio.

Specific Objectives

This dissertation will carry out a computational investigation on low Reynolds number flow starting jets, inflow jets, and fully oscillating jets. The following objectives are targeted:

1. Validate the computational model against experimental and theoretical results (Chapter 2).
2. Verify the computational model to ensure independent solutions with respect to space and time (Chapters 2, 3, and 4).
3. Examine the performance of starting jets based on vortex formation, thrust, and efficiency under various pressures and blocking ratios (Chapter 2).
4. Examine the performance of jet inflows based on vortex formation, thrust, and efficiency under various pressures and blocking ratios (Chapter 3).
5. Examine the performance of fully oscillating jets based on vortex formation, thrust, and efficiency under various pressures and blocking ratios (Chapter 4).
6. Compare the performance of the starting jet, inflow jet, and fully oscillating jet (Chapter 5).

Important Terminology

Starting Jet: Refers to a moving fluid that is exposed to a quiescent fluid.

Outflow Jet: Refers to a starting jet and is used to emphasize the flow direction.

Inflow Jet (or Jet Inflow): Refers to a jet that is opposite in direction to the starting or outflow jet.

Unit Pulsation: Refers to a velocity boundary function that is made up of a period of constant velocity following by an equal period of no flow.

Sinusoidal Pulsation: Refers to a velocity boundary function that consists of a sine function.

Impulsive Jet: Refers to a velocity boundary function of constant value. Note that the use of the term 'impulsive jet' is not to be confused with the way it was used by Gharib et al. (1998). The use of the term "impulsive jet" by Gharib et al. (1998) actually resembles the unit pulsation of this study since the piston in their experiment eventually stopped.

Fully Oscillating Jet: Refers to a velocity boundary with either unit or sinusoidal pulsation in the outflow and inflow directions

CHAPTER 2

COMPUTATIONAL INVESTIGATION OF LOW REYNOLDS NUMBER STARTING ANNULAR JETS[*]

Abstract

A computational model was used to examine low Reynolds number annular jets. The investigation focused on the effects of blocking ratio and ambient pressure on vortex formation, thrust, and propulsive efficiency for impulsively started, unit pulsed, and sinusoidal pulsed annular jets. The impulsively started jets were used to validate the computational model. Among the major findings was that pulsed jets were noted to pinch-off, i.e. reach maximum entrainment, in time ranges independent of the blocking ratio and ambient pressure. On the other hand, the vortices from impulsively started jets continued to entrain more fluid and did not pinch-off during the investigated time. It was also noted that incorporating blockage and increasing the ambient pressure enhanced the entrainment of the three jet types. In addition, the vortex formation from the three jet types contributed to the thrust outputs by augmenting thrust (i.e. higher exit thrust than thrust due to momentum at the entry). The changes in the thrust output due to blockage occurred within a close range of about 8 to 12%. On the other hand, ambient pressure changes (from 101 kPa to 0.670 kPa) affected the thrust of impulsively started, unit pulsed, and sinusoidal pulsed jets by 2, 11, and 120%, respectively. It was also noted that reducing the ambient pressure decreased the propulsive efficiency of the three jet types.

[*] Note. This chapter is based on "Computational Investigation of Low Reynolds Number Starting Annular Jets," by E. Abdel-Raouf, J. Baker, and M. Sharif, submitted to the *Journal of Fluids Engineering* on 9/14/2010.

Introduction

The terms starting jets is used to describe the sudden exposure of a moving fluid to a stationary fluid. Starting jets are common in many applications including fuel and oxidizer jets in combustion chambers, pressurized vessel breaches, tidal jets, and animal propulsion (Pawlak et al., 2007). In addition, starting jets are either steady or pulsating, where the latter type in particular is widely utilized in aquatic propulsion (Linden & Turner, 2001). Previous starting jet studies (Hill, 1972; Kulman, 1987; Joshi & Schreiber, 2006; Hill, 1894; Norbury, 1973; Morton, 2004) have mostly targeted two topics: the jet flow characteristics (i.e. velocity profile, entrainment, thrust, etc.) and the vortex ring formation, which is a phenomenon that characterizes starting jets.

One of the most commonly studied flow aspects of the starting jet is the associated velocity profile. Studies have shown that the velocity profile of a starting jet can be divided into three zones: the initial zone, the intermediate zone, and the fully developed zone (Ko & Chan, 1978; Ko & Lam 1985). In the initial zone, the dimensionless velocity profile along the radial position varies with the dimensionless axial position. In the intermediate zone, the dimensionless velocity profile begins to converge along the dimensionless axial position. In the fully developed zone, the dimensionless velocity profile becomes constant along the dimensionless axial position.

Another topic that has been extensively looked at in starting jet studies is the vortex formation. Many of the engineering studies on vortex formation focused on obtaining vortex ring measurements (i.e. vorticity, impulse, energy, etc.). For example, Kambe and Oshima (1975) presented a numerical simulation for viscous vortex rings and were able to calculate the rings' energy and impulse, which are difficult to determine experimentally. Didden (1979)

obtained an expression for the dimensionless circulation of the vortex rings generated by a piston and cylinder device as a function of the dimensionless piston-stroke ratio (i.e. L/D). Didden (1979) based his calculations on the slug model assumption, where the fluid velocity out of the cylinder is assumed equal to the piston velocity. Such an assumption produces inaccurate vorticity calculations because the boundary layer effects on velocity are ignored. To remedy the problem, Shusser et al. (2002) and Dabiri and Gharib (2004) incorporated correction terms to the exit velocity of the flow, while Krueger (2005) incorporated the effects of pressure.

Recently, there has been an interest in optimizing the vortex ring formation associated with starting jets. Gharib et al. (1998) suggested that for their piston and cylinder experiment, circulation is maximized at a piston stroke to diameter ratio (L/D) of approximately 4, which they called the 'formation number.' They noted that increasing the stroke ratio above the formation number causes the vortex ring to 'pinch-off', i.e. no longer entrain additional voriticity from the starting jet. Maximizing the circulation of starting jet vortex rings through the formation number was further investigated and verified analytically by Mohseni and Gharib (1998) and numerically by Rosenfeld et al. (1998). The three studies (Gharib et al., 1998; Mohseni & Gharib, 1998; Rosenfeld et al., 1998) explained the concept of a vortex 'pinch-off' at an optimized 'formation number' based on a principle by Kelvin (1880) and Benjamin (1976) that a steady vortex moving along an axis is maintained as long as the rate of energy supplied allows the vortex to possess "the maximum energy with respect to alternative arrangements of the vorticity with the same total impulse" (Dabiri, 2009). Shusser and Gharib (2000) showed that vortex pinch-off occurs when the translational velocity of the vortex ring equals the velocity of the jet flow near the ring, hence confirming the explanation based on the Kelvin-Benjamin principle.

Optimal vortex formation studies have also been extended to biological flow applications. Dabiri (2009) pointed out that biological flow applications such as blood flow in the human heart, flow of microorganisms, and propulsion of marine life like jellyfish and squid are characterized by the formation of vortex rings. Dabiri and Gharib (2005) and Linden and Turner (2004) suggested that aquatic propulsion behavior might be driven by optimal vortex formation. Bartol et al. (2009) studied the vortex rings generated by the propulsion of squid hatchlings and were able to calculate efficiency as a function of empirically determined vorticity. Jiang and Grosenbaugh (2006) numerically investigated the effects of background flow on starting jets. When comparing the steady (which was referred to as long jets) and pulsating jets at the presence of background flow, they realized that the former had a better performance, which (according to their claim) explains why adult squids use the steady flow mechanism.

In this study, a computational investigation is carried out to examine the effects of blockage and ambient pressure on the propulsion of low Reynolds number impulsively started and pulsating air jets. The tested blocking ratios are 0, 0.5, and 0.75. The simulated ambient pressures are 101 kPa, 6.51 kPa, and 0.670 kPa, which correspond to 1.00, 0.0642, and 0.00661 atmospheric pressures, respectively. The analyzed propulsion quantities are thrust and efficiency, where the latter is calculated indirectly based on the motion of the generated vortex rings. Since the vortex formation is critical to the efficiency calculations, vortex formation is also studied under various conditions. Overall, this endeavor combines elements of both the traditional starting jet flow and recent vortex formation studies. In addition, the low Reynolds number pulsating jets that are characteristic of this study make this computational investigation relevant to numerous biological flow applications.

Problem Description

A starting air jet subjected to ambient pressures of 101, 6.51, and 0.670 kPa passes through an annulus shown by Figure 2.1. The annulus, which is similar to the one used by Krueger and Gharib (2003), has a hydraulic diameter, D, of 1.27cm and a tip angle, α, of 7°. The length of the annulus is expressed in terms of the hydraulic diameter such that

$$L = 6.125D \tag{2.1}$$

To ensure that the jet is fully developed as it exits the annulus, the length of the annulus is assumed equal to the hydrodynamic length for internal laminar flow such that (Langhaar, 1942)

$$\frac{L}{D} \approx 0.05\,\mathrm{Re} \tag{2.2}$$

The Reynolds number Re in Eq. (2.2) is defined as

$$\mathrm{Re} = \frac{V_o D}{\nu} \tag{2.3}$$

where the kinematic viscosity ν was obtained from atmospheric data tabulated in U.S. Standard Atmosphere (1976).

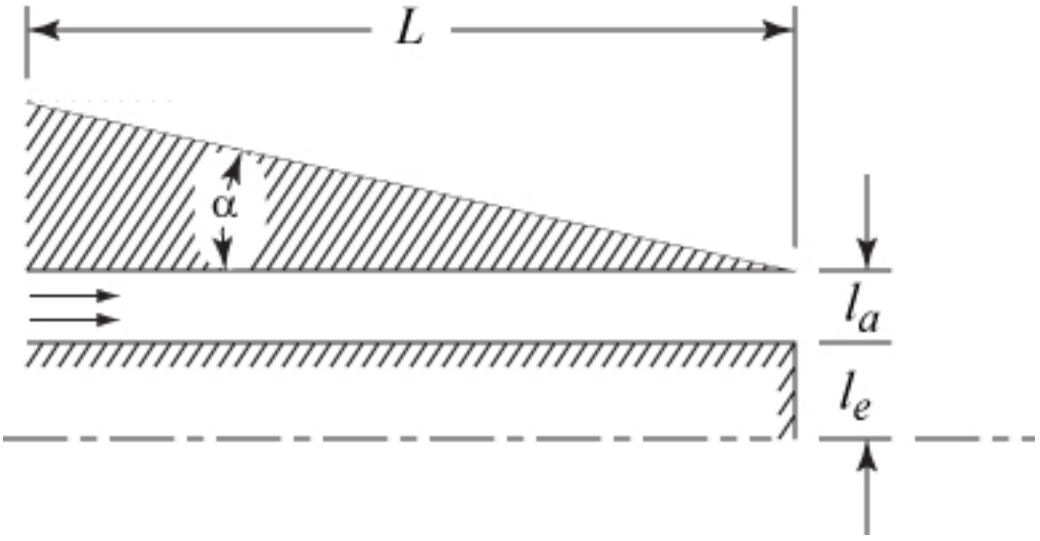

Figure 2.1. Annulus schematic.

By substituting Eq. (2.1) into Eq. (2.2), the Reynolds number used throughout this study is calculated as 122.5. At this Reynolds number, the inlet flow velocities under the ambient pressures of {101, 6.51, and 0.670} kPa are calculated from Eq. (2.3) as {0.141, 1.31, and 14.6} m/s, respectively. The Mach numbers at the three inlet conditions are significantly less than 0.3, which makes the flow of this computational study incompressible.

Numerical Model

Equations & Boundary Conditions

FLUENT 6.3, a commercially available CFD package, was used to model the starting jet described in the previous section under laminar, axisymmetric, and incompressible flow conditions. The normalized Navier-Stokes equations of this flow are (Rosenfeld et al., 1998)

$$\frac{\partial U_R}{\partial T} + U_R \frac{\partial U_R}{\partial R} + U_X \frac{\partial U_R}{\partial X} = \frac{1}{R}\frac{\partial}{\partial R}\left(R\sigma_{RR}\right) - \frac{1}{R}\sigma_{\theta\theta} + \frac{\partial \sigma_{RX}}{\partial X} \tag{2.4}$$

$$\frac{\partial U_X}{\partial T} + U_R \frac{\partial U_X}{\partial R} + U_X \frac{\partial U_X}{\partial X} = \frac{1}{R}\frac{\partial}{\partial R}\left(R\sigma_{RX}\right) + \frac{\partial \sigma_{XX}}{\partial X} \tag{2.5}$$

$$\sigma_{RR} = -P + \frac{2}{\mathrm{Re}}\frac{\partial U_R}{\partial R} \tag{2.6}$$

$$\sigma_{\theta\theta} = \frac{2}{\mathrm{Re}}\frac{\partial U_R}{\partial R} \tag{2.7}$$

$$\sigma_{RX} = \frac{1}{\mathrm{Re}}\left(\frac{\partial U_R}{\partial X} + \frac{\partial U_X}{\partial R}\right) \tag{2.8}$$

$$\sigma_{XX} = -P + \frac{2}{\mathrm{Re}}\frac{\partial U_X}{\partial X} \tag{2.9}$$

$$\frac{1}{R}\frac{\partial}{\partial R}\left(RU_R\right) + \frac{\partial U_X}{\partial X} = 0 \tag{2.10}$$

where Eq. (2.4) and (2.5) respectively represent the momentum equation in the radial and axial directions, Eq. (2.6)-(2.9) represent the stress components of the momentum equation, and Eq. (2.10) represents the continuity equation.

The labeled sides of Figure 2.2 represent the outer boundaries of the mesh used by the numerical model, and the arrow shows the flow direction. Label a represents a velocity inlet boundary condition, where

$$U_R = 0 \tag{2.11}$$

$$U_X = U_0 \tag{2.12a}$$

$$U_X = \begin{cases} 2U_0, & 0 \le T \le N/2 \\ 0, & N/2 < T \le N \end{cases} \tag{2.12b}$$

$$U_X = U_0\left[1 - \sin\left(2\pi \cdot T/N + \pi/2\right)\right], \quad 0 \le T \le N \tag{2.12c}$$

where Eq. (2.11) represents the radial component of the inlet velocity and Eq. (2.12a)-(2.12c) respectively represent the axial component of the inlet velocity for impulsively started, unit pulsed, and sinusoidal pulsed jets. Labels b through f represent non-slip wall boundary conditions such that

$$U_X = U_R = 0 \tag{2.13}$$

Labels g, h, and i represent pressure inlet/outlet boundary conditions where

$$P_{gage} = 0 \tag{2.14}$$

Label j represents an axial boundary condition. Note that label e represents the blockage such that the blocking ratio can be defined as

$$BR = \frac{l_e}{l_a + l_e} \tag{2.15}$$

where variable l denotes a boundary length. When the blocking ratio, BR, is zero (i.e. $l_e = 0$), labels f and j will both represent an axial boundary condition.

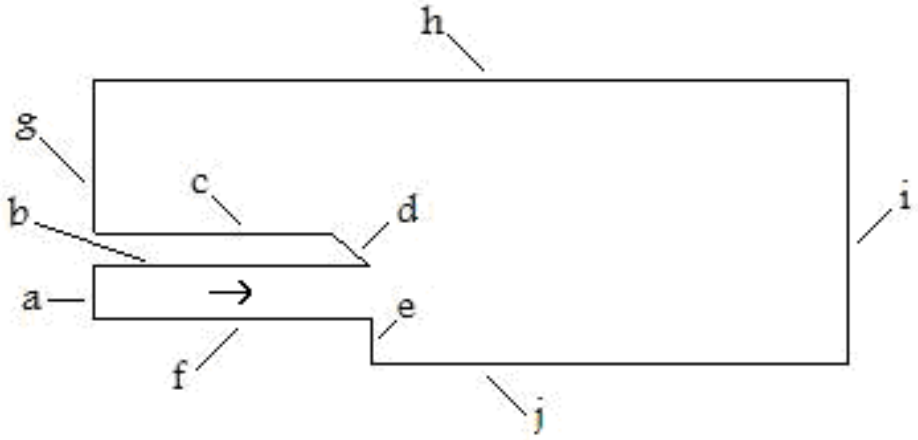

Figure 2.2. Outer boundaries of numerical model.

Verification

A vortex generated by an oscillatory pulsed starting round jet with a 0.1 s period at an ambient pressure of 101 kPa is analyzed at the end of a single pulse cycle using different grid sizes and time steps to determine the spatial and temporal convergence criteria, respectively. Figure 2.3 shows the average vorticity along an axial position of $x = 0.0814\,\text{m}$ using several equally incremented grid sizes outer dimensions of 0.045 m and 0.12 m (i.e. along the radial and axial directions, respectively) and a single time step of 0.0005 s. The percent difference between the average vorticity values from the 60000 and 86000 cell grid sizes is approximately 2%, which indicates that spatial convergence is obtained using the 60000-cell grid. Note that the 60000-cell grid was meshed using uniform square cells of length 0.03cm. This specific cell size will be used throughout the computational study to mesh grids of other outer dimensions and blocking ratios.

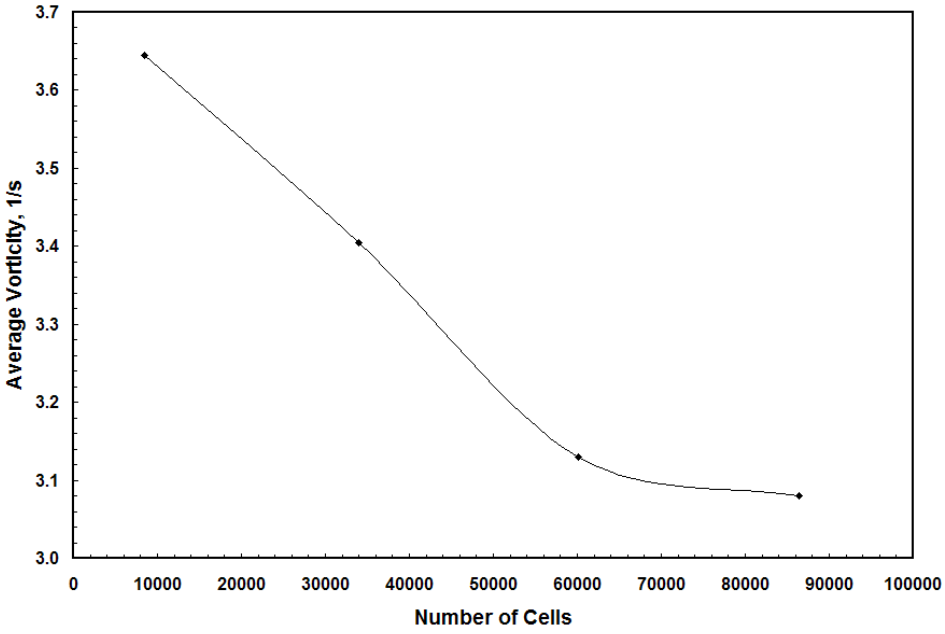

Figure 2.3. Grid convergence plot.

In order to test for temporal convergence, the time step is varied using various orders of magnitude. Relative to a $2.5*10^{-6}$ second time step, the percent difference in the area weighed average vorticity is 0.4% for a $2.5*10^{-5}$ second time step and 7% for a $2.5*10^{-4}$ second time step. Thus, temporal convergence is obtained using the $2.5*10^{-5}$ second time step, which will be the time step used throughout the computational study.

Validation

In a previous numerical study by Abdel-Raouf et al. (2010), the same commercial CFD package and flow type (i.e. axisymmetric, laminar, and incompressible) were used to model a similar starting jet problem. Figure 2.4 shows their numerical results compared against the experimental results of Obot et al. (1986) and the related theoretical results based on a derivation by Uyttendaele and Shambaugh (1989). Note that the plots of Figure 2.4 represent the dimensionless velocity profile along the radial direction of a fully developed starting round jet at a dimensionless axial position of $X = 100$. The numerical results (Abdel-Raouf et al., 2010)

were obtained from a starting jet with the same Reynolds number of 122.5 used by this study and under an ambient pressure of 101 kPa. As observed from Figure 2.4, the numerical plot is bounded by the experimental and theoretical plots, indicating the validity of the computational model.

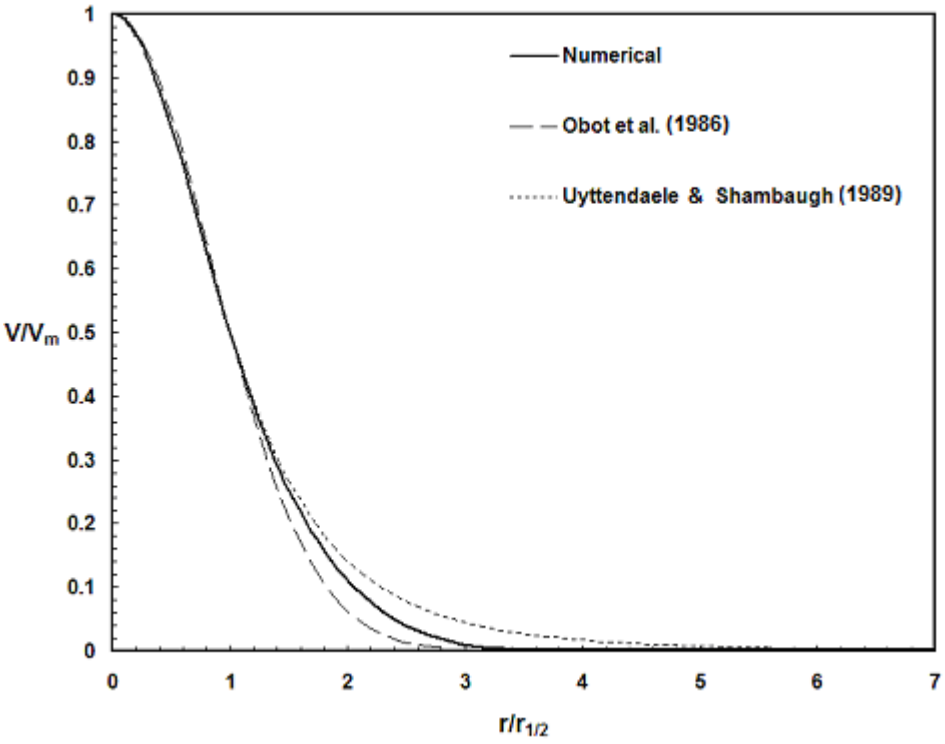

Figure 2.4. Numerical results validation (Abdel-Raouf et al., 2010).

Results & Discussion

Vortex Formation

As previously mentioned in the introduction, vortex formation is a characteristic of starting jets. Figure 2.5 shows an example of the typical vortex formation triggered by pulsed starting jets. The vorticity contour plots of Figure 2.5 show the vortex development at times $T = \{1.38, 2.76, 4.14, 5.52\}$ of a unit pulsed starting jet with cycle frequency $St = 0.18$ under zero blockage and an ambient pressure of 0.670 kPa. Time T and frequency St (or Strouhal

number) are the normalized dimensions of time t and frequency ω, respectively, such that (Dabiri, 2009)

$$T = \frac{V_0 t}{D} \tag{2.16}$$

$$St = \frac{D\omega}{V_0} \tag{2.17}$$

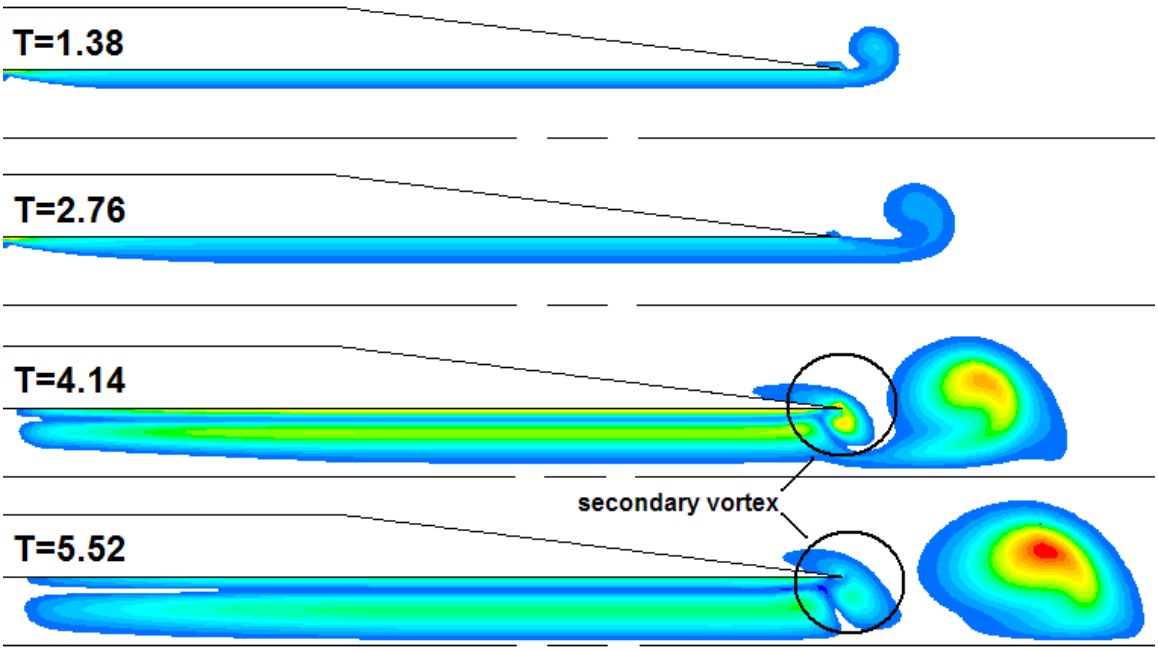

Figure 2.5. Vorticity contour plots of vortex development at St=0.18 (generated using unit pulsation).

At times $T = 1.38$ and $T = 2.76$, the velocity inlet boundary has not yet been pulsed (i.e. $U_X \neq 0$), and hence, the respective vortices are expected to resemble those triggered by an impulsively started jet. On the other hand, at times $T = 4.14$ and $T = 5.52$, the velocity inlet boundary has been pulsed (i.e. $U_X = 0$), and a secondary vortex is triggered near the edge of the annulus. The secondary vortex, which has a circulation opposite to that of the leading edge vortex, has been previously reported experimentally (Didden, 1979) and numerically (James &

Madnia, 1996) and is triggered by the vortex shedding of the leading vortex as a result of its higher induced velocity relative to the lower velocity near the edge of the annulus.

Figure 2.5 also shows that the leading vortex detaches from the trailing jet by time $T = 5.52$, indicating that vortex pinch off (i.e. when the vortex no longer entrains additional circulation) must have occurred at an earlier time. The time of vortex pinch is determined by tracking the vortex circulation as done in Table 2.1, where the circulation is calculated across the central vertical plane of the leading vortex and represented in dimensionless form such that (Krueger & Gharib, 2003)

$$\Gamma^* = \frac{\Gamma}{\nu} \tag{18}$$

Note that Table 2.1 also shows leading vortex circulation for the cases of $BR = 0.75$ with 0.670 kPa ambient pressure and $BR = 0.75$ with 101 kPa ambient pressure in order to examine the effects of blockage and ambient pressure on vortex formation. In addition, Table 2.1 shows the circulation of the vortex development that result from sinusoidal pulsed jets and impulsively started jets under similar conditions.

Table 2.1

Dimensionless Circulation, Γ^*, of Leading Vortices

Time	BR=0.0 & 0.670 kPa			BR=0.75 & 0.670 kPa			BR=0.75 & 101 kPa		
(nominal)	Unit	Sinusoidal	Impulsive	Unit	Sinusoidal	Impulsive	Unit	Sinusoidal	Impulsive
1.38	2360	850	840	8840	4060	3490	9760	3810	3580
2.76	2610	1760	890	9460	7170	3650	12610	8630	4120
4.14	2450	2290	950	9050	8750	3710	12070	11960	4490
5.52	2320	2080	1110	8090	7830	4040	11790	10720	4940

From the circulation values of Table 2.1, several observations can be made. The leading vortices triggered by pulsation have higher circulation (and thus more entraining capabilities) than those triggered by impulsive jets. In addition, increasing both blockage and ambient

pressure enhanced the vortex circulation. On the other hand, neither blockage nor ambient pressure seems to affect the time range at which the formation number falls (i.e. the time of vortex pinch off). Regardless of blockage and ambient pressure, the formation number falls between 2.76 and 4.14 for unit pulsed jets and between 4.14 and 5.52 for sinusoidal pulsed jets, which indicates that unit pulsed jets have a faster vortex formation process than sinusoidal pulsed jets. Furthermore, no vortex pinch off is noted by impulsively started jets under the examined times as indicated by the continuous increase of the vortex circulation with respect to time. Hence, impulsively started jets have a slower vortex formation process than pulsed jets.

The vorticity distribution along the horizontal center line of the leading vortex for unit pulsed, sinusoidal pulsed, and impulsively started jets is shown in Figures 2.6-2.8, respectively, where the curves peak at the center of the vortices. The plots present the vorticity Ω in dimensionless form such that (Yehoshua & Seifert, 2006)

$$\Omega^* = \frac{\Omega D}{V_0} \tag{19}$$

For all flow types, incorporating blockage increased the vorticity along the center of the leading vortex (maximum with $BR = 0.5$) and shifted the distribution closer to the edge of the annulus. On the other hand, increasing the ambient pressure shifted the vorticity distribution away from the edge of annulus while increasing the vorticity of the unit pulsed jets and impulsively started jets (maximum at 6.51 kPa) and decreasing the vorticity of the sinusoidal pulsed jets.

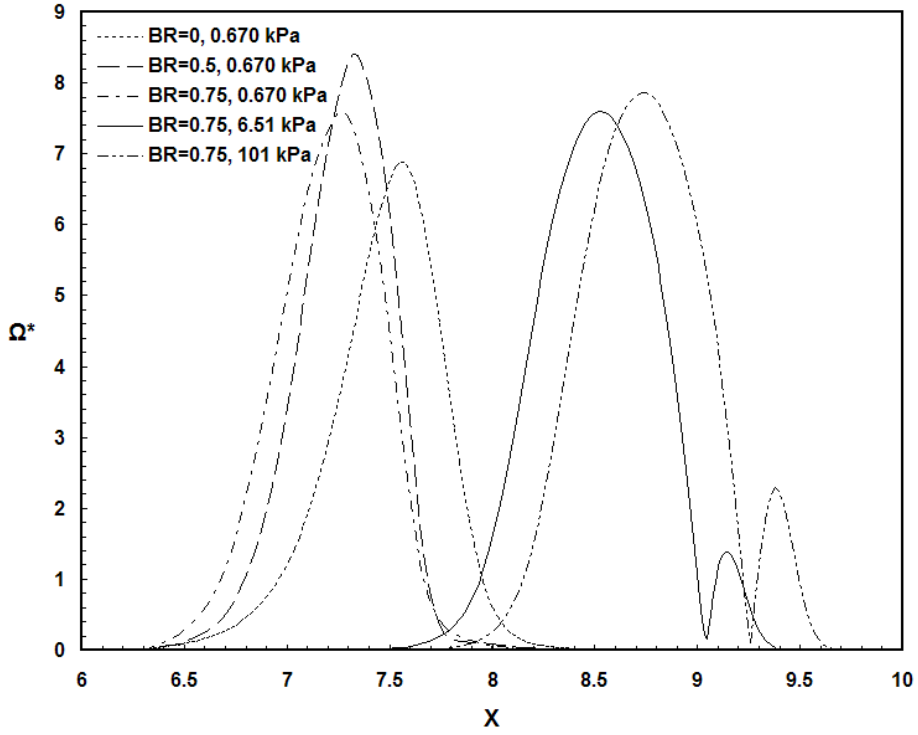

Figure 2.6. Unit pulsed starting jet vortex distribution at St=0.18

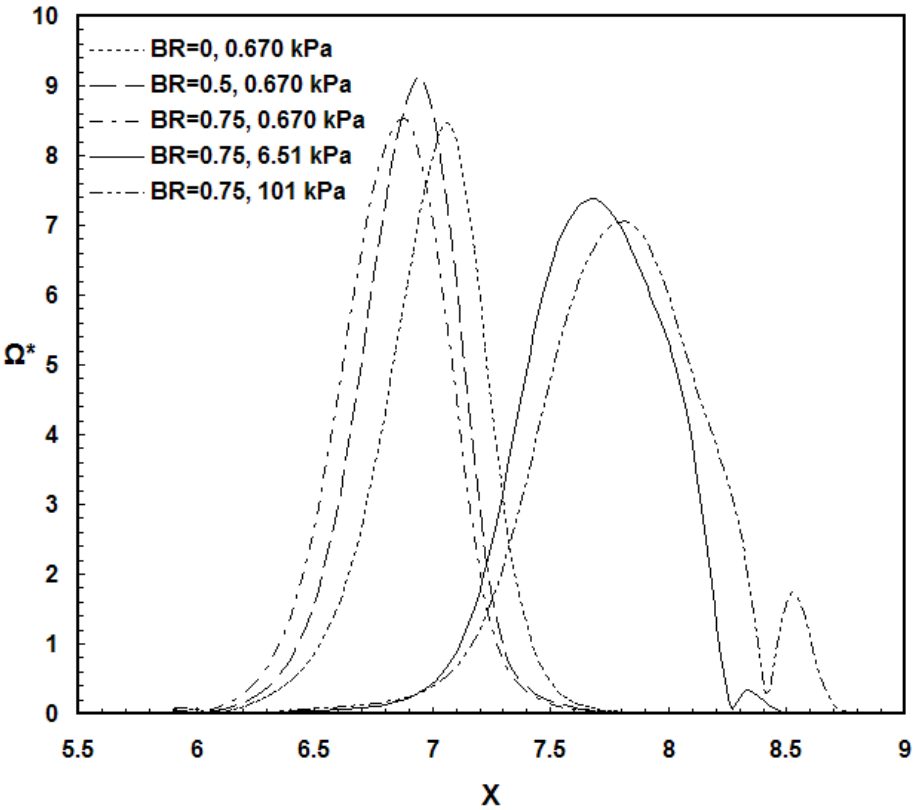

Figure 2.7. Sinusoidal pulsed starting jet vortex distribution at St=0.18.

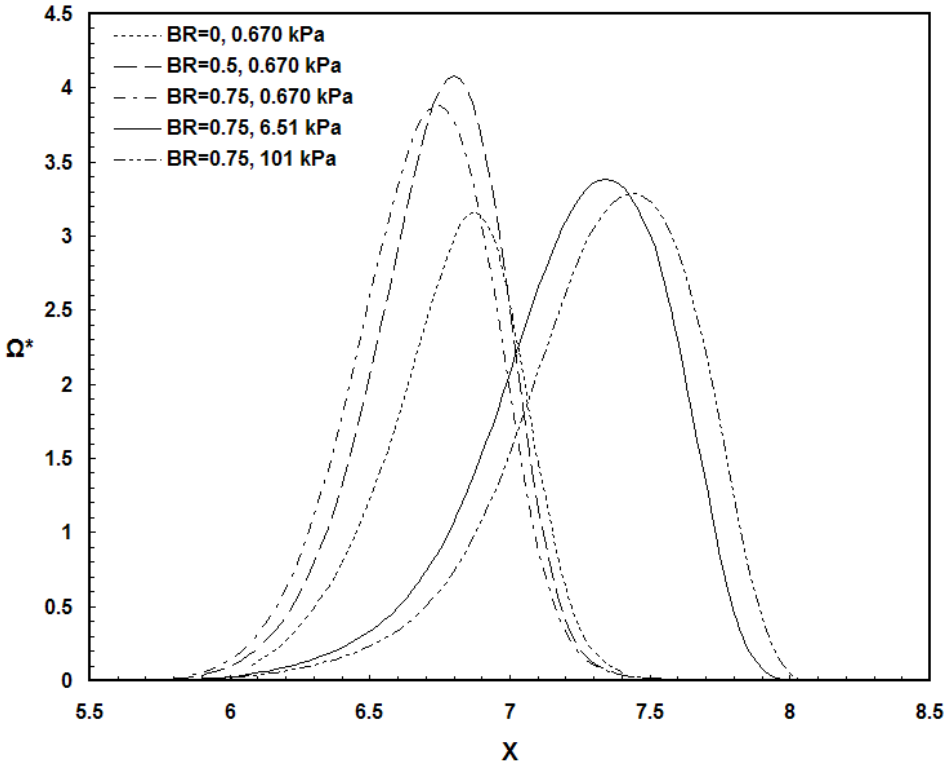

Figure 2.8. Impulsively started jet vortex distribution at T=5.52.

In addition, some of the plots in Figures 2.6 and 2.7 show secondary minor peaks, which are portions of the vortices induced by the circulation due to blockage, for which an example is shown by lower vortex of Figure 2.9. The fact that portions of the lower vortex are present along the vorticity distribution at the horizontal centerline of the upper vortex indicates that the lower vortex is in the process of engulfing the upper vortex. In general, for any two closely located vortices initially comparable in size and moving along the same axis of symmetry, one will end up engulfing the other in what has been described as 'leapfrogging' motion (Riley & Stevens, 1993). For the pulsed jet vorticity distribution plots of Figures 2.6 and 2.7, the leapfrogging motion is enhanced by increasing the ambient pressure. The impulsively started jet vorticity distributions of Figure 2.8 do not contain any secondary peaks, which indicates that leapfrogging is triggered faster by pulsation for low Reynolds number flows.

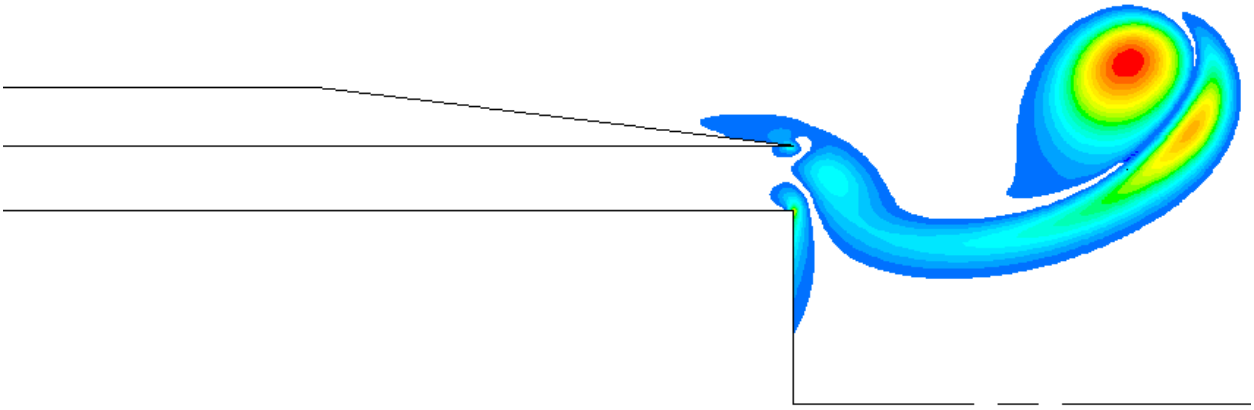

Figure 2.9. Vortex leapfrogging.

Thrust Analysis

The average thrust, f_{avg}, of a starting jet can be calculated at the exit of the annulus by

$$f_{avg} = \frac{1}{t}\left[\int_0^t \int_A [pV_x^2(r,\tau) + p_{gage}(r,\tau)] \; dsd\tau\right] \tag{2.20}$$

where A is the cross sectional area of the annulus and t is the duration of an impulsively started jet or the time period of a pulsating jet. The first term of the integrand of Eq. (2.20) represents the thrust due to momentum, and the second term represents the thrust due to pressure.

Impulsively Started Jets

The effects of the blocking ratio and ambient pressure on the thrust output of an impulsively started jet are shown in Figure 2.10, where the dimensionless thrust F is defined as

$$F = \frac{f_{avg}}{\rho A V_0^2} \tag{2.21}$$

As shown in Figure 2.10, the thrust curve is initially dominated by transient behavior where its values drop rapidly with increasing time. The time range between $T = 2$ and $T = 3$ marks the transition to steady state, where the thrust levels offs with increasing time. The steady state thrust value under zero blockage and an ambient pressure of 101 kPa is $F = 1.2$. Incorporating

blockage decreases the steady state value by approximately 9% for $BR = 0.5$ and 10% for $BR = 0.75$, while decreasing the ambient pressure to 6.51 and 0.670 kPa decreases the steady state thrust by 0.4% and 2%, respectively. Hence, the steady state thrust values are strong functions of blockage and weak functions of ambient pressure.

In addition, the dimensionless thrust values of the impulsively started jets of Figure 2.10 have values that are greater than F>1 (particularly in the transient state). Such thrust augmentation was noted by Krueger and Gharib (2005) in their experimental study with starting pulsed jets and is a direct effect of the fluid entrainment caused by the vortex formation.

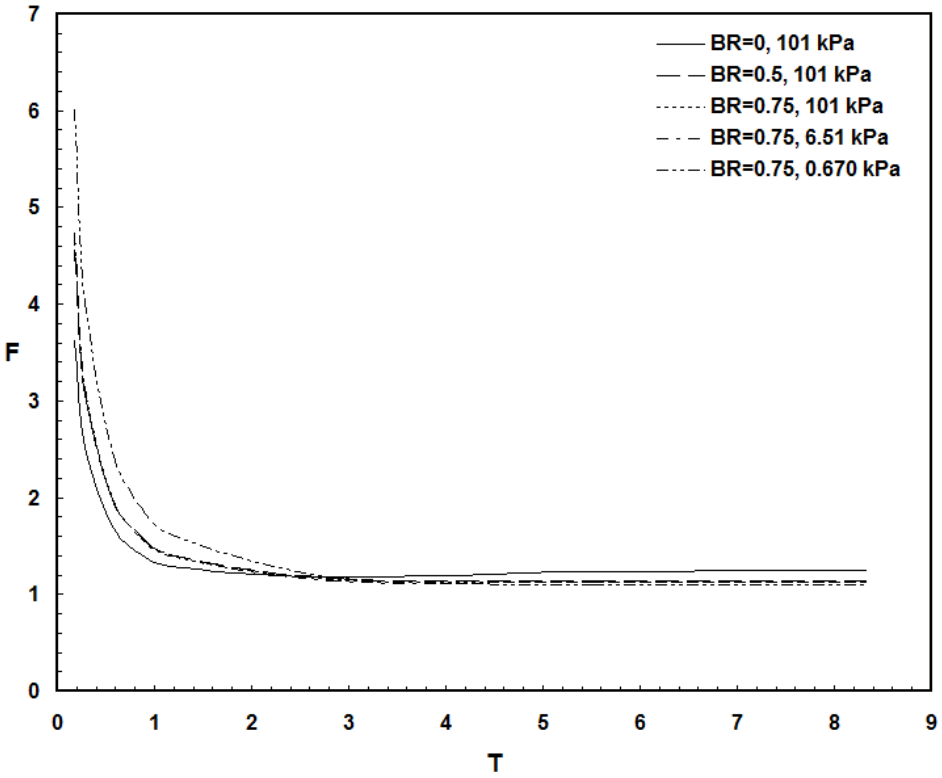

Figure 2.10. Thrust output of impulsively started jets.

In Figure 2.11, the momentum and pressure terms of the total thrust output presented in Figure 2.10 are plotted separately. The momentum component of the thrust is nearly constant throughout the flow time. On the other hand, the pressure component of the thrust drops rapidly during the initial flow time and then levels out. When comparing both thrust components, the

pressure component has more contribution to the total thrust at the start of the flow. As time increases, however, the pressure contribution decreases, and eventually, the thrust is completely produced by the momentum of the flow. Therefore, the transient behavior of the total thrust from Figure 2.10 is due to the behavior of the thrust's pressure component. Such high initial values of the pressure thrust are due to the reaction of the flow to the pressure wave caused the sudden motion of the impulsively started jet.

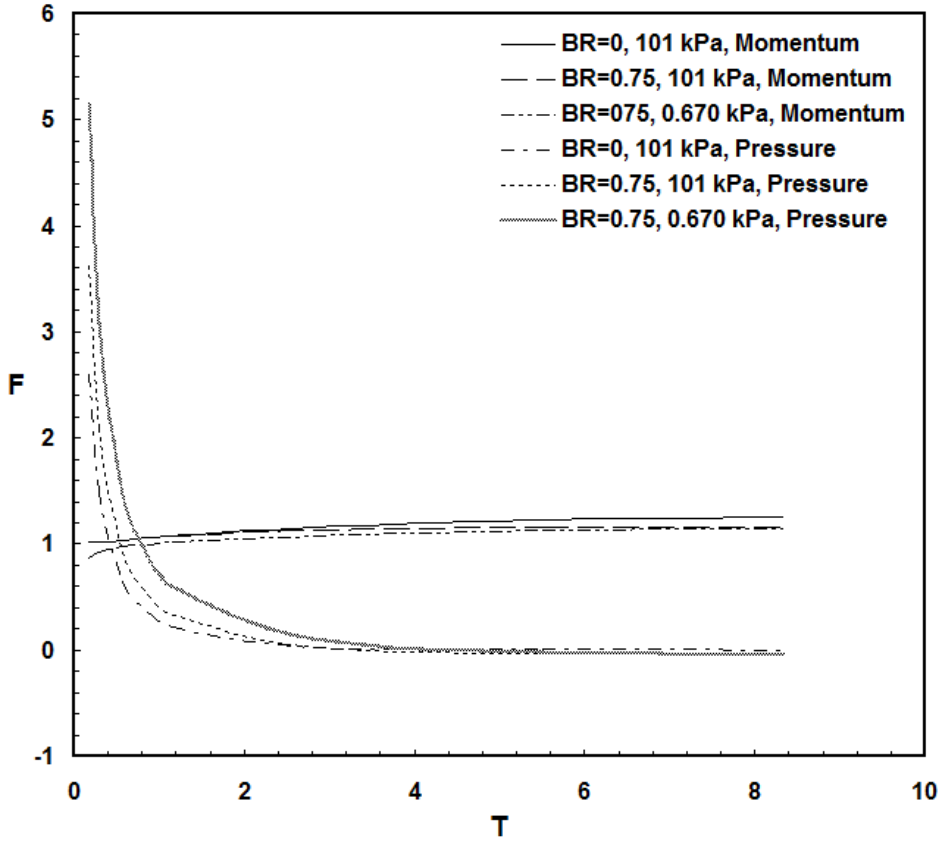

Figure 2.11. Thrust components of impulsively started jets.

Pulsed Jets

The dimensionless thrust of the unit and sinusoidal pulsating starting jets is plotted in Figure 2.12 as a function of the normalized frequency. Under all tested conditions, as shown in Figure 2.12, the thrust output of unit pulsed jets decreases to a minimum at the frequency range

of $St = 0.2$ and $St = 0.3$ and then increases with increasing frequency. The thrust output from sinusoidal pulsed jets, on the other hand, generally decreased with increasing frequency; the only exception is when under an ambient pressure of 0.670 kPa, where the thrust decreases and then increases with increasing frequency.

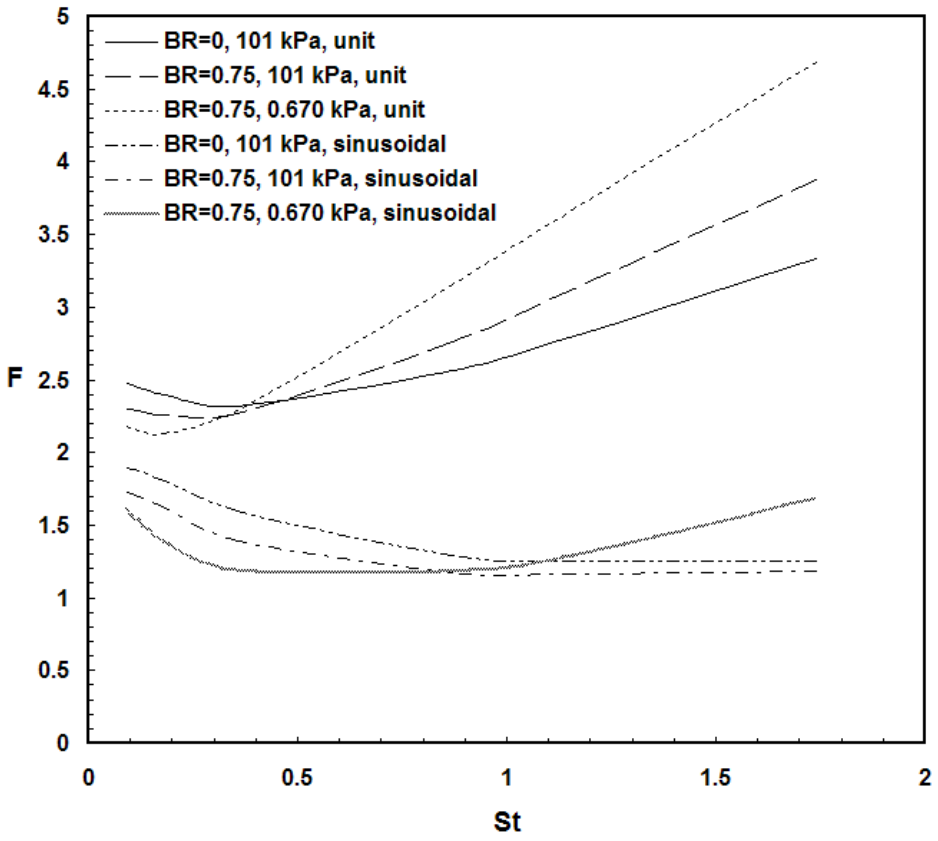

Figure 2.12. Thrust output of pulsating starting jets.

The change of the thrust output plot behavior of sinusoidal pulsed jets at an ambient pressure of 0.670 kPa indicates that sinusoidal jets are sensitive to ambient pressure changes. In fact, for a blocking ratio of $BR = 0.75$, decreasing the ambient pressure from 101 kPa to 0.670 kPa changes the average thrust output of the sinusoidal pulsed jet by 120% over the examined range of frequencies. For the same blockage and ambient pressure changes, the average thrust output change for the unit pulsed jet is only 11%.

The sensitivity of sinusoidal and unit pulsed jets to changes in blockage, on the other hand, are quite similar. Under an ambient pressure of 101 kPa, changing the blocking ratio from $BR = 0$ to $BR = 0.75$ causes an average thrust output change of 7.6% for sinusoidal pulsed jets and 12% for unit pulsed jets.

From Figure 2.12, it can also be noted that the thrust output from the unit pulsed jets is greater than the thrust output from sinusoidal pulsed jets under all examined frequencies. For example, under $BR = 0$ and 101 kPa ambient pressure conditions, the ratio of the thrust outputs between unit and sinusoidal pulsed jets varied between 1.3 at $St = 0.1$ and 4.9 at $St = 1.7$, where the increase in the thrust ratio at higher frequencies is primarily due to the high pressure thrust components that are shown in Figure 2.13 for unit pulsed jets.

The thrust components of the total thrust output from Figure 2.12 are shown in Figures 2.13 and 2.14 for unit and sinusoidal pulsed jets, respectively. For both pulsation types, the momentum thrust component decreases gradually with increasing frequency, which is the same behavior reported by Krueger and Gharib (2005) during their experimental study on thrust augmentation due to fully pulsed jets. In particular, the values of the momentum thrust component from the sinusoidal pulsed jet resemble the experimental results of Krueger and Gharib (2005), which were produced using a piston velocity profile similar to the sinusoidal inlet velocity boundary of this study.

The noted decrease in the momentum thrust component with increasing frequency can be rationalized by the fact the vortex formation is more developed (i.e. has more circulation) at lower frequencies than at higher frequencies and hence has more entrainment capabilities at the former. Note that a low frequency means a large cycle period and hence ample time for the

vortex to develop and entrain more fluid than a vortex triggered at a high frequency (i.e. small cycle period and lesser development time).

The pressure component of thrust from both pulsed jets, on the other hand, behaves differently. For unit pulsed jets, the pressure thrust component increases with increasing frequency as a result of the decrease in the cycle period, which makes the fluid react faster to the disturbance caused by the upcoming pressure wave. Note that the effects of such a disturbance has been noted in impulsively started jets and is shared by the constant velocity inflow portion of the unit pulsed jets. The velocity inflow of sinusoidal pulsed jets, on the other hand, changes gradually and hence does not cause the disturbance noted in impulsively started and unit pulsed jets. Thus, the pressure thrust component of sinusoidal pulsed jets is not the dominating thrust component. However, for a low ambient pressure of 0.670 kPa, the flow disturbance due to the pressure wave is evident at higher frequencies.

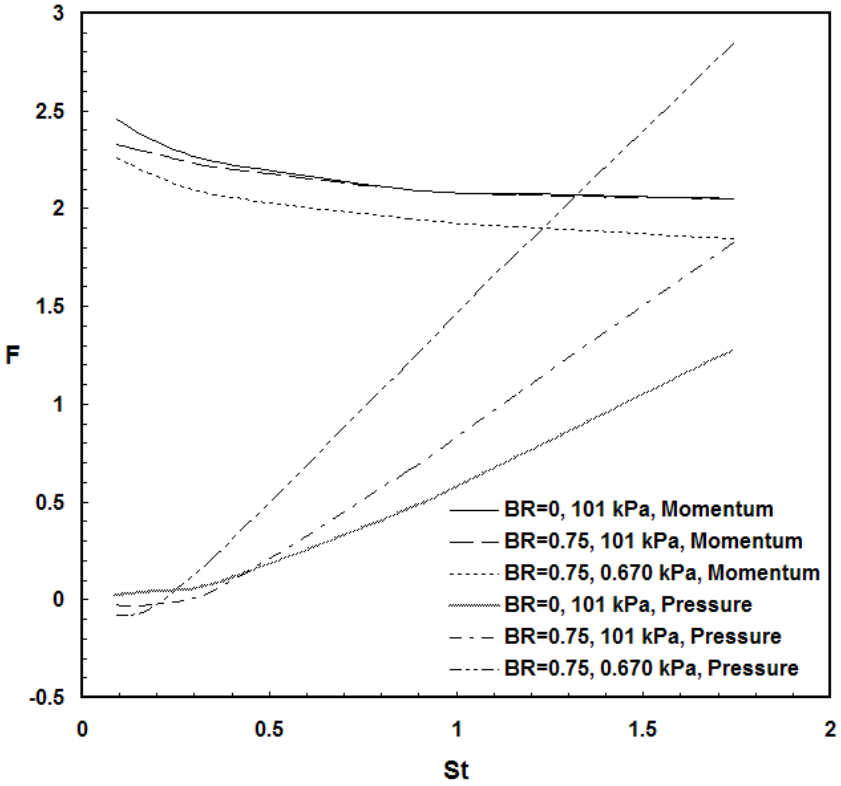

Figure 2.13. Thrust components of unit pulsation.

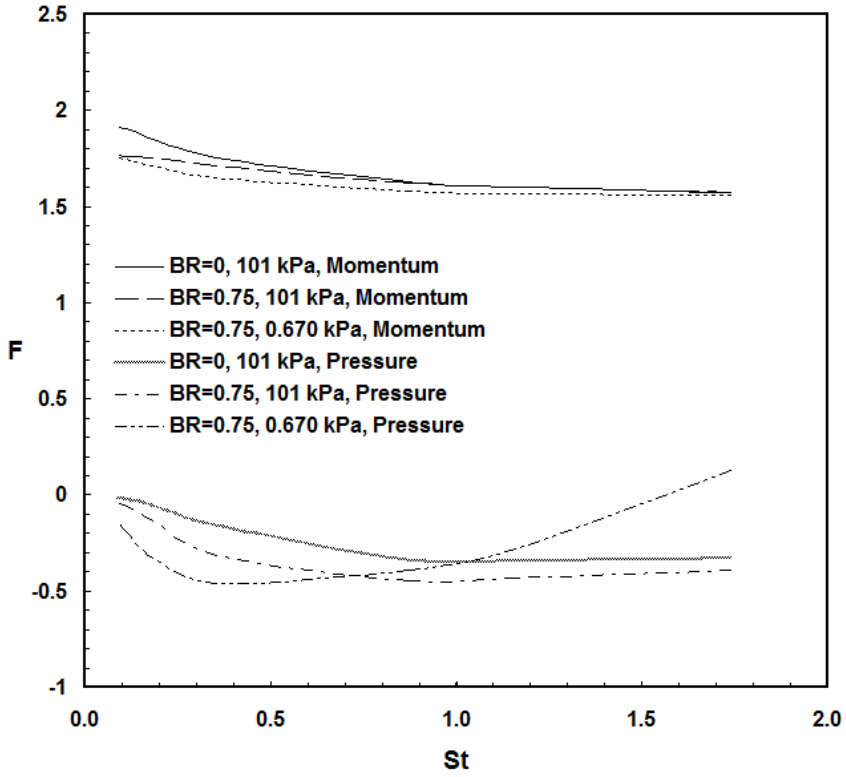

Figure 2.14. Thrust components of sinusoidal pulsation.

Propulsive Efficiency

The propulsive efficiency η of the impulsively started, unit pulsed, and sinusoidal pulsed jets under various conditions are calculated based on both the work done by the leading vortex along the axial direction over a specific time and the excess kinetic energy ke during the process such that

$$\eta = \frac{\tilde{f} \cdot \Delta x}{\tilde{f} \cdot \Delta x + ke} \tag{2.22}$$

where $\tilde{f}$ is average thrust at the end of the work process and Δx is the axial distance traveled by the center of the leading vortex during work process. The average thrust of the leading vortex is calculated from the impulse such that $\tilde{f} = I / t$, where the impulse I is determined from the vorticity of the vortex using (Barton et al., 2009)

$$I = \rho\pi \int_{jet} \Omega_\theta r^2 dr dx \tag{2.23}$$

The kinetic energy along the axial direction is calculated by

$$ke = \rho \int_{jet} \frac{V^2}{2} d\forall \tag{2.24}$$

Figure 2.15 shows the propulsive efficiency of impulsively started jets as a function of time. Similar to the noted behavior of the thrust output of impulsive jets, the efficiency undergoes a transient stage followed by a steady state stage. The efficiency increases with time during the transient stage and then nearly flattens out to a constant value during the steady-state stage. For a blocking ratio of $BR = 0$, the steady state efficiency of an impulsively started jet decreases from approximately 49% under a 6.51 kPa ambient pressure condition to 23% under a 0.670 kPa ambient pressure condition (i.e. 53% drop). Under the latter pressure condition, the steady state efficiency of the impulsively started jet decreases from about 23% to 19% (i.e. 17% drop) for blocking ratios of $BR = 0$ and $BR = 0.75$, respectively. Thus, incorporating blockage and decreasing the ambient pressure reduces the steady state efficiency of impulsively started jets.

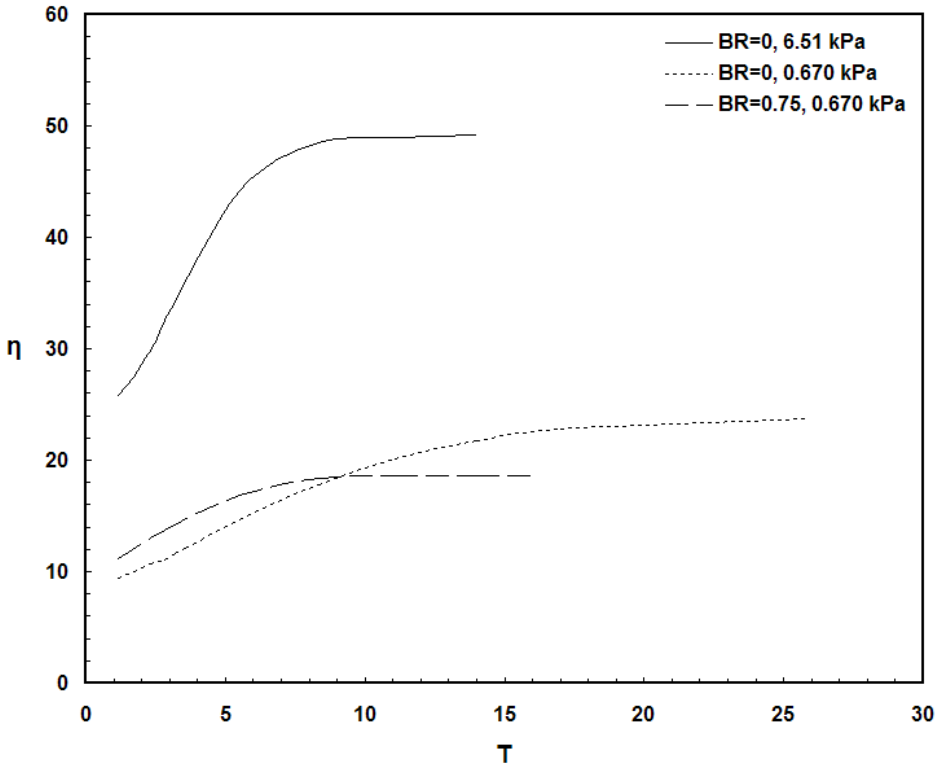

Figure 2.15. Propulsive efficiency of impulsively started jets.

Unlike the steady-state efficiency behavior of impulsively started jets with respect to time, pulsed jets have no steady-state efficiency with respect to the dimensionless frequency, as evident from Figures 2.16 and 2.17. The overall pattern of the propulsive efficiency of pulsed jets is a brief increase to a maximum efficiency value within the frequency range of $St = 0.15$ to $St = 0.35$ followed by a decline with increasing frequency. In addition, incorporating blockage enhances the efficiency of unit and sinusoidal pulsed starting jets by 26% and 31%, respectively. On the other hand, decreasing the ambient pressure decreases the efficiency of both types of pulsed starting jets by 18% and 20%, respectively.

It can also be noted that starting jets triggered by unit pulsation generally produced higher efficiencies than those triggered by sinusoidal pulsation for the examined blockage and ambient pressures. For example, under a block ratio of $BR = 0$ and an ambient pressure of 6.51 kPa, the

average propulsion efficiency of the unit pulsed jet is greater than that of sinusoidal pulsed jet by about 15% over the examined frequencies. However, the maximum efficiency values remain in the range of 52 to 56% (i.e. within a 7% difference) at frequencies ranging from $St = 0.15$ to $St = 0.35$ regardless of pulsation type, blockage, and ambient pressure.

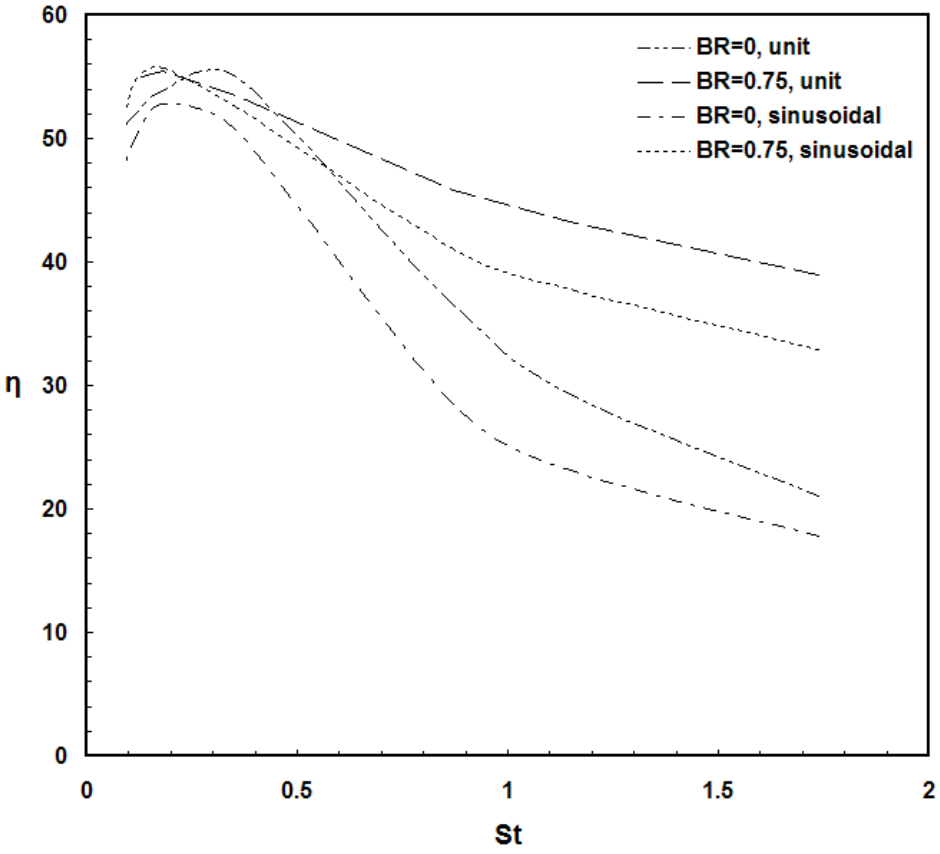

Figure 2.16. Propulsive efficiency of pulsed jets at various blocking ratios.

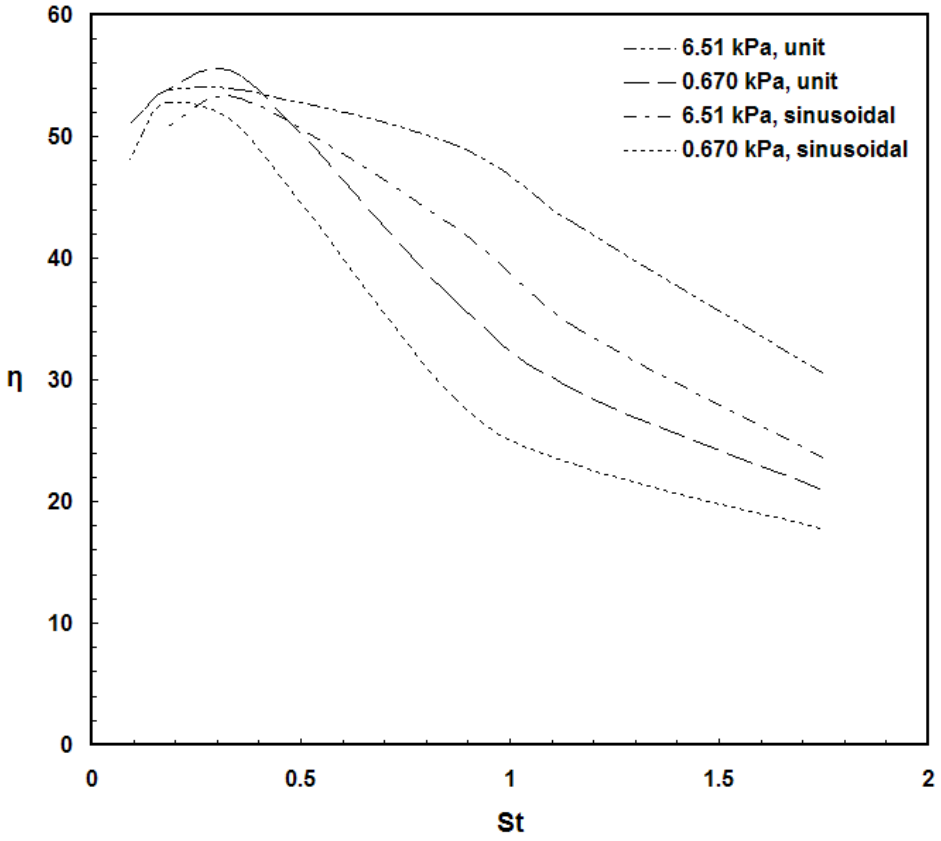

Figure 2.17. Propulsive efficiency of pulsed jets at various pressures.

Conclusion

Low Reynolds number flow starting air jets triggered by steady, unit pulsed, and sinusoidal pulsed flow were numerically examined for the blocking ratios of 0, 0.5, and 0.75 and at ambient pressure conditions of 101, 6.51, and 0.670 kPa. The analysis was conducted for vortex formation, thrust, and propulsive efficiency. The following points present the main finding.

1. Unit pulsed jets were noted to have faster vortex formation development than sinusoidal pulsed jets. Vortex 'pinch-off' took place in the range of $T = 2.76$ to $T = 4.14$ for unit pulsed jet but at a later time range of $T = 4.14$ to $T = 5.52$ for sinusoidal pulsed jets. Unit pulsed jets also had superior entrainment capabilities relative to sinusoidal pulsed jet, as evident from the higher circulation values of the former relative to the later. In addition, vortex

formation triggered by impulsively started jets had inferior entrainment capabilities relative to pulsed jets, and they also had slower vortex development since 'pinch-off' was not noted by time $T = 5.52$.

2. Both unit and sinusoidal pulsed jets were noted to generate a secondary vortex (Didden, 1979; James & Madnia, 1996) at the annulus exit plane because of the shedding of the leading vortex. The shedding was triggered by the higher induced velocity of the leading vortex and the lower velocity at the edge of the nozzle.

3. Incorporating blockage and increasing the ambient pressure increased the circulation (i.e. higher entrainment) of the leading vortices for impulsively started, unit pulsed, and sinusoidal pulsed jets. Furthermore, neither blockage nor ambient pressure were noted to affect the vortex formation number (i.e. time at which pinch off occurs).

4. Thrust augmentation (i.e. F>1) was noted from the thrust outputs of impulsively started, unit pulsed, and sinusoidal pulsed jets. The thrust augmentation phenomenon was previously reported by Krueger and Gharib (2005) and is the caused by the entrainment effects of the lead vortex.

5. The normalized momentum component of thrust of the sinusoidal pulsed jet for a Reynolds number of 122.5 with BR=0 and an ambient pressure condition of 101 kPa closely resembled values obtained from the experimental work of Krueger and Gharib (2005) for a piston velocity profile similar to the sinusoidal velocity input of this study and a Reynolds number of approximately 13000. Note that the annulus geometry of this study was the same as the one used by Krueger and Gharib (2005). This leads to the possible conjecture that the normalized thrust outputs from starting jets are not highly dependent on the Reynolds number. However, more research is needed in order validate that claim.

6. Unit pulsation generally delivered more efficient leading vortices than sinusoidal pulsation. However, the maximum efficiency remained in the efficiency range of 52 to 56% occurring within the frequency range of St=0.15 to St=0.35.

Acknowledgements

The authors would like to thank the U.S. Department of Education for its support through the Graduate Assistance in Areas of National Need (GAANN) Fellowship.

References

Abdel-Raouf, E., Baker, J., & Sharif, M. (2010). Computational investigation of low Reynolds number impulsively started annular jets (The effects of blocking ratio and atmospheric altitude on starting annular jets). *Proceedings of the ASME 2010 3rd Joint US-European Fluids Engineering Summer Meeting and 8th International Conference on Nanochannels, Microchannels, and Minichannels*, FEDSM-ICNMM2010-30767.

Bartol, I., Krueger, P., Stewart, W., & Thompson, J. (2009). Pulsed jet dynamics of squid hatchlings at intermediate Reynolds numbers. *Journal of Experimental Biology*, 212, 1506-1518.

Benjamin, T. (1976). The alliance of practical and analytical insights into the non-linear problems of fluid mechanics. *Application of Methods of Functional Analysis to Problems in Mechanics*, Lecture Notes in Mathematics, 503, 8-29.

Dabiri, J. (2009). Optimal vortex formation as a unifying principle in biological propulsion. *Annual Review of Fluid Mechanics*, 41, 17-33.

Dabiri, J., & Gharib, M. (2004). A revised slug model boundary layer correction for starting jet vorticity flux. *Theoretical and Computational Fluid Dynamics*, 17, 293-295.

Dabiri, J., & Gharib, M. (2005). The role of optimal vortex formation in biological fluid transport. *Proceedings of the Royal Society B*, 272, 1557-1560.

Didden, N. (1979). On the formation of vortex rings: rolling-up and production of circulation. *Zeitschrift für Angewandte Mathematik und Physik* (ZAMP), 30(1), 101-116.

Gharib, M., Rambod, E., & Shariff, K. (1998). A universal time scale for vortex ring formation. *Journal of Fluid Mechanics*, 360, 121-140.

Hill, B. (1972). Measurement of local entrainment rate in the initial region of axisymmetric turbulent air jets. *Journal of Fluid Mechanics*, 51(4), 773-779.

Hill, M. (1894). On a spherical vortex. *Proceedings of the Royal Society of London*, 55, 219-224.

James, S., & Madnia, C. (1996). Direct numerical simulation of a laminar vortex ring. *Physics of Fluids*, 8(9), 2400-2414.

Jiang, H., & Grosenbaugh, M. (2006). Numerical simulation of vortex ring formation in the presence of background flow with implications for squid propulsion. *Theoretical and Computational Fluid Dynamics*, 20(2), 103-123.

Joshi, A., & Schreiber, W. (2006). An experimental examination of an impulsively started incompressible turbulent jet. *Experiments in Fluids*, 40, 156-160.

Kambe, T., & Oshima, Y. (1975). Generation of decay of viscous vortex rings. *Journal of the Physical Society of Japan*, 38(1), 271-280.

Kelvin, L. (1880). Vortex statics. *Philosophical Magazine Series 5*, 10(60), 97-109.

Ko, N., & Chan, W., 1978. Similarity in the initial region of annular jets: three configurations. *Journal of Fluid Mechanics*, 84(4), 641-656.

Ko, N., & Lam, K. (1985). Flow structures of a basic annular jet. *AIAA Journal*, 23(8), 1185-1190.

Krueger, P. (2005). An over-pressure correction to the slug model for vortex ring circulation. *Journal of Fluid Mechanics*, 545, 427-443.

Krueger, P., & Gharib, M. (2003). The significance of vortex ring formation to the impulse and thrust of a starting jet. *Physics of Fluids*, 15(5), 1271-1281.

Krueger, P., & Gharib, M. (2005). Thrust augmentation and vortex ring evolution in a fully pulsed jet. *AIAA Journal*, 43(4), 792-801.

Kulman, J. (1987). Variation of entrainment in annular jets. *AIAA Journal*, 35(3), 373-379.

Langhaar, H. (1942). Steady flow in the transition length of a straight tube. *Journal of Applied Mechanics*, 9, 55-58.

Linden, P., & Turner, J. (2001). The formation of 'optimal' vortex rings, and the efficiency of propulsion devices. *Journal of Fluid Mechanics*, 427, 61-72.

Linden, P., & Turner, J. (2004). 'Optimal' vortex rings and aquatic propulsion mechanisms. *Proceeding of the Royal Society of London B*, 271, 647-653.

Mohseni, K., & Gharib, M. (1998). A model for universal time scale of vortex ring formation. *Physics of Fluids*, 10(10), 2436-2438.

Morton, T. (2004). The velocity field within a vortex ring with a large elliptical cross-section. *Journal of Fluid Mechanics*, 503, 247-271.

Norbury, J. (1973). A family of steady vortex rings. *Journal of Fluid Mechanics*, 57, 417-431.

Obot, N., Trabold, T., Graska, M., & Gandhi, F. (1986). Velocity and temperature fields in turbulent jets issuing from sharp-edged inlet round nozzles. *Industrial & Engineering Chemistry Fundamentals*, 25(3), 425-433.

Pawlak, G., Cruz, C., Bazan, C., & Hrdy, P. (2007). Experimental characterization of starting jet dynamics. *Fluid Dynamics Research*, 39, 711-730.

Riley, N., & Steven, D. (1993). A note on leapfrogging vortex rings. *Fluid Dynamics Research*, 11(5), 235-244.

Rosenfeld, M., Rambod, E., & Gharib, M. (1998). Circulation and formation number of laminar vortex rings. *Journal of Fluid Mechanics*, 376, 297-318.

Shusser, M., & Gharib, M. (2000). Energy and velocity of a forming vortex ring. *Physics of Fluids*, 12(3), 618-621.

Shusser, M., Gharib, M., Rosenfeld, M., & Mohseni, K. (2002). On the effect of Pipe Boundary layer growth on the formation of a laminar vortex ring generated by a piston/cylinder arrangement. *Theoretical and Computational Fluid Dynamics*, 15, 303-316.

Uyttendaele, M., & Shambaugh, R. (1989). The flow of annular jets at moderate Reynolds numbers. *Industrial & Engineering Chemistry Research*, 28, 1735-1740.

Yehoshua, T., & Seifert, A. (2006). Active boundary layer tripping using oscillatory vorticity generator. *Aerospace Science and Technology*, 10, 175-180.

U.S. Standard Atmosphere. (1976). Washington, DC: U.S. Government Printing Office.

CHAPTER 3

IMPULSIVELY STARTED AND PULSATED ANNULAR INFLOWS[*]

Abstract

A computational investigation was carried out on low Reynolds number inflow starting annular jets using multiple blocking ratios and ambient pressure conditions. The inflow velocity boundary was selected in such as to mimic the impulsive, unit pulsed, and sinusoidal pulsed starting jet propulsion mechanisms that are common among biological marine flow. The behavior of the three propulsion modes was analyzed based on the vortex formation, the resultant of the momentum and pressure forces at the entry of the annulus, and the efficiency of the inflow jets. The results showed that impulsively started inflow jets did not trigger vortex formation, while both unit pulsed and sinusoidal pulsed inflow jets triggered the formation of a standing vortex inside the annulus. Furthermore, unit pulsed inflow jets triggered the formation of a secondary vortex outside the annulus. Force augmentation was also noted from sinusoidal pulsed inflow jets and was directly related to the vortex formation inside the annulus. In addition, the efficiency of the sinusoidal pulsed inflow jet was higher than that of the unit pulsed inflow jet because of the formation of a secondary vortex (by the latter) with opposite circulation to the primary vortex.

[*] Note. This chapter is based on "Impulsively Started and Pulsating Annular Inflows," by E. Abdel-Raouf, J. Baker, and M. Sharif, submitted to the *International Journal of Heat and Fluid Flow* on 2/23/2011.

Introduction

Starting jets are a category of fluid flow problems that involve the exposure of a moving fluid to a dormant fluid; such jets generally trigger the formation of vortices. Starting jets are found in numerous applications that range from the production of microfibers (Uyttendaele & Shambaugh, 1989) to biological propulsion (Dabiri, 2009). As an important phenomenon, starting jets have been the subject of various studies that typically focused on the overall jet characteristics (Joshi & Schreiber, 2006; Satti & Agrawal, 2008) and/or the vortex formation (Seno et al., 1988; Syed & Sung, 2009).

Vortex formation, in particular, has been the subject that attracted the recent trend of starting jets studies. In their investigation of vortices generated from impulsively starting jets delivered by a piston/cylinder device, Gharib et al. (1998) realized that vortex formation could be optimized as a function of the piston's velocity profile. Dabiri and Gharib (2005) then suggested that biological flow kinematics, such as those of squids, can be correlated with optimal vortex formation.

Most of the previous studies have addressed vortex formation using starting outflow jets. For example, the effects of blockage and ambient pressure on low Reynolds number steady jets, unit pulsed jets, and sinusoidal pulsed jets in the outflow direction were studied in Chapter 2. Among the main findings was that neither blockage nor pressure had significant effects on the vortex formation number. In addition, the leading vortices caused thrust augmentation (i.e. higher thrust at annulus exit relative to annulus entry), which had been previously noted experimentally by Krueger and Gharib (2005).

Unlike the abundant studies of starting jets in the outflow direction, the literature is lacking in the studies of starting jets in the inflow direction due to its limited practical

applications. For example, suction feeding is employed by the fish's rapid expansion of its oral cavity, which in turn draws water into its mouth and captures the prey in the process (Bishop et al., 2008). Theoretical (Muller et al., 1982), experimental (Lauder, 1980), and computational (Van Wassenbergh & Aerts, 2009) studies have been carried out on the topic to better understand the suction feeding mechanism. In another research area, Dabiri et al. (2005) indirectly studied jet inflows by examining the recovery stroke of a jellyfish during which the formation of a stopping vortex was noted to occur. With the exception of the suction feeding of marine vertebrates and the recovery stroke of a jellyfish, the authors are not aware of any other studies that would fall under the category of inflow starting jets.

The current endeavor seeks to computationally examine the behavior of starting inflow jets that are triggered by impulsive flow, unit pulsation, and sinusoidal pulsation. These three mechanisms are commonly used by low and intermediate Reynolds number marine flow (Bartol et al., 2009). In order to make this computational investigation relevant to as many applications as possible, the inflow starting jets will be subjected to several blocking ratios along with multiple ambient pressure conditions. The resulting inflow jets will be analyzed based on the vortex formation, the resultant of the momentum and pressure forces at the annulus entry, and the efficiency. Note that the current jet inflow study is conducted using air; nevertheless, the results from the investigation will still be comparable with the results from the previous biological flow studies by using a similar low Reynolds flow regime.

Problem Description

The inflow air jet of this study is assumed to pass through the same annulus used in the outflow starting air jet study of Chapter 2, where the incline angle, α, is 7° and the hydraulic diameter, D, is 1.27 cm. The length of the annular tube, L, is $6.125D$, as shown by the

schematic of Figure 3.1. In addition, the jet is tested for the following blocking ratio: $BR = \{0, 0.5, 0.75\}$, where

$$BR = \frac{l_e}{l_a + l_e} \tag{3.1}$$

Furthermore, the ambient pressure effects on the inflow starting jet are investigated using the following pressures: 101 kPa, 6.51 kPa, and 0.670 kPa, which correspond to atmospheric pressures at sea level, edge of near space, and near space altitudes, respectively. Note that the atmospheric properties needed in this study at the given altitudes are obtained from the US Standard Atmosphere (1976).

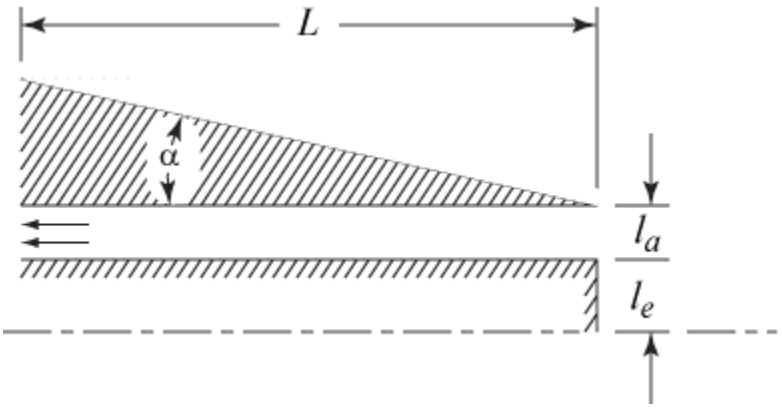

Figure 3.1. Annulus schematic.

As previously stated, the inflow air jet is limited to low Reynolds number flow, and hence, the findings of this investigation will only be applicable to laminar flow. Similar to the starting outflow jet study, a Reynolds number of 122.5 is used throughout this study. Based on the selected Reynolds number value, the jet inlet velocity V_0 is calculated from the definition of the Reynolds number, where

$$\mathrm{Re} = \frac{V_0 D}{\nu} \tag{3.2}$$

Hence, at the ambient pressures of 101, 6.51, and 0.670 kPa, the inlet velocities are 0.141, 1.31, and 14.6 m/s, respectively, due to the changes of the atmospheric viscosity. Under an ambient pressure of 0.670 kPa and its corresponding intake speed, the Mach number is 0.046, which is the highest value from all investigated conditions. Hence, since the calculated Mach number values are less than 0.3, the inflow air jet of this study can be assumed incompressible.

Numerical Model

The inflow air jet under study is analyzed using an axisymmetric, unsteady, and incompressible flow model. A commercial CFD package based on a finite volume numerical technique is utilized using a second order upwind numerical scheme. The momentum and continuity equations for the chosen model were presented during the outflow analysis (refer to Chapter 2). In addition, the numerical model was validated during the outflow study with experimental and theoretical results.

The outer contour of the mesh grid used in this study is shown in Figure 3.2. The arrow in Figure 3.2 indicates the flow direction, and the lettered side labels represent the boundary conditions of this study.

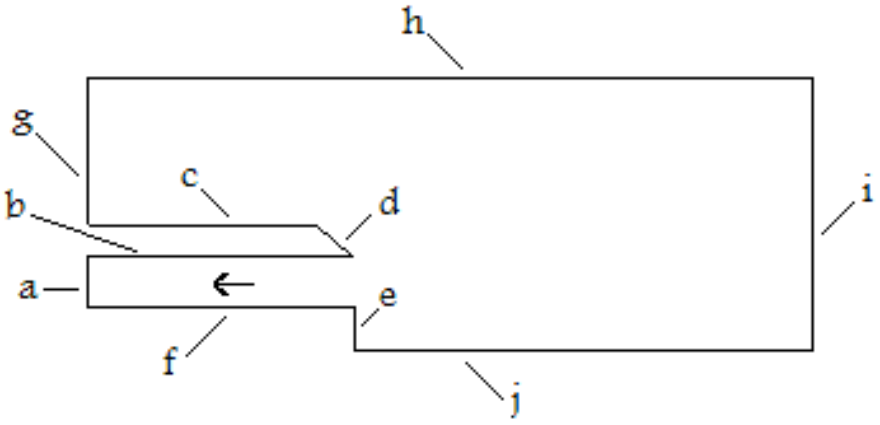

Figure 3.2. Outer contours of mesh.

Due to the flow direction, side a is treated as the exit of the annulus, which represents a velocity outlet boundary such that

$$U_R = 0 \tag{3.3}$$

$$U_X = -U_0 \tag{3.4a}$$

$$U_X = \begin{cases} -2U_0, & 0 \le T \le N/2 \\ 0, & N/2 < T \le N \end{cases} \tag{3.4b}$$

$$U_X = -U_0\left[1 - \sin\left(2\pi \cdot T/N + \pi/2\right)\right], \quad 0 \le T \le N \tag{3.4c}$$

where Eq. (3.3) and (3.4) represent the dimensionless radial and axial velocity components, respectively. Equations (3.4a)-(3.4c) respectively represent the outlet velocity (as indicated by the negative signs) for impulsive flow, unit pulsation, and sinusoidal pulsation. Furthermore, sides b through f represent a wall boundary, and sides g, h, and i represent a pressure inlet/outlet boundary. Side j represents an axial boundary. Note that the angle formed by sides b and d is the incline angle, α, described in the previous section and that the length of side e controls the blocking ratio, BR. For a blocking ratio of zero, side f is leveled with side j, and both are treated as an axial boundary.

In order to ensure that the selected model produces grid independent results with respect to space and time, an inflow sinusoidal pulsed jet with a cycle frequency of 10 Hz is tested under zero blockage and an ambient pressure condition of 101 kPa using multiple grid sizes and time steps. The target of the grid spatial and temporal convergence tests is to accurately characterize the vortex formation that occurs inside the annulus. Note that this phenomenon is discussed in detail in the following section.

Grid spatial convergence was tested using grid sizes of 15000, 34000, 60000, and 86000 cells. Relative to the 86000-cell grid size, the error in calculating the average vorticity along the

vertical axis of the generated vortex was 20%, 5%, and 0.04% using grid sizes of 15000, 34000, and 60000 cells, respectively. Hence, spatial grid convergence is achieved using a grid size of around 60000 cells. Note that the 60000-cell grid was constructed using square grids of length 0.03 cm, and thus, changes made to the overall grid to implement the various blockage ratio configurations are carried out using the same square grid dimensions.

In addition, in order to test for temporal convergence, several time steps are used to obtain the average vorticity along the vortex. Relative to the average vorticity obtained using a time step of $2.5*10^{-6}$ s, the percent difference is 9% for a time step of $2.5*10^{-4}$ s and 0.9% for a time step of $2.5*10^{-5}$ s. Hence, temporal convergence is achieved using a time step of $2.5*10^{-5}$ s, which will be using by this computational study.

Results & Discussion

Vortex Formation

In this section, vortex formation is analyzed for impulsively started, unit pulsed, and sinusoidal pulsed inflow jets. The analysis is carried out by examining both the vorticity contour plot inside the annulus and the circulation plot along the annulus entry plane. The former is used to visually indicate the vortex development, while the latter is used to compare the blocking ratio and ambient pressure effects on the inflow jet.

Impulsively Started Inflow Jet

Figure 3.3 shows the vorticity contour plots of impulsively started jets under various blockage and ambient pressure conditions at times $T = 0.86$ and $T = 2.8$, where the normalized time T is calculated by (Dabiri, 2009)

$$T = \frac{V_0 t}{D} \tag{3.5}$$

The vorticity contour plots of Figure 3.3 show no indication that impulsively started inflow jets trigger vortex formation regardless of blockage and ambient pressure. In addition, the selected times of $T = 0.86$ and $T = 2.8$ show the vorticity contour plots respectively during transient and steady state times (as evident from Figure 3.4), further indicating that impulsively started inflow jets do not trigger the formation of vortices at any given time.

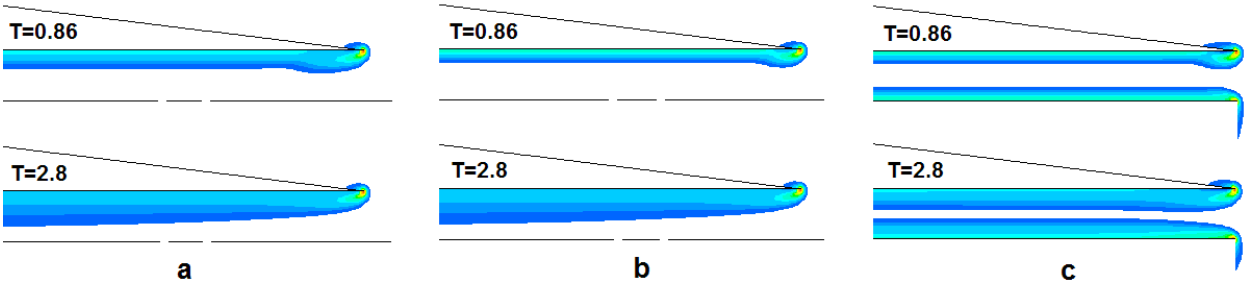

Figure 3.3. Vorticity contours of impulsive inflow jets for a) BR=0 & 101 kPa, b) BR=0 & 0.670 kPa, and c) BR=0.75 & 0.670 kPa.

Figure 3.4 shows the circulation of impulsively started jets along the annulus entry plane as a function of time, where the dimensionless circulation Γ^* is calculated by (Krueger & Gharib, 2003)

$$\Gamma^* = \frac{\Gamma}{\nu} \tag{3.6}$$

As evident from Figure 3.4, the circulation of impulsively started inflow jets undergoes a transient period following by a steady period that begins around time $T = 1$, regardless of blockage and ambient pressure conditions. Varying blockage from $BR = 0$ to $BR = 0.75$ increases the steady state circulation by about seven fold. On the other hand, decreasing the ambient pressure condition from 101 kPa to 0.670 kPa increases the steady state circulation of impulsively started jets by approximately 0.6%, indicating that ambient pressure variation has negligible effects on the circulation of impulsive inflow jets at the annulus entry cross section.

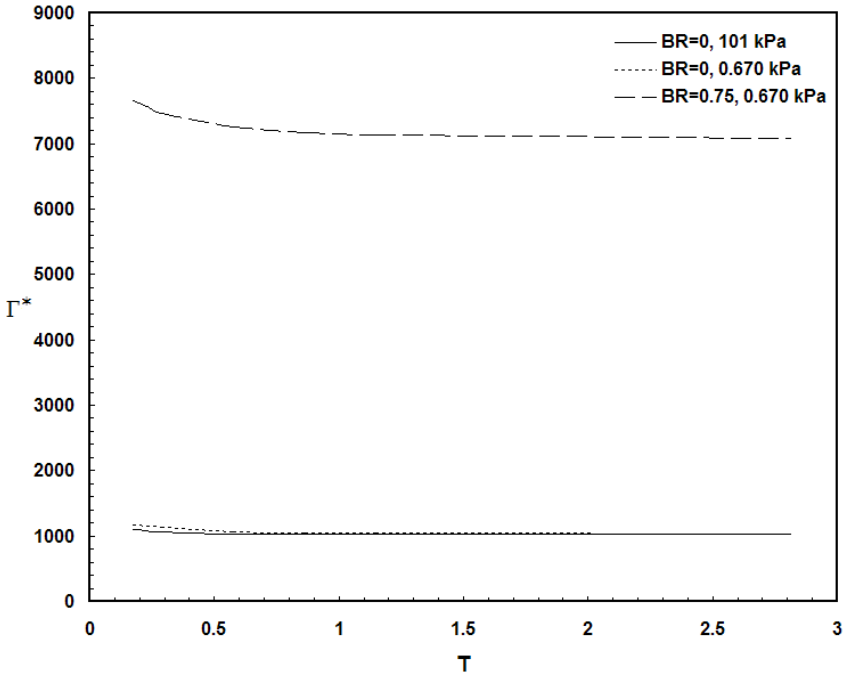

Figure 3.4. Circulation of impulsive inflow jets (calculated at the annulus entry).

Pulsed Inflow Jets

Unlike impulsively started inflow jets, pulsed inflow jets trigger the formation of vortices. Figures 3.5 and 3.6 show the vorticity contour plots of unit pulsed and sinusoidal pulsed inflow jets, respectively, at various frequencies under zero blockage and a 101 kPa ambient pressure condition. Note that the dimensionless frequency is expressed in terms of the Strouhal number St, which is defined as (Dabiri, 2009)

$$St = \frac{D\omega}{V_0} \tag{3.7}$$

As shown in both figures, vortex size is enhanced with decreasing frequency such that the vortex is localized near the annulus entry at a frequency of $St = 1.7$ but fills the inside of the annulus by a frequency of $St = 0.36$. Such phenomenon can be rationalized by the fact that prior to pulsation, the regions of high vorticity inside the annulus expand with increasing time (as shown by Figure 3.3) as the flow becomes fully developed. When pulsation is triggered, the flow

disturbance instigated by the imposed zero inflow velocity boundary causes the region of high vorticity to circulate and form a stationary vortex. Thus, if the region of high vorticity is only limited within the immediate vicinity of the annulus wall (i.e. small cycle period/high frequency), a localized vortex is formed. On the other hand, if the regions of high vorticity covers a large portion of the annulus (i.e. large cycle period/low frequency), a considerable vortex is formed.

In addition to forming a vortex inside the annulus, unit pulsed inflow jets form a secondary vortex with opposite rotation (i.e. anticlockwise) outside the annulus. The secondary vortex is triggered by the impulsive nature of unit pulsation. Note that immediately prior to pulsation, the inflow velocity of a sinusoidal pulsed jet has near zero value, and the inflow velocity of a unit pulsed jet has non-zero constant value. As a result, the flow around the edge of the annulus (i.e. the corner of the incline angle) will have low vorticity for the former and high vorticity for the latter. Hence, the subsequent flow disturbance due to pulsation is more prominent with the unit pulsed jets and causes the formation of a secondary vortex outside the annulus.

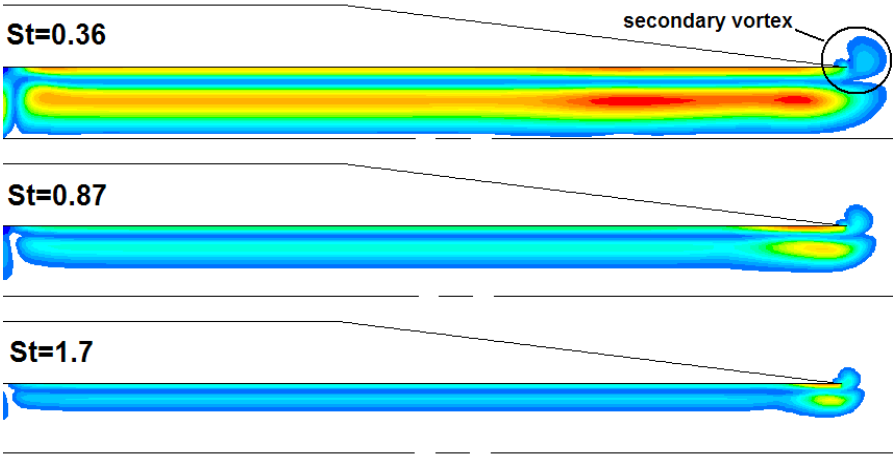

Figure 3.5. Vorticity contours of unit pulsed inflow jets (calculated at the end of one cycle).

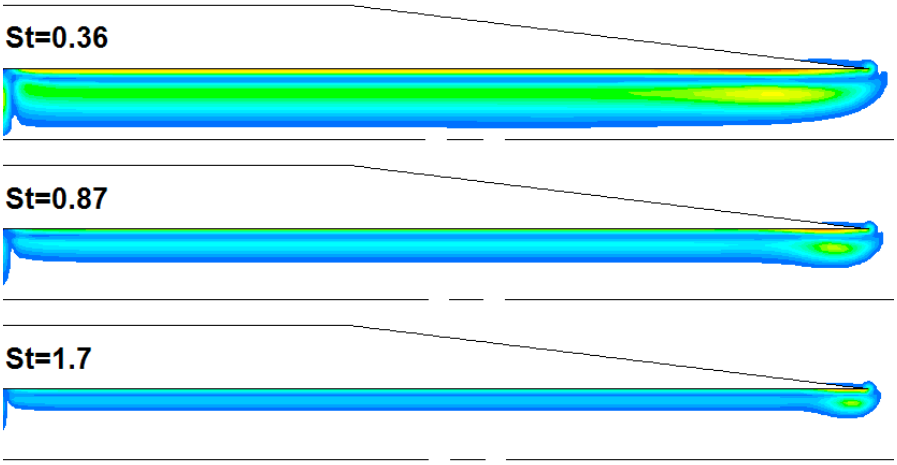

Figure 3.6. Vorticity contours of sinusoidal pulsed inflow jets (calculated at the end of one cycle).

It is important to note that unlike vortices triggered by unit pulsation, vortices triggered by sinusoidal pulsation are not just the product of the pulsatile nature of the flow but also the rolling of the shear layer. As indicated by Figure 3.3, vortex formation is not triggered by impulsive jets. Similarly, vortex formation is not triggered by unit pulsed inflow jets until pulsation takes place, i.e. when the inflow velocity is zero. On the other hand, vortex formation is triggered with sinusoidal pulsation during the presence of a jet inflow, i.e. a non-zero inflow velocity. Velocity magnitude vector plots (not shown) indicated the presence of vortex formation inside the annulus at time $T < N$, where the boundary velocity is $U_x \neq 0$. Hence, certain inflow pulsation types can cause the momentum boundary layer to roll and generate a toroidal vortex.

Figure 3.7 shows the circulation at the end of a single inflow starting jet cycle triggered by unit and sinusoidal pulsations as a function of frequency. As noted from the figure, increasing the frequency increases the circulation. Under zero blockage and a 101 kPa ambient pressure condition, the average dimensionless circulations of unit and sinusoidal pulsed inflow jets over the examined frequencies are 245 and 335, respectively. Decreasing the ambient

pressure to 0.670 kPa increases the average circulation by 170% for unit pulsed inflow jets and 83% for sinusoidal pulsed inflow jets. In addition, incorporating a blockage of $BR = 0.75$ increases the average circulation by 650% and 620% for unit pulsed and sinusoidal pulsed inflow jets, respectively.

Altogether, the reported percent increases indicate that the circulation from unit pulsation is more sensitive to ambient pressure conditions than the circulation from sinusoidal pulsation. The percent increases also indicate that variation of blockage has comparable effects on the circulation from both pulsation types.

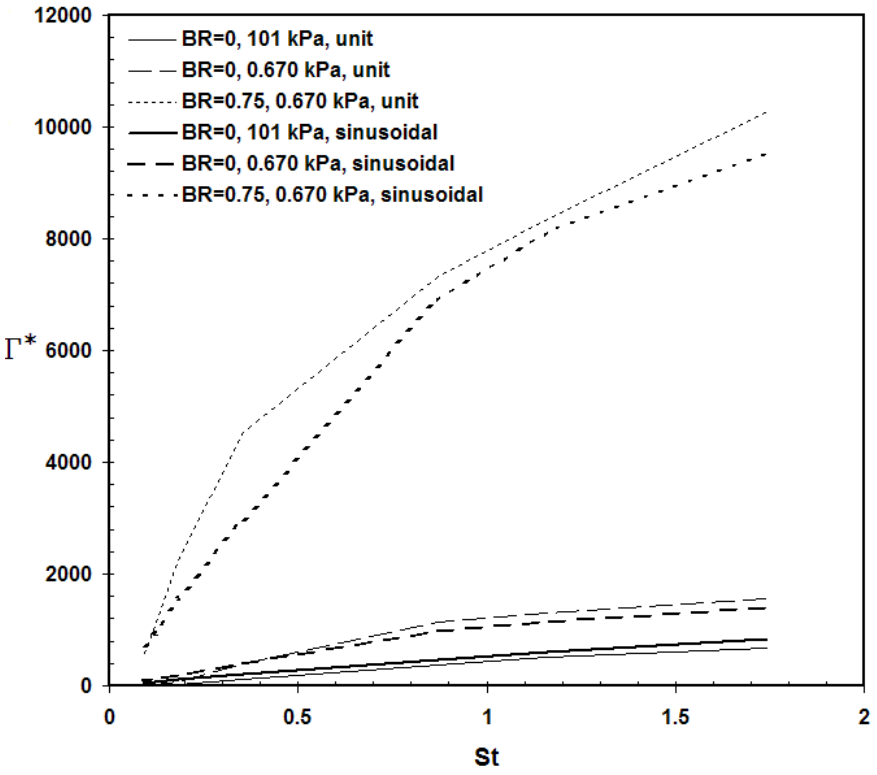

Figure 3.7. Circulation of pulsed inflow jets (calculated at the end of one cycle).

Net Force Analysis

The net force $\sum f$ generated by the jet inflow and calculated in this study at the entry of the annulus is the resultant of the momentum and pressure forces such that (Krueger & Gharib, 2003)

$$\sum f = f_{mom} + f_{pres} \tag{3.8}$$

where

$$f_{mom} = \frac{\int_{t_1}^{t_2} \int_{A} \rho u_x^2(r,\tau) \; ds d\tau}{t_2 - t_1} \tag{3.9}$$

$$f_{pres} = \frac{\int_{t_1}^{t_2} \int_{A} p(r,\tau) \; ds d\tau}{t_2 - t_1} \tag{3.10}$$

The effects of the two force components on the net force are investigated for impulsively started and pulsed inflow jets. Note that based on Eq. (3.8) and the flow configuration dictated by Figure 3.2, a positive net force behaves as a suction force pointing in the flow direction, while a negative net force behaves as a thrust force opposing the flow direction.

Impulsively Started Inflow Jet

Figure 3.8 shows the net force of the impulsively started inflow jet under various blocking ratios and ambient pressure conditions. The plots are presented in dimensionless form, where the normalized force F is calculated by (Dabiri, 2009)

$$F = \frac{f}{\rho A V_0^2} \tag{3.11}$$

As noted, the net force of the impulsively started inflow jet undergoes a transient period followed by a steady period. During the transient period, the net force points towards the outflow direction, as indicated by the negative force values, thus producing a thrust. As the time increases, the value of the force magnitude along the outflow direction decreases until it eventually points in the inflow direction, as indicated by the positive force values in Figure 3.8. Once the net force of the inflow jet begins behaving like a suction force, it immediately reaches a steady state value of approximately $F = 0.081$ under zero blockage and an ambient pressure of 101 kPa. Decreasing the ambient pressure to 6.51 kPa and 0.670 kPa changes the steady state value by 3.7% and 13%, respectively, while increasing the blocking ratio to $BR = 0.5$ and $BR = 0.75$ changes the steady state value by 6.5% and 23%, respectively. Thus, large changes to the ambient pressure and blockage can significantly affect the steady state suction force value of impulsively started jets.

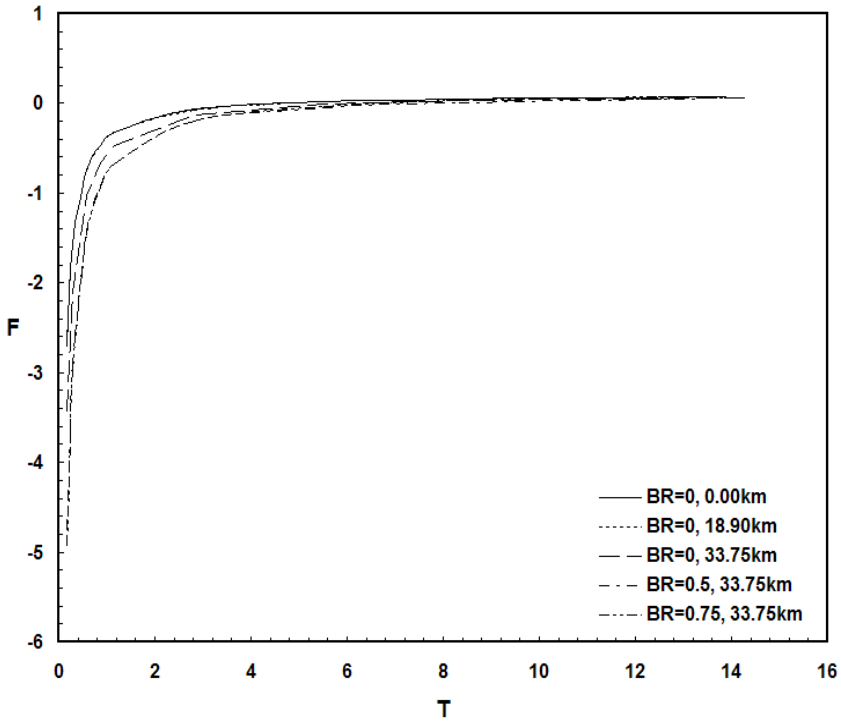

Figure 3.8. Net force of impulsive inflow jets (calculated at annulus entry).

Figure 3.9 shows the momentum and pressure components of the net force of the impulsively started inflow jets presented in Figure 3.8. The momentum component is nearly constant in magnitude and points towards the flow direction. On the other hand, the pressure component of the net force is negative (i.e. the absolute flow pressure was less than the ambient pressure), and its magnitude decreases with time until it reaches a constant value. Thus, the thrust output of the impulsively started inflow jet during the transient period (as noted in Figure 3.8) is due to the initial large pressure force drop of the flow, which is not countered in magnitude by the momentum force, causing the net force to point in the opposite direction of the flow. Furthermore, during the steady period, the pressure force nearly offsets the momentum force, causing a steady insignificant net force in the flow direction.

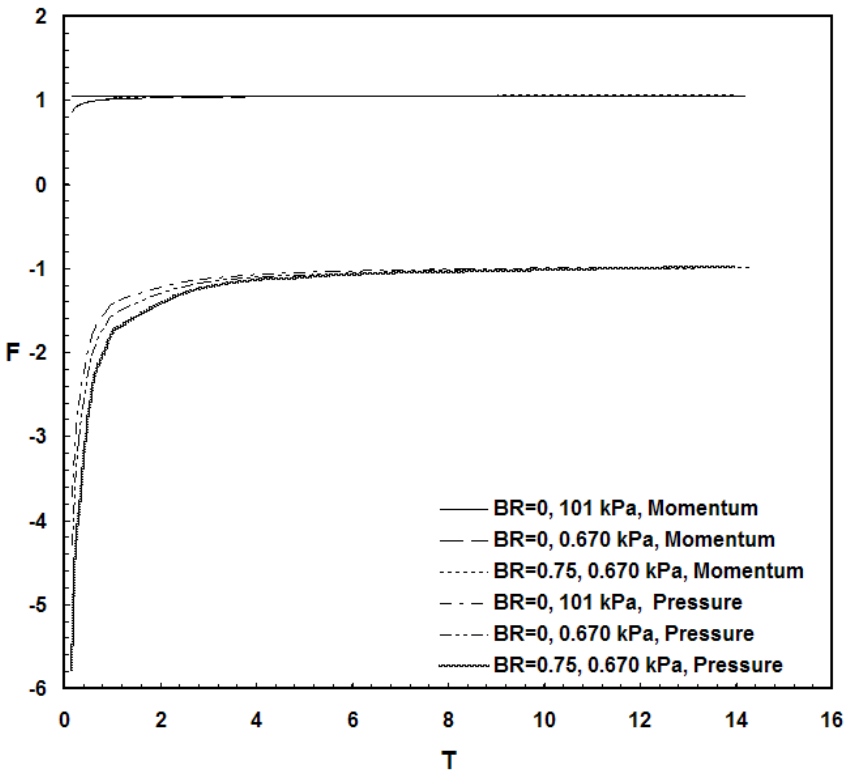

Figure 3.9. Force components of impulsive inflow jets (calculated at annulus entry).

Pulsed Inflow Jets

Since unit pulsed inflow jets prior to pulsation behave as impulsively started inflow jets, which have been discussed in the previous section, this section will only examine the sinusoidal pulsed inflow jets for the net force analysis. Figure 3.10 shows the dimensionless net force as a function of the dimensionless frequency for sinusoidal pulsed inflow jets at the annulus entry. At low frequencies, a net suction force is produced at the entry. The force plots have a negative rate of change with respect to frequency. Hence, with increasing frequency, the net force becomes a weaker suction force until it eventually turns into a thrust force. Note that for an inflow jet, a net thrust force occurs when the force component due to a vacuum pressure (i.e. a flow pressure less than the ambient pressure) is greater than the force component due to the momentum of the jet inflow. Hence, the force component due to a vacuum pressure can be thought of as a reaction force that opposes the force component due to momentum.

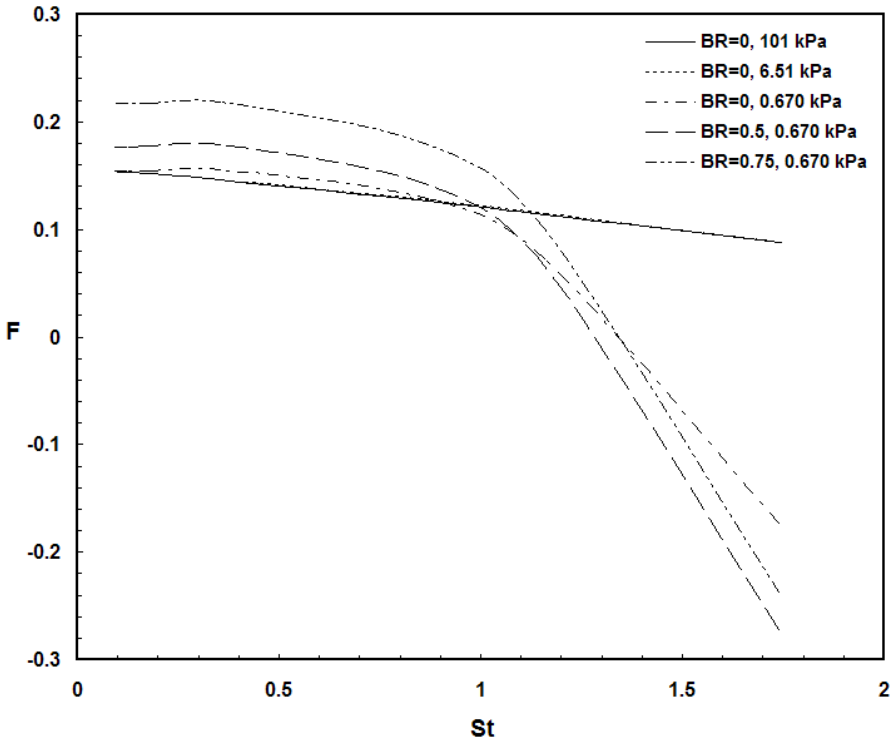

Figure 3.10. Net force of sinusoidal pulsed inflow jets (negative sign indicates thrust behavior).

The behavior of the net force plots from Figure 3.10 can be explained by the momentum and pressure forces components of Figure 3.11. As shown, the momentum force components of the sinusoidal pulsed inflow jets behave as a suction force of nearly steady values with respect to frequency. Furthermore, the dimensionless suction forces have values greater than one (i.e. $F > 1$), which indicates that suction at the annulus entry is augmented relative to the suction imposed by the velocity inflow boundary. Such force augmentation was previously noted experimentally by Krueger and Gharib (2005) and numerically in Chapter 2 for outflow pulsed jets. The reason for the pulsed inflow force augmentation of this study is that the generated toroidal vortex partially blocks the annulus entry to the incoming flow, which effectively causes the flow velocity to increase in accordance with the conservation of mass for an incompressible fluid. As a result, the average momentum force at the annulus entry over a given cyclic period is augmented for pulsed inflow jets. Note that when vortex formation is absent (as in the case with impulsively started inflow jets), the dimensionless momentum force is $F = 1$ (refer to Figure 3.9).

In addition, Figure 3.11 shows the effects of the ambient pressure and blockage on the momentum force component. For example, under zero blockage and an ambient pressure condition of 101 kPa, the average momentum force components for sinusoidal pulsed inflow jets over the examined frequencies is $F = 1.6$. Decreasing the ambient pressure to 0.670 kPa increases the average momentum force by 0.79%. Similarly, incorporating a blockage of $BR = 0.75$ increases the average momentum force by 1.2%. Thus, ambient pressure and blockage have insignificant effects on the momentum force component of sinusoidal pulsed inflow jets.

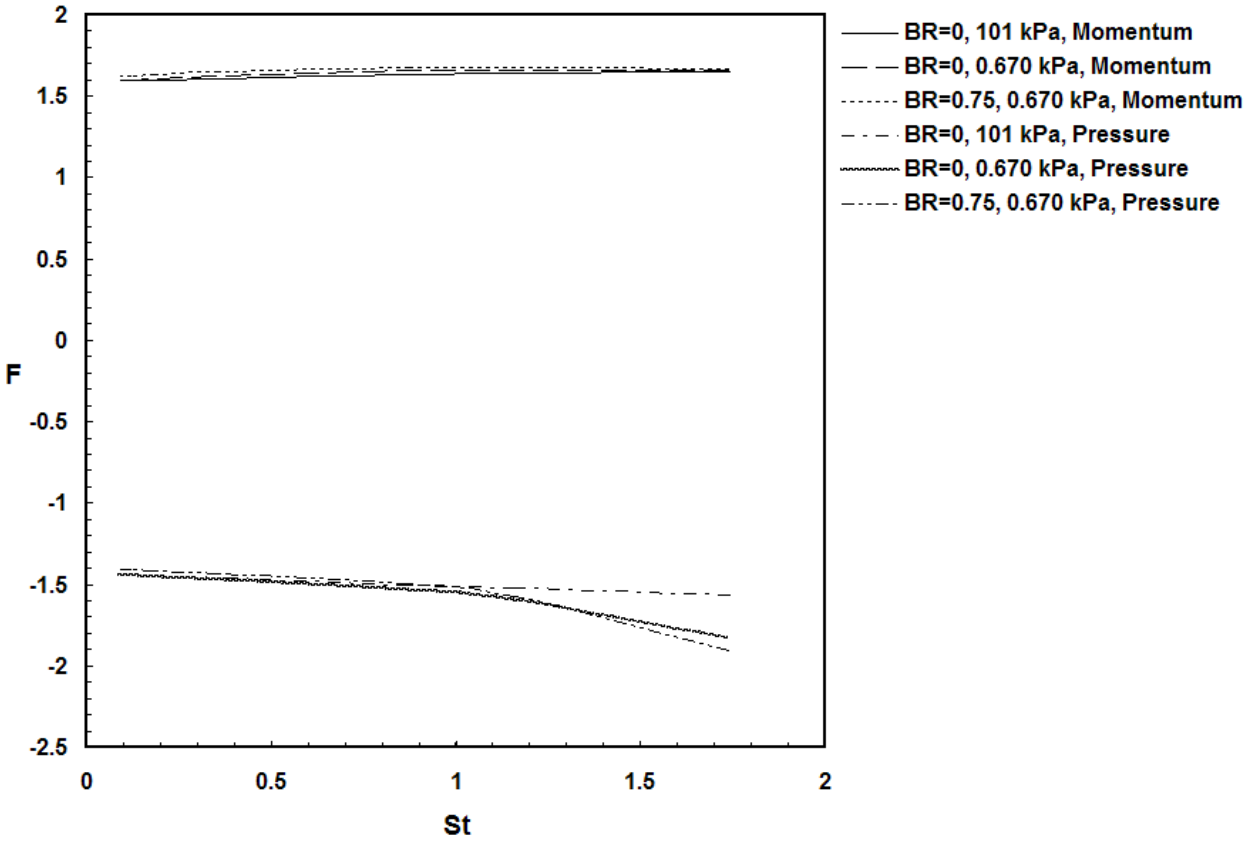

Figure 3.11. Force components of sinusoidal pulsed inflow jets (negative sign indicates thrust behavior).

Figure 3.11 also shows the pressure force components of Figure 3.10 for sinusoidal pulsed inflow jets. The pressure force components have negative signs, indicating that they act as a thrust force. Under zero blockage and an ambient condition of 101 kPa, the thrust delivered by the pressure force components increases with increasing frequency and have an average of $F = 1.5$. Decreasing the ambient pressure to 0.670 kPa increases the pressure thrust component by 3.6% for sinusoidal pulsed inflow jets. On the other hand, incorporating a blockage of $BR = 0.75$ decreases the average pressure thrust by 1.2%. Thus, the pressure force component of sinusoidal pulsed inflow jets is not significantly affected by blockage.

Efficiency Analysis

The efficiency analysis of this section is based on the potential work that can be produced by the vortex circulation of inflow starting jets at a given time. Since steady inflow jets do not trigger vortex formation, the analysis is limited to pulsating inflow jets. The efficiency is calculated at the end of a pulsating inflow cycle with dimensionless time period N such that

$$\eta = \left.\frac{\Delta ke}{ke}\right|_N \tag{3.12}$$

where both ke and Δke respectively represent the total axial kinetic energy of the inflow jet and the change of the axial kinetic energy calculated over a specified amount of time. Hence, Δke is determined between times $T = N$ and $T = N + dT$, where $dT = 0.028$ is used throughout the analysis and corresponds to the temporal convergence time step (i.e. 0.000025 s) for an ambient pressure of 0.670 kPa.

Figure 3.12 shows the efficiency plots of inflow jets triggered by unit and sinusoidal pulsation as a function of the dimensionless frequency. From observation, the efficiency generally increases with increasing frequency. Furthermore, Figure 3.12 shows that sinusoidal pulsation produces more efficient inflow jets (at an increasing rate with increasing frequency) than unit pulsation. Under zero blockage and a 101 kPa ambient pressure condition, the average efficiency over the examined frequencies is 6.2% for unit pulsed and 9.6% for sinusoidal pulsed inflow jets. The lower efficiency of unit pulsation relative to sinusoidal pulsation can be attributed to the fact that for unit pulsed inflow jets, a portion of the potential work from the circulation of the primary vortex is countered with the potential work from the circulation of the secondary vortex because both vortices rotate in opposite directions.

Figure 3.12 also shows that decreasing the ambient pressure and incorporating blockage improves the average efficiency. Decreasing the ambient pressure to 0.670 kPa increases the

average efficiency by 13% for unit pulsed and 10% for sinusoidal pulsed inflow jets. In addition, incorporating a blockage of $BR = 0.75$ enhances the average efficiency of the unit pulsed inflow jet by 11% and the sinusoidal pulsed inflow jet by 9.9%.

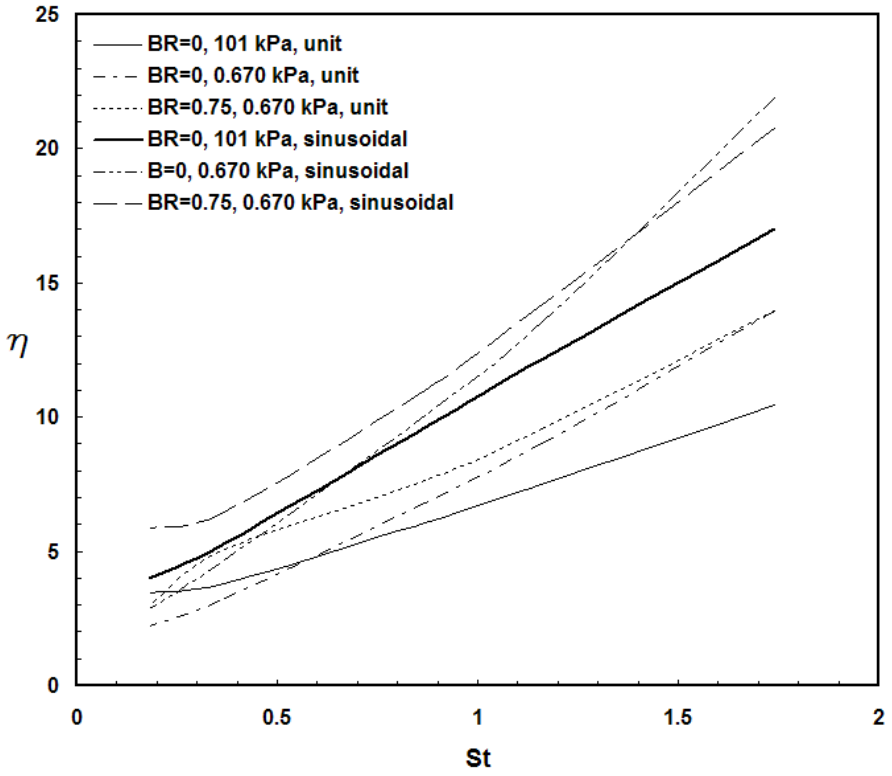

Figure 3.12. Efficiency of pulsed inflow jets.

Conclusion

In this computational study, low Reynolds number impulsively started annular jet inflows were investigated using impulsively started, unit pulsed, and sinusoidal pulsed velocity boundary conditions. The jet performance was assessed based on the jet vortex formation, the net force generated by the jets at the annulus entry, and the efficiency of the jets. The jets were also analyzed using several blocking ratios to examine the effects of the annulus blockage on the jet performance. In addition, the jets were studies under multiple ambient pressures to examine the effects of environmental conditions on the jet performance. The main findings of this study are listed as follows.

1. Impulsively started inflow jets did not trigger vortex formation, regardless of blockage and ambient pressure. On the other hand, unit pulsed and sinusoidal pulsed inflow jets triggered the formation of a standing vortex inside the annulus. The resulting vortex increased in size and decreased in circulation with decreasing frequency. In addition, unit pulsed inflow jets triggered the formation of a secondary vortex outside the annulus. The secondary vortex rotated counterclockwise, i.e. opposing the primary vortex.

2. The resultant forces due to momentum and pressure at the annulus entry are approximately zero ($F = 0.081$) at steady state for impulsively started inflow jets. Unit pulsed inflow jets, on the other hand, provided a suction force that increased in magnitude with increasing frequency, while sinusoidal pulsed inflow jets initially (i.e. at low frequencies) provided a suction force that decreased in magnitude with increasing frequency until it turned into a thrust force. Note that the jet inflow causes the pressure of the fluid at the annulus entry to drop below the ambient pressure. As a result, this vacuum pressure causes the pressure component of the net force at the annulus entry to behave as a reaction force that opposes the momentum force component, where the latter behaves as suction force. Thus, when the pressure force component is larger than the momentum force component, the net force behaves as a thrust force.

3. The behavior of the force plots of the sinusoidal pulsed inflow jets followed the same pattern as their pressure force components. Note that the momentum force component of the sinusoidal pulsed inflow jet had a near constant dimensionless force values that was greater than one, indicating the presence of a force augmentation (relative to the inflow velocity boundary) caused by the increased velocity at the annulus entry due to the partial blockage of the entry by the generated vortex.

4. The efficiency of pulsed inflow jets increased with increasing frequency because of the circulation increase of the generated vortices with increasing frequency. Furthermore, sinusoidal pulsed jets had a higher efficiency than unit pulsed jets, which is caused by the circulation offset of the opposing primary and secondary vortices triggered by unit pulsation.

5. Incorporating blockage and decreasing the ambient pressure generally enhanced the circulation, force magnitude, and propulsive efficiency of the all inflow examined inflow jet types. Additional study is needed to draw general conclusions regarding this behavior.

Acknowledgements

The authors would like to thank the U.S. Department of Education for its support through the Graduate Assistance in Areas of National Need (GAANN) Fellowship.

References

Bartol, I.K., Krueger, P.S., Stewart, W.J., & Thompson, J.T. (2009). Pulsed jet dynamics of squid hatchlings at intermediate Reynolds numbers. *Journal of Experimental Biology*, 212, 1506-1518.

Bishop, K.L., Wainwright, P.C., & Holzman, R. (2008). Anterior-to-posterior wave of buccal expansion in suction feeding fishes is critical for optimizing fluid flow velocity profile. *Journal of the Royal Society Interface*, 5, 1309-1316.

Dabiri, J. (2009). Optimal vortex formation as a unifying principle in biological propulsion. *Annual Review of Fluid Mechanics*, 41, 17-33.

Dabiri, J., Colin, S., Costello, J., & Gharib, M. (2005). Flow patterns generated by oblate medusan jellyfish: field measurements and laboratory analyses. *Journal of Experimental Biology*, 208, 1257-1265.

Dabiri, J., & Gharib, M. (2005). The role of optimal Vortex formation in biological fluid transport. *Proceedings of the Royal Society B*, 272, 1557-1560.

Gharib, M., Rambod, E., & Shariff, K. (1998). A universal time scale for vortex ring formation. *Journal of Fluid Mechanics*, 360, 121-140.

Joshi, A., & Schreiber, W. (2006). A experimental examination of an impulsively started incompressible turbulent jet. *Experiments in Fluids*, 40, 156-160.

Krueger, P., & Gharib, M. (2003). The significance of vortex ring formation to the impulse and thrust of a starting jet. *Physics of Fluids*, 15(5), 1271-1281.

Krueger, P., & Gharib, M. (2005). Thrust augmentation and vortex ring evolution in a fully pulsed jet. *AIAA Journal*, 43(4), 792-801.

Lauder, G.V. (1980). The suction feeding mechanism in sunfishes (Lepomis): an experimental analysis. *Journal of Experimental Biology*, 88, 49-72.

Muller, M., Osse, J.W., & Verhagen, J.H. (1982). A quantitative hydrodynamical model of suction feeding in fish. *Journal of Theoretical Biology*, 95, 49-79.

Satti, R.P., & Agrawal, A.K. (2008). Computational study of buoyancy effects in a laminar starting jet. *International Journal of Heat and Fluid Flow*, 29, 527-539.

Seno, T., Kageyama, S., & Ito, R. (1988). A modeling of vortex rings in an axisymmetric pulsed jet. *Journal of Chemical Engineering of Japan*, 21(1), 1-5.

Syed, A.H., & Sung, H.J. (2009). Propagation of orifice- and nozzle-generated vortex rings in air. *Journal of Visualization*, 12(2), 139-156.

U.S. Standard Atmosphere. (1976). Washington, DC: U.S. Government Printing Office.

Uyttendaele, M.A., & Shambaugh, R.L. (1989). The flow field of annular jets at moderate Reynolds numbers. *Industrial & Engineering Chemistry Research*, 28(11), 1735-1740.

Van Wassenbergh, S., & Aerts, P. (2009). Aquatic suction feeding dynamics: insights from computational modeling. *Journal of the Royal Society Interface*, 6, 149-158.

CHAPTER 4

COMPUTATIONAL INVESTIGATION INTO THE STRUCTURE OF FULLY OSCILLATING ANNULAR JETS[*]

Abstract

A computational study was carried out on low Reynolds number fully oscillating annular jets, where the term fully oscillating is used to describe an inflow stroke followed by an outflow stroke. The study was implemented using an unsteady, incompressible and laminar axisymmetric CFD flow model. Using the numerical model, the investigation examined the effects of the pulsation type (i.e. imposed velocity boundary), entrance geometry of the annulus, and ambient pressure on the fully oscillating jets. The jet performance was analyzed by examining the vortex formation behavior, thrust output, and propulsive efficiency. Among the major findings was that thrust augmentation was noted to occur as a direct effect of the vortex formation triggered by the fully oscillating pulsed jets. In addition, the choice of pulsation was noted to affect the performance of the jet such that sinusoidal pulsation out performed unit pulsation in enhancing the thrust output and propulsive efficiency of fully oscillating jets.

[*] Note. This chapter is based on "Computational Investigation into the Structure of Fully Oscillating Annular Jets," by E. Abdel-Raouf, J. Baker, and M. Sharif, submitted to *Theoretical and Computational Fluid Dynamics* on 2/4/2011.

Introduction

This study is a computational investigation on low Reynold's number pulsating staring annular jets. The purpose of this endeavor is to examine the effects of the imposed velocity boundary, the annulus entry geometry, and the ambient pressure conditions on the vortex formation, thrust, and propulsive efficiency of the annular jets. Note that vortex formation is a characteristic phenomenon of starting jets. Recent studies (Gharib et al., 1998; Rosenfeld et al., 1998; Mohseni & Gharib, 1998) have respectively proved experimentally, numerically, and theoretically that the vortices generated from the ensuing jet of a piston/cylinder device can be optimized under what was named the vortex 'formation number,' which is equivalent to the piston stroke to diameter ratio. Beyond the vortex 'formation number,' the vortex is said to 'pinch-off' such that is no longer entrains circulation or energy. Further studies by Dabiri and Gharib (2005) and Linden and Turner (2004) related the vortex formation number to the propulsion mechanism used by numerous marine life.

The starting jet, which is characteristic of many propulsion systems including that of fish propulsion, was examined in Chapter 2. Among the major findings was that the vortex development was fastest for unit pulsed jets, followed by sinusoidal pulsed jets and then impulsively started jets. The vortex 'formation number' was also not affected by changes in blockage and ambient pressure. In addition, the triggering of vortex formation enhanced the thrust output of the jets by augmenting the thrust at the annulus exit plane relative to the thrust at the imposed velocity inlet boundary. Note that thrust augmentation had been previously reported experimentally (Krueger & Gharib, 2005) using sinusoidal pulsed jets. The work done by the vortices was also used to calculate the propulsive efficiency of the jets, where the maximum

efficiency of unit and sinusoidal pulsed jets occurred in the frequency range of $St = 0.15$ and $St = 0.35$ (where the Strouhal number, St, will be defined in the Results Section).

The inflow jet, which is not a mechanism commonly used by propulsion systems but does have an applicable use with biological marine suction feeding, was studied in Chapter 3. The results showed that impulsively started inflow jets did not trigger the formation of vortices, while both unit and sinusoidal pulsed inflow jets triggered standing vortices whose circulation increased with increasing frequency. Another major results was that impulsively started jets produced a near zero suction force (i.e. a force oriented towards the inflow direction), while unit pulsed jets produced a suction force that increasing with increasing frequency. Sinusoidal pulsed jets, on the other hand, produced a suction force that decreased with increasing frequency until eventually becoming a thrust force. In addition, sinusoidal pulsed jets were noted to have a higher efficiency that unit pulsed jets.

This study will examine fully oscillating starting jets, which incorporates an inflow jet stroke followed by an outflow jet stroke. Such oscillating jet flow mechanism is the method of propulsion utilized by squids and jellyfish. According to Anderson and DeMont (2000), squids propel themselves by filling their mantle cavity with sea water and then pressurizing the water by contracting their mantel walls. The water is then jetted through a funnel-like body organ, creating the propulsive force. Similarly, according to DeMont and Gosline (1998), a jellyfish propels itself by contracting its bell, which forces the water in the bell cavity through the velum and creates a thrust. Water then refills the bell cavity when the bell recoils.

Problem Description

This study numerically investigates fully oscillating impulsively started air jets through an annulus that is shown by the Figure 4.1 schematic. The annulus has a hydraulic diameter of

$D = 1.27$ cm, a length of $L = 6.125D$, and a tip angle of $\alpha = 7^{\circ}$, which are the same dimensions used by Krueger and Gharib (2003). The effects of pulsation type on the performance of the fully oscillating starting jets are examined by using unit and sinusoidal velocity imposed flow boundaries that are functions of cycle frequency. For each tested frequency, a single fully oscillating cycle is considered, where the cycle consists of an inflow stroke followed by an outflow stroke. Note that both strokes have equal durations. During the two strokes, the average Reynolds number used in this study is 122.5. With the given annulus dimensions, this Reynolds number is the maximum value that guarantees fully developed flow based on the hydrodynamic length for internal laminar flow, which is defined as (Langhaar, 1942)

$$\frac{L}{D} \approx 0.05\,\mathrm{Re} \tag{4.1}$$

where

$$\mathrm{Re} = \frac{V_o D}{\nu} \tag{4.2}$$

The effects of the annulus entry geometry on fully oscillating jets are investigated by varying the blocking ratio, BR, to the values of 0, 0.5, and 0.75. In addition, the environmental effects are examined by varying the ambient pressure to 101 kPa, 6.51 kPa, and 0.670 kPa, which correspond to atmospheric pressures of approximately 1.00, 0.0642, and 0.00661, respectively. Note that the selected Reynolds number and the specified ambient pressures produce jets with Mach number well below 0.3, which indicated that the flow is incompressible.

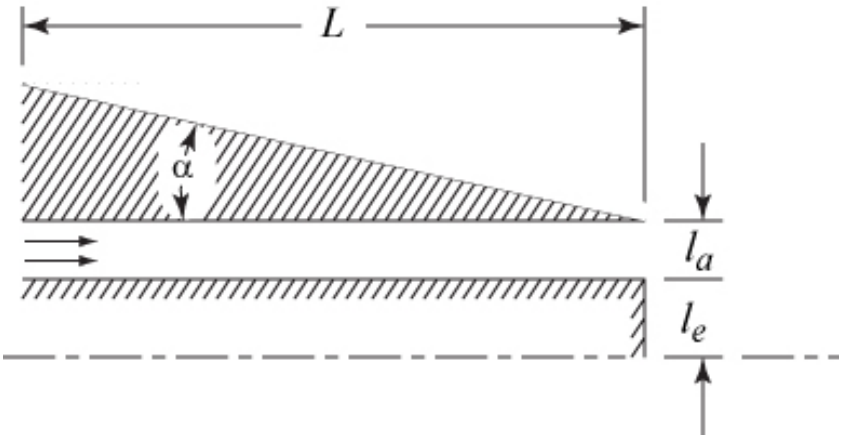

Figure 4.1. Annulus schematic.

Numerical Model

Formulation

The computational study is carried out using the axisymmetric laminar, incompressible Navier Stokes equations and implemented with a commercial CFD package that utilizes a finite volume numerical scheme (Rosenfeld, 1998). The outer contours of the mesh used by the model are shown in Figure 4.2. The two numbered arrows indicate the order of the flow directions, which respectively represents the inflow and outflow strokes for a single cycle fully oscillating jet. In addition, the labeled sides represent the boundary conditions. Side a represents the fully oscillating velocity imposed boundary such that

$$U_R = 0 \tag{4.3}$$

$$U_X = \begin{cases} -U_0, & 0 \le T \le N/2 \\ U_0, & N/2 < T \le N \end{cases} \tag{4.4a}$$

$$U_X = -\frac{\pi}{2} U_0 \sin(2\pi \cdot T/N), \qquad 0 \le T \le N \tag{4.4b}$$

where Eq. (4.3) and (4.4) respectively represent the radial and axial velocities in dimensionless form. Equations (4a) and (4b) represent the axial boundary velocities for unit and sinusoidal oscillations, respectively. Note that U_0 is the dimensionless form of velocity V_0 from Eq. (4.2)

and that the average velocity for both the unit and sinusoidal fully oscillating cycles is U_0 (or effectively V_0 in dimensional form). In addition, sides b, c, d, and f represent wall boundaries, while sides g, h, and i represent pressure input/output boundaries. Side j represents an axial boundary. Note that for zero blockage, i.e. $BR = 0$, sides f and j are lined-up and represent an axial boundary.

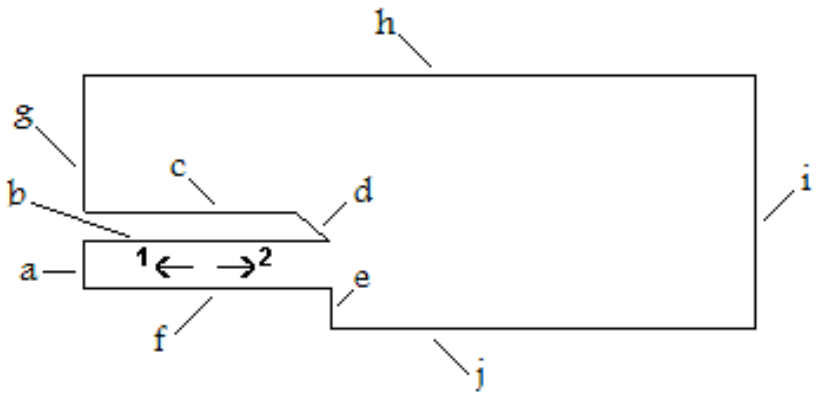

Figure 4.2. Outer contour of numerical mesh.

Verification and Validation

The computational model is verified by testing for grid spatial and temporal convergence on a fully oscillating sinusoidal started jet with a cycle frequency of 10 Hz under zero blockage and an ambient pressure of 101 kPa. As will later be shown in the results, fully oscillating jets triggers the formation of vortices outside the annulus at the end of a pulsed cycle. Thus, the convergence criteria target the vortex formation.

To test for spatial convergence, various grid sizes are generated using the same outer dimensions of 0.07 m and 0.2 m along the radial and axial directions, respectively, and a single time step of 0.00025 s. Relative to a grid size of 180000 cells, the errors obtained in calculating the average vorticity along the horizontal axis of the generated vortex are 13%, 3%, 0.6%, and 0.3% using grid sizes of approximately 40000 cells, 70000 cells, 110000 cells, and 160000 cells,

respectively. Hence, grid spatial convergence is achieved using a grid size of 160000 cells, which were meshed using 0.03 cm x 0.03 cm square grids. These cell dimensions are employed for the rest of the blocking ratio configurations to ensure spatial convergence.

Furthermore, temporal convergence is checked by solving the same problem with several time steps of different orders of magnitude. Relative to a time step of $2.5*10^{-6}$ s, the errors obtained in determining the average vorticity are 58%, 1.7%, and 0.26% using time steps of $2.5*10^{-3}$ s, $2.5*10^{-4}$ s, and $2.5*10^{-5}$ s, respectively. Hence, a time step of $2.5*10^{-5}$ s is used throughout the study to ensure temporal convergence.

In addition, the numerical model of this study was previously validated by the numerical model of Abdel-Raouf et al. (2010) against experimental (Obot et al., 1986) and theoretical (Uyttendaele & Shambaugh, 1989) results, as shown in Figure 4.3 for an outflow starting jet in the fully developed velocity region. The figure shows (in dimensionless form) the axial velocity as a function of the radial position at a specified axial position. As observed, the numerical results are bounded by the experimental and theoretical results, indicating the validity of the numerical model.

Results & Discussion

Vortex Formation

In this section, the vortex generation triggered by fully oscillating unit and sinusoidal pulsed starting jets are studied by analyzing their entrainment capabilities, development, and structure under various blockage and ambient pressure conditions. The vortex entrainment is determined by examining the behavior of the vortex circulation at the annulus exit plane, while the vortex development is studied by the examining the vorticity contour plots. The vorticity is also used to examine the vortex structure.

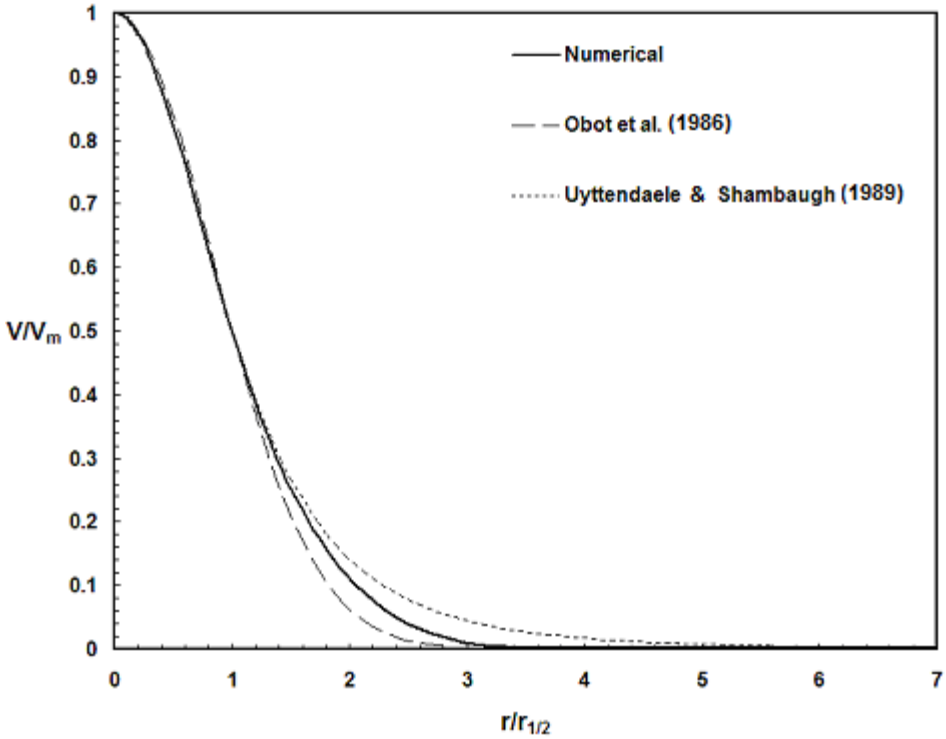

Figure 4.3. Numerical results validation (Abdel-Raouf et al., 2010).

Vortex Entrainment

Figures 4.4 and 4.5 respectively show the vortex circulation at the annulus exit plane as a function of frequency for unit and sinusoidal pulsations. The two figures are presented in dimensionless form, where the dimensionless circulation Γ^* is calculated by (Krueger & Gharib, 2003)

$$\Gamma^* = \frac{\Gamma}{\nu} \tag{4.5}$$

and the dimensionless frequency is defined in terms of the Strouhal number St such that (Dabiri, 2009)

$$St = \frac{D \cdot \omega}{V_0} \tag{4.6}$$

The plots from both figures have opposite behaviors. The circulation from the fully oscillating unit pulsed jets decreases to a minimum and then increases with increasing frequency, as shown

in Figure 4.4. On the other hand, the circulation form the fully oscillating sinusoidal pulsed jets increase to a maximum and then decrease with increasing frequency, as shown in Figure 4.5. The reason for this behavior will be explained in the following section.

Under zero blockage and an ambient pressure of 101 kPa, the average dimensionless circulations of the unit and sinusoidal pulsed fully oscillating jets are respectively $\Gamma^* = 550$ and $\Gamma^* = 540$, indicating that vortices generated by unit pulsation have similar entrainment capabilities to the ones generated by sinusoidal pulsation. Decreasing the ambient pressure to 6.51 kPa nad 0.670 kPa respectively increases the average circulation by 3.0% and 28% for unit pulsed jets and 0.92% and 0.35% for sinusoidal pulsed jets. Such average percent increases of circulation suggest that the vortex entrainment from sinusoidal pulsed fully oscillating jets are not as sensitive to ambient pressure changes as unit pulsed fully oscillating jets. In addition, incorporating blockage to blocking ratio values of $BR = 0.5$ and $BR = 0.75$ increases respectively increases the average circulation by 210% and 610% for unit pulsed jets and 200% and 590% for sinusoidal pulsed jets, which indicates that the entrainment causes by the vortex formation from both pulsation types are nearly as sensitive to entry geometry variations.

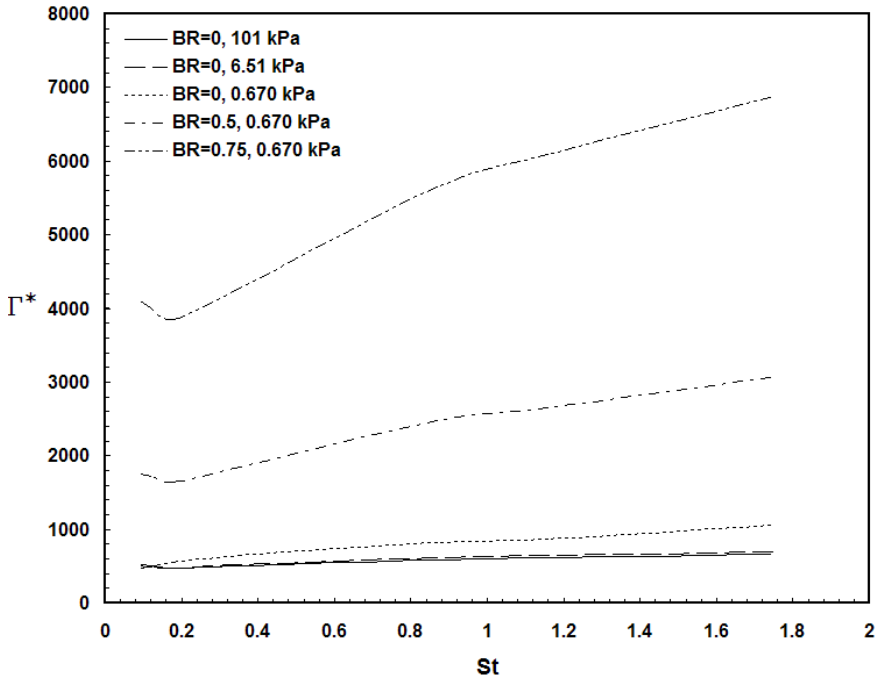

Figure 4.4. Vortex circulation of fully oscillating unit pulsed jets.

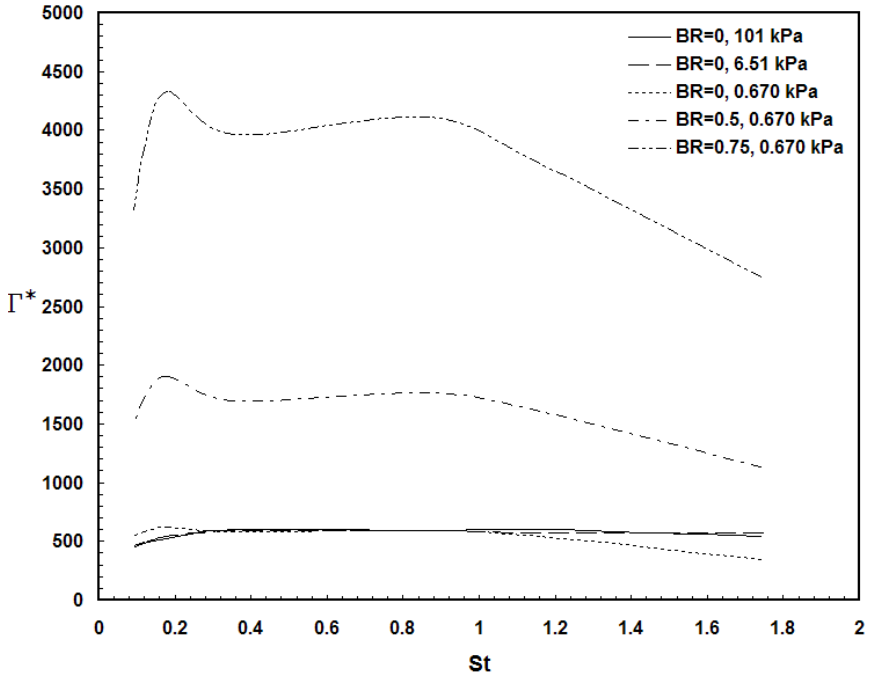

Figure 4.5. Vortex circulation of fully oscillating sinusoidal pulsed jets.

Vortex Development

Complimenting the circulation plots of Figure 4.4 and 4.5, Figures 4.6 and 4.7 respectively show the vorticity contour plots of fully oscillating unit and sinusoidal pulsed jets at the end of a single cycle under zero blockage and an ambient pressure of 101 kPa. An apparent similarity between the two figures is that the leading edge vortex grows in size and travels farther away from the annulus exit plane with decreasing frequency. Such behavior can be rationalized by the fact that lower frequencies mean higher cycle periods and hence more time for vortex growth and movement. A noted difference between Figures 4.6 and 4.7, on the other hand, is that the plots produced by sinusoidal pulsations indicate that a region of backflow exists near the edge of the incline angle, as shown by Figure 4.7. Since fluid flow moves in the direction of high energy to low energy, the higher velocity outside the annulus (caused by the vortex entrainment) relative to the lower velocity inside the annulus (at the end of a sinusoidal pulsed cycle) induces the backflow. Such behavior is not noted for unit pulsed jets, where the velocity remains constant for each inflow and outflow stroke.

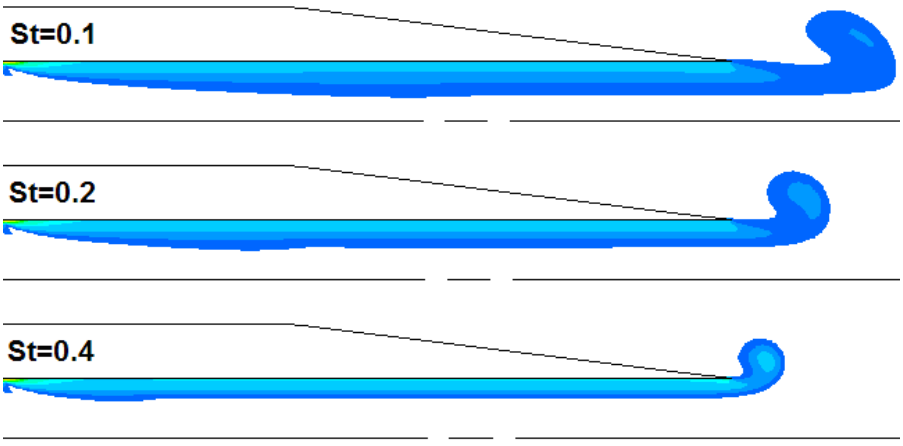

Figure 4.6. Vorticity contours of fully oscillating unit pulsed jets.

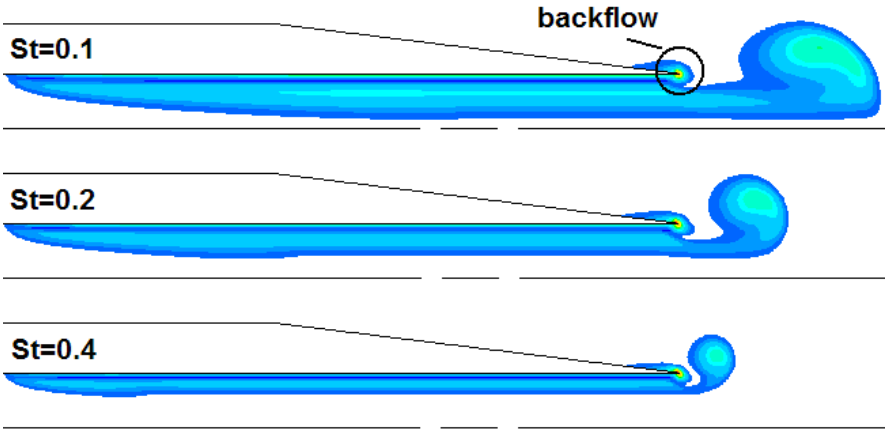

Figure 4.7. Vorticity contours of fully oscillating sinusoidal pulsed jets.

Furthermore, the two noted observations regarding vortex movement/growth, (pertaining to unit and sinusoidal pulsations) and backflow (pertaining only to sinusoidal pulsation) explain the behavior of the circulation plots of Figures 4.4 and 4.5. As previously mentioned with the explanation of Figure 4.4, the circulation from the fully oscillating unit pulsed jets initially decreases to a minimum and then increases with increasing frequency. In light of the observation regarding the increase in vortex movement and growth with increasing frequency, the fact that the circulation at the annulus generally increases with increasing frequency indicates that circulation (and hence entrainment in general) is dominated by vortex displacement rather than size. Thus, for fully oscillating unit pulsed jets, a generated vortex that is localized but close to the annulus exit plane has a higher entrainment capability at the annulus than a developed vortex that has traveled farther away. Note that at the low frequency value (i.e. large vortex size and displacement) corresponding to the minimum circulation (and hence entrainment) in Figure 4.4, the effects of vortex size and displacement are equally balanced.

In addition to the vortex displacement, fluid backflow into the annulus affects the circulation at the annulus exit plane for fully oscillating sinusoidal jet. Since the entrainment

capabilities increase with increasing frequency, the velocity outside the annulus that is induced due to entrainment also increases, which in turn enhances the backflow. Such increase in backflow with increasing frequency is evident from the thinning of the vorticity region between the vortex and its trailing jet, as shown in Figure 4.7. In addition, the effects of the backflow on entrainment are evident from the circulation plots of Figure 4.5, where the circulation from the fully oscillating sinusoidal pulsed jets increase to a maximum and then decrease with increasing frequency. Instead of obtaining an increase in circulation at higher frequencies as is the case with unit pulsation, the circulation from sinusoidal pulsation decreases because of backflow. Hence, backflow hinders the vortex entrainment in fully oscillating sinusoidal pulsed jets.

Vortex Structure

The structure of the generated vortices triggered by fully oscillating unit and sinusoidal pulsed jets is examined in this section. Figure 4.8 shows the vorticity distribution along the horizontal central plane of the leading vortex from the two pulsation modes at various blockage and ambient pressure conditions at the end of a fully oscillating cycle with frequency $St = 1.7$. The plots present the vorticity Ω in dimensionless form such that (Yehoshua & Seifert, 2006)

$$\Omega^* = \frac{\Omega D}{V_0} \tag{4.7}$$

The vorticity distribution of both pulsation modes is quite similar in shape, which indicates that the vortices of fully oscillating starting jets have the same structure under unit and sinusoidal pulsations. In addition, the both figures indicate that incorporating blockage increases the vorticity magnitude but not its structure. On the other hand, decreasing the ambient pressure from 101 kPa to 0.670 kPa not only increases the vorticity magnitude but also affects the vortex structure by shifting the vorticity distribution towards the annulus exit.

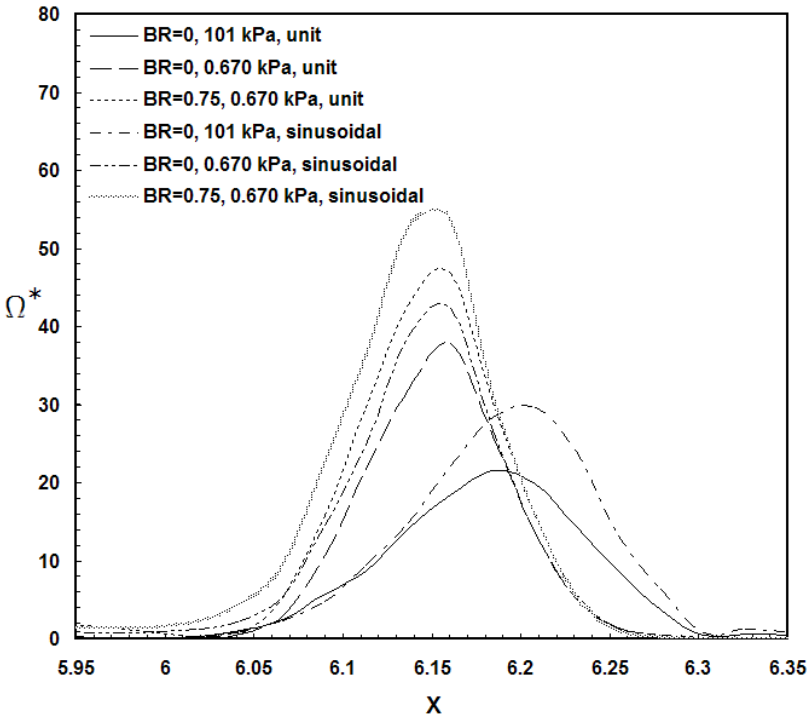

Figure 4.8. Vorticity distribution of fully oscillating jets.

Thrust Analysis

The average thrust output at the end of one fully oscillating cycle, i.e. consisting on an inflow stroke followed by an outflow stroke, is calculated with

$$f_{avg} = \frac{1}{t}\left[\int_0^t \int_A \left[pV_x^2(r,\tau) + p_{gage}(r,\tau)\right] \; dsd\tau\right] \tag{4.8}$$

where the first and second integrand terms are the momentum and pressure components of thrust, respectively, at the annulus exit plane.

Figure 4.9 shows the thrust output of fully oscillating unit and sinusoidal pulsed jets, respectively, as a function of frequency. The figure is presented in dimensionless form, where the thrust F is normalized with (Dabiri, 2009)

$$F = \frac{f}{\rho A V_0^2} \tag{4.9}$$

Calculated at the annulus exit plane, the thrust generally increases with increasing frequency, which is related to the vortex formation, where the generated vortices are closer to the annulus exit plane at higher frequencies. As shown in Figure 4.9, fully oscillating sinusoidal pulsed jets produce more thrust than fully oscillating unit pulsed jets. For example, at zero blockage and an ambient pressure of 101 kPa, the average thrust outputs under unit and sinusoidal pulsations are respectively $F = 0.23$ and $F = 1.3$

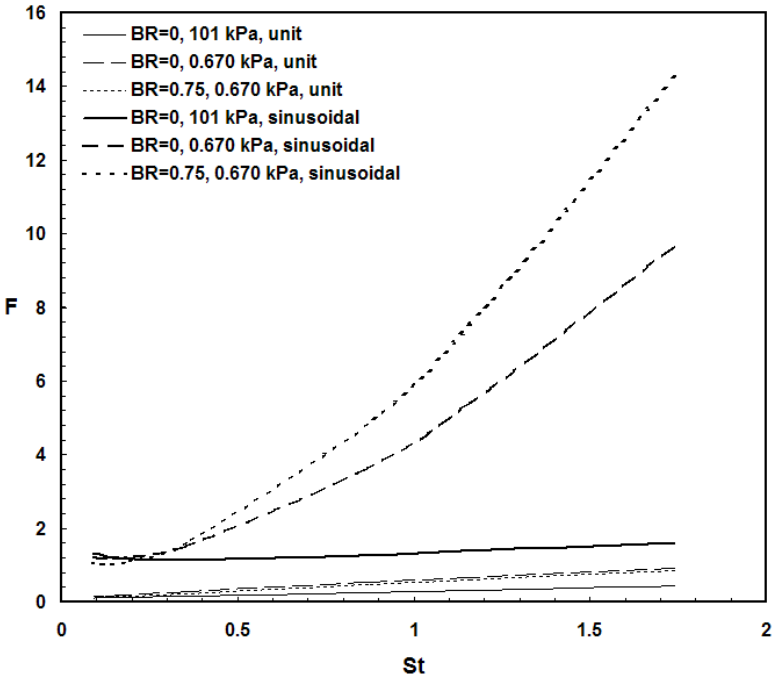

Figure 4.9. Thrust output of fully oscillating jets.

In addition, examining the results from Figure 4.9 indicates that fully oscillating sinusoidal pulsed jets are more sensitive to ambient pressure and nearly as sensitive to entry geometry conditions relative to fully oscillating unit pulsed jets. At zero blockage, decreasing the ambient pressure from 101 kPa to 0.670 kPa increases the average thrust output of sinusoidal and unit pulsed jets by 140% and 66%, respectively. On the other hand, under an ambient pressure of 0.670 kPa, incorporating a blockage of $BR = 0.75$ increases the average thrust output

of sinusoidal jets by 13% and decreases the thrust output of unit pulsed jets by 18%. Hence, the blockage effects on the thrust output of both pulsation types are of the same order of magnitude.

An example of the thrust components of Figure 4.9 is shown in Figure 4.10 for fully oscillating unit and sinusoidal pulsed jets with a blockage of $BR = 0.75$ and an ambient pressure of 0.670 kPa. As shown in Figure 4.10, the average momentum thrust components from both unit and sinusoidal pulsations over the examined frequencies are respectively $F = 0.013$ and $F = 0.084$, while the average pressure thrust components are $F = 0.35$ and $F = 4.4$, respectively. Thus, for this particular example, the pressure thrust components of unit and sinusoidal pulsations respectively contribute 96% and 98% of the total thrust output. Similar percent values are also obtained under various blockage and pressure conditions, as evident from Figure 4.11. Hence, the momentum component of thrust is insignificant relative to the pressure component for fully oscillating pulsed jets.

Besides the significance of the pressure component of thrust, an important observation can be made regarding the low momentum thrust component. Note that in the present study, the velocity imposed boundaries during the inflow and outflow strokes of the fully oscillating cycle have the same magnitude but opposite directions. Therefore, the force due to momentum during the inflow and outflow strokes should also have equal magnitudes but opposite directions, resulting in a total thrust output of zero. The fact that the momentum thrust output values of the current study are non-zero (as shown by Figure 4.10 and 4.11) indicates the presence of thrust augmentation, caused by entrainment of the generated vortex located outside the annulus exit plane.

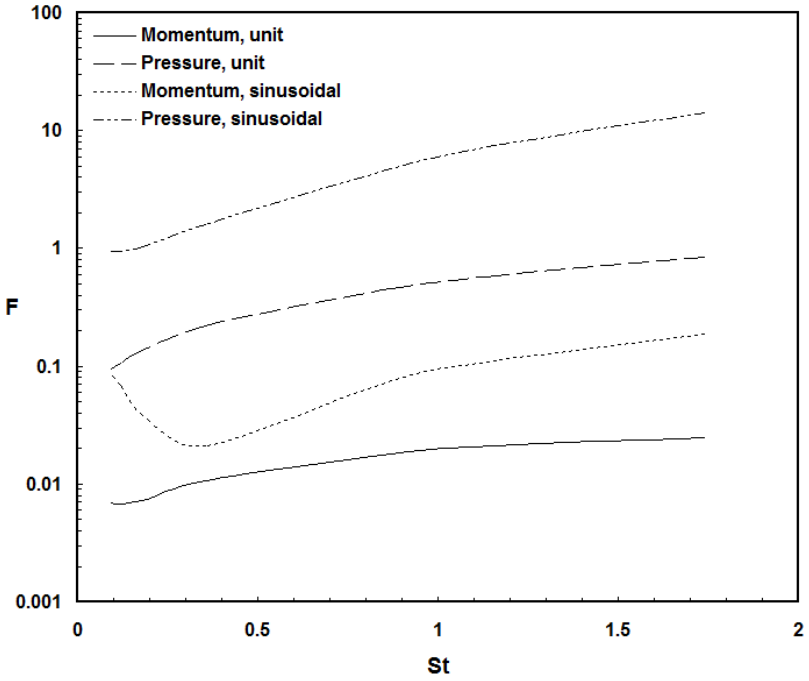

Figure 4.10. Thrust components of fully oscillating jets (for BR=0.75 & 0.670 kPa).

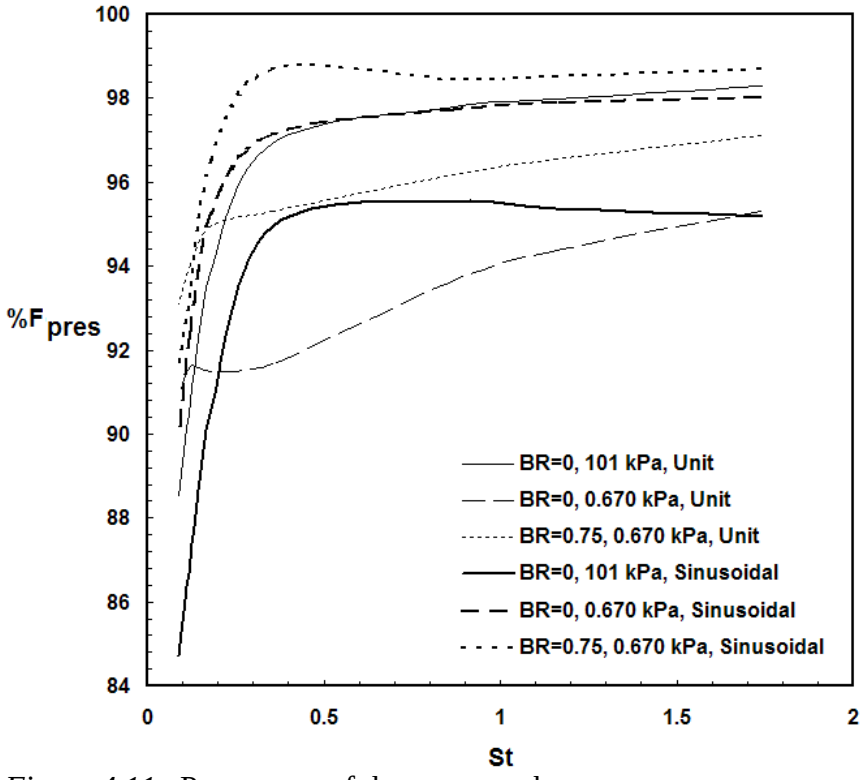

Figure 4.11. Percentage of the pressure thrust component.

Propulsive Efficiency

The propulsive efficiency η in this study is calculated based on the work done by the leading vortex during a $\Delta T = 0.028$ time duration at the end of a single fully oscillating pulsed cycle such that

$$\eta = \frac{\tilde{f} \cdot \Delta x}{\tilde{f} \cdot \Delta x + ke} \tag{4.10}$$

where Δx is the distance traveled by the vortex (measure between the vortex centers), and $\tilde{f}$ and ke are respectively the average thrust and excess kinetic energy of the vortex during the work process. The average thrust $\tilde{f}$ is determined from the vortex impulse I at both ends of the work process such that

$$f = I / t \tag{4.11}$$

$$I = \rho\pi \int_{jet} \Omega_\theta r^2 dr dx \tag{4.12}$$

The kinetic energy at both ends of the work process is determined with

$$ke = \rho \int_{jet} \frac{V^2}{2} d\forall \tag{4.13}$$

where the higher of the two values is used as the excess kinetic energy in Eq. (4.10).

Figure 4.12 shows the propulsive efficiency of unit and sinusoidal pulsed starting jets as a function of frequency under various blockage and pressure conditions. Note that the reported efficiencies are calculated at the end of a single fully oscillating jet cycle. As shown, the propulsive efficiency from unit pulsation increases with increasing frequency while the efficiency from sinusoidal pulsation increases and then reaches a near steady state value. Nevertheless, sinusoidal pulsed jets are more efficient than unit pulsed jets under the examined frequencies. It can also be noted that incorporating blockage increases the propulsive efficiency

of both pulsation modes. On the other hand, decreasing the ambient pressure increases the propulsive efficiency of unit pulsed jets but decreases the efficiency of sinusoidal pulsed jets.

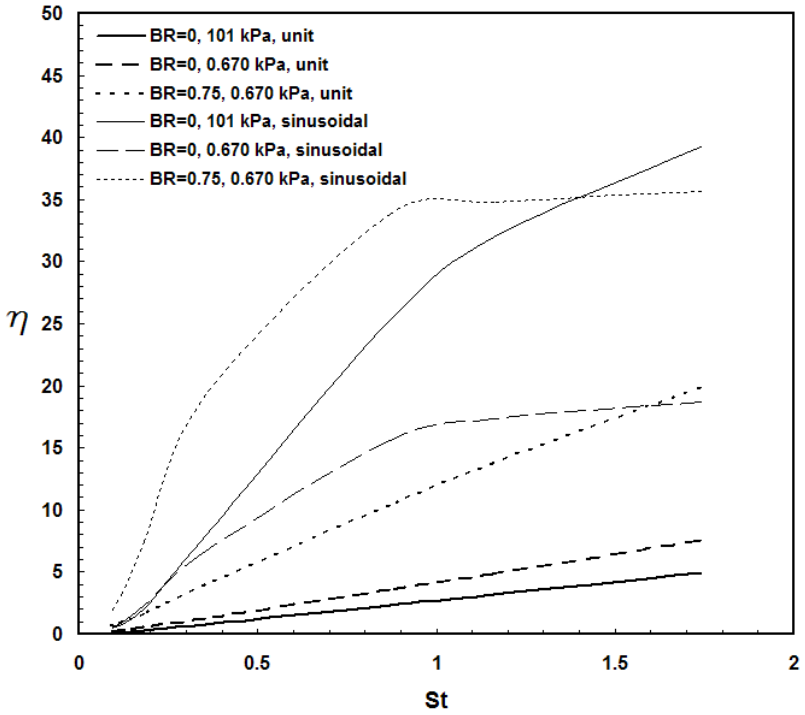

Figure 4.12. Propulsive efficiency of fully oscillating jets.

While Figure 4.12 shows the propulsive efficiency at the end of the fully oscillating cycles, Figure 4.13 investigates the efficiency changes within a given cycle with frequency $St = 0.18$. As evident from Figure 4.13, propulsive efficiency of unit pulsed starting jets decreases with increasing cycle time. On the other hand, the propulsive efficiency of sinusoidal pulsed starting jets resembles a quadratic function of cycle time with a local minimum. It is also important to note that the sinusoidal pulsed jet has a higher propulsive efficiency than the unit pulsed jet throughout the given fully oscillating cycle. Thus, the efficiency comparisons that were noted at the end of fully oscillating cycles (in Figure 4.12) between the two pulsation modes still hold throughout the duration of the pulsed cycles.

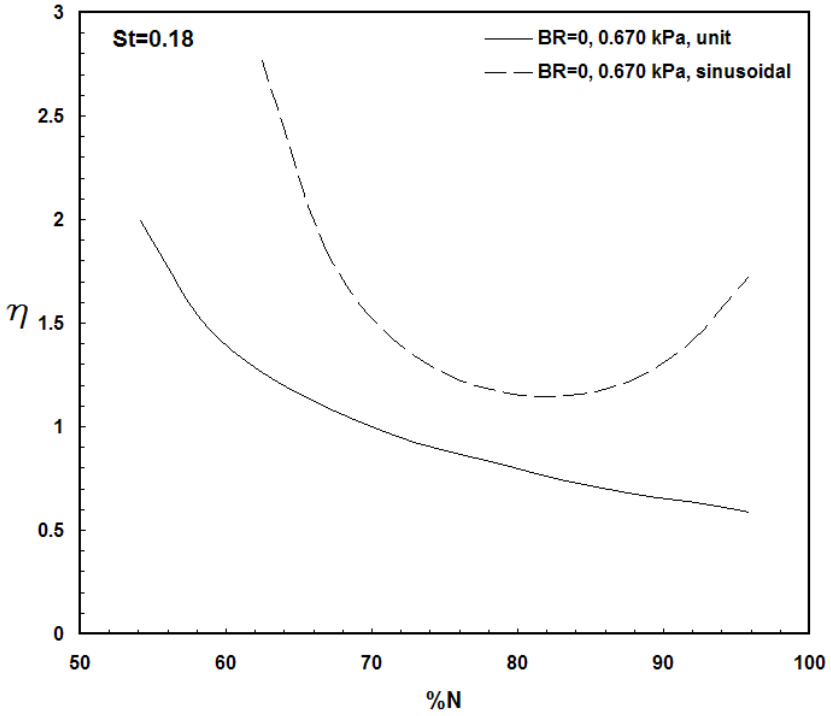

Figure 4.13. Propulsive efficiency cycle patterns.

Conclusion

In this study, a computational investigation was carried out on low Reynolds number fully oscillating impulsively started annular jets triggered by unit and sinusoidal pulsations. The fully oscillating cycle consisted of an inflow stroke followed by an outflow stroke. At the end a single cycle, the performance of the jets was measured based on the thrust output, vortex formation, and propulsive efficiency. In addition, the effects of the annulus entry geometry and ambient conditions were examined by varying the blocking ratio and the surrounding pressure, respectively. The main findings of this study are listed as follows.

1. The leading edge vortex formation is a prominent feature of fully oscillating jets. As the frequency decreases, the leading edge vortex at the end of a fully oscillating cycle period grows in size and travels farther away from the annulus. Calculated at the annulus exit plane, the circulation, which is indicative of vortex entrainment, is more dependent on the vortex displacement than size. Hence, for unit pulsed jets, entrainment increases with increasing

frequency, where the vortex is closer to the annulus. For sinusoidal pulsed jets, on the other hand, the effect (on entrainment) of the vortex's close proximity to the annulus at high frequencies is opposed with the effect of the backflow, which is noted to occur near the incline angle for sinusoidal pulsed jets and increases with increasing frequency.

2. The average circulation calculations under the examined frequencies indicate that vortex formation from fully oscillating unit and sinusoidal pulsed jets have approximately equivalent entrainment capabilities. Varying the ambient pressure had minimal effects (i.e. less than 1%) on the average circulation from sinusoidal pulsation but a more visible effect on the average circulation from unit pulsation (i.e. 28% at 0.670 kPa). In addition, varying the blocking ratio caused a change of the same order of magnitude on the average circulation from unit and sinusoidal pulsations.

3. The thrust output of fully oscillating jets was higher from sinusoidal pulsation than unit pulsation. Under zero blockage and an ambient pressure of 101 kPa, the average thrust output over the examined frequencies from sinusoidal pulsation was approximately 6 folds higher than that of unit pulsation. In addition, the thrust output of sinusoidal pulsation was more sensitive to ambient pressure changes than unit pulsation. Both pulsation were nearly as sensitive to blockage.

4. The pressure component of thrust was the primary contributor to the average thrust output (i.e. generally greater than 90% of total thrust). In addition, the non-zero total momentum thrust component (i.e. total from both inflow and outflow strokes) indicates the presence of thrust augmentation in fully oscillating jets due to the entrainment caused by the vortex formation.

5. The propulsive efficiency of fully oscillating starting jets was calculated based on the excess energy and work done by the leading edge vortices. The results showed that sinusoidal pulsed jets are more efficient than unit pulsed jets.

Acknowledgements

The authors would like to thank the U.S. Department of Education for its support through the Graduate Assistance in Areas of National Need (GAANN) Fellowship.

References

Abdel-Raouf, E., Baker, J., & Sharif, M. (2010). Computational investigation of low Reynolds number impulsively started annular jets (The effects of blocking ratio and atmospheric altitude on starting annular jets). *Proceedings of the ASME 2010 3rd Joint US-European Fluids Engineering Summer Meeting and 8th International Conference on Nanochannels, Microchannels, and Minichannels*, FEDSM-ICNMM2010-30767.

Anderson, E., & DeMont, M. (2000). The mechanics of locomotion in the squid Loligo Pealei: locomotory function and unsteady hydrodynamics of the jet and intramantle pressure. *Journal of Experimental Biology*, 203, 2851-2863.

Bartol, I., Krueger, P., Stewart, W., & Thompson, J. (2009). Pulsed jet dynamics of squid hatchlings at intermediate Reynolds numbers. *Journal of Experimental Biology*, 212, 506-1518.

Dabiri, J. (2009). Optimal vortex formation as a unifying principle in biological propulsion. *Annual Review of Fluid Mechanics*, 41, 17-33.

Dabiri, J., & Gharib, M. (2005). The role of optimal vortex formation in biological fluid transport. *Proceedings of the Royal Society of London B*, 272, 557-1560.

DeMont, M., & Gosline, J. (1998). Mechanics of jet propulsion in the hydromedusan jellyfish, Polyorchis Penicillatus II. Energetics of the jet cycle. *Journal of Experimental Biology*, 134, 333-345.

Gharib, M., Rambod, E., & Shariff, K. (1998). A universal time scale for vortex ring formation. *Journal of Fluid Mechanics*, 360, 121-140.

Krueger, P., & Gharib, M. (2003). The significance of vortex ring formation to the impulse and thrust of a starting jet. *Physics of Fluids*, 15(5), 1271-1281.

Krueger, P., & Gharib, M. (2005). Thrust augmentation and vortex ring evolution in a fully pulsed jet. *AIAA Journal*, 43(4), 792-801.

Langhaar, H. (1942). Steady flow in the transition length of a straight tube. *Journal of Applied Mechanics*, 9, 55-58.

Linden, P., & Turner, J. (2004). 'Optimal' vortex rings and aquatic propulsion mechanisms. *Proceedings of the Royal Society of London B*, 271, 647-653.

Mohseni, K., & Gharib, M. (1998). A model for universal time scale of vortex ring formation. *Physics of Fluids*, 10(10), 2436-2438.

Obot, N., Trabold, T., Graska, M., & Gandhi, F. (1986). Velocity and temperature fields in turbulent jets issuing from sharp-edged inlet round nozzles. *Industrial & Engineering Chemistry Fundamentals*, 25(3), 425-433.

Rosenfeld, M., Rambod, E., & Gharib, M. (1998). Circulation and formation number of laminar vortex rings. *Journal of Fluid Mechanics*, 376, 297-318.

Uyttendaele, M., & Shambaugh, R. (1989). The flow of annular jets at moderate Reynolds numbers. *Industrial & Engineering Chemistry Research*, 28, 1735-1740.

Yehoshua, T., & Seifert, A. (2006). Active boundary layer tripping using oscillatory vorticity generator. *Aerospace Science and Technology*, 10, 175-180.

CHAPTER 5

CONCLUSION

This dissertation studied the following jet types at low Reynolds number flow in Chapters 2, 3, and 4, respectively: starting jet, inflow jet, and fully oscillating jet. The fully oscillating jet consisted of a starting jet followed an inflow jet similar to jet propulsion of a squid and jellyfish, where the full cycle (i.e. fully oscillating jet) consists of a filling phase (i.e. the inflow jet) followed by a propulsion phase (i.e. the staring jet). The investigation of those three jet types was achieved by analyzing the net force (either thrust or suction force) at the annulus exit along with the jet efficiency. Special attention was also given to the vortex dynamics, for which vortex formation is known to be triggered by starting jets.

Vortex formation was triggered by the three jet types. Chapter 2 showed that the pulsed starting jets (particularly from unit pulsation) produced moving vortex rings with similar vortex formation numbers to the previously published results. In addition, the results showed that ambient pressure and blockage did not affect the vortex formation number.

Chapter 3 showed that pulsed inflow jets triggered standing vortices inside the annulus. The size of the standing vortex depended on the pulsation frequency, where low and high frequencies respectively triggered large and small standing vortices. At the low frequencies (i.e. large cycle periods), there was more time prior to pulsation for the inflow jet to become fully developed causing a thicker boundary layer and subsequently larger distribution of vorticity within the fluid (as detected by the vorticity contour plots). Pulsation then triggered a large

vortex ring out of the large distribution of vorticity, and vice versa took place for high pulsation frequencies.

Both Chapters 2 and 3 indicated that vortex formation is not as strong of a phenomenon in impulsive jets as it is for pulsed jets. For example, the moving vortex rings triggered by impulsive starting jets did not show pinch off characteristics, as shown in Chapter 2. Furthermore, impulsive inflow jets did not trigger standing vortex rings, as pointed out in Chapter 3.

Chapter 4 showed that a moving vortex is triggered by the end of a fully oscillating jet cycle similar to the vortex triggered by starting jets. However, comparing the vorticity contour plots and circulation measurements from Chapters 2 and 4 indicated that the vortices from the fully oscillating jets were not as developed and had lower entrainment than the vortices triggered by the starting jets alone.

The presence of vortex formation triggered by the three jet types led to thrust augmentation. Note that the term 'thrust augmentation' is used to describe a greater momentum force component at the annulus exit than the force due to mass flux. The results form both impulsive and pulsed starting jets of Chapter 2 showed thrust augmentation. Similarly, the pulsed inflow jets from Chapter 3 augmented thrust.

The relationship between vortex formation and thrust augmentation is more self-evident with the impulsive inflow jets and the fully oscillating jets. The absence of vortex formation from the impulsive inflow jets of Chapter 3 did not lead to thrust augmentation, but rather, the suction force due to the mass out flux of the inflow jet equaled the force due to momentum at the annulus exit. On the other hand, the fully oscillating jets of Chapter 4 showed evidence of thrust augmentation because of vortex formation. The fully oscillating jet, which consists of equal but

opposite inflow and starting jets, should have had a net momentum thrust of zero since the effects of the two mass fluxes would cancel out. However, the presence of vortex formation enhanced the mass entrainment causing thrust augmentation.

In addition to affecting the jet resultant forces, vortex formation affected the propulsion efficiency. Unit pulsed starting jets were generally more efficient than sinusoidal pulsed starting jets, while the opposite was true for inflow jets. For starting jets after vortex pinch off, it is important to note that vortex ring behavior of both pulsation types was similar such that there was a moving leading edge vortex and a standing secondary trailing vortex of opposite rotation, as shown in Chapter 2. On the other hand, the vortex ring behavior of both pulsation types was different for inflow jets where although both pulsation triggered standing vortices inside the annulus, the unit pulsed pulsation triggered a secondary vortex of opposite rotation outside the annulus. Based on the method for calculating the efficiency of the inflow jets in Chapter 3, the secondary vortex triggered by the unit pulsed inflow jet countered the main standing vortex and hence lowered the efficiency relative to that of sinusoidal inflow pulsation.

Note that sinusoidal pulsed fully oscillating jets were also more efficient than the ones produced by unit pulsation. The apparent reason, however, was not due to vortex formation but because the pressure component of thrust from sinusoidal pulsation was greater by an order of magnitude than the pressure component of thrust from unit pulsation for the same average mass flux. For both pulsation types, the thrust due to pressure supplied over 90% of the total thrust of fully oscillating jets.

REFERENCES

Abdel-Raouf, E., Baker, J., & Sharif, M. (2010). Computational investigation of low Reynolds number impulsively started annular jets (The effects of blocking ratio and atmospheric altitude on starting annular jets). *Proceedings of the ASME 2010 3rd Joint US-European Fluids Engineering Summer Meeting and 8th International Conference on Nanochannels, Microchannels, and Minichannels*, FEDSM-ICNMM2010-30767.

Anderson, E., & DeMont, M. (2000). The mechanics of locomotion in the squid Loligo Pealei: locomotory function and unsteady hydrodynamics of the jet and intramantle pressure. *Journal of Experimental Biology*, 203, 2851-2863.

Bartol, I., Krueger, P., Stewart, W., & Thompson, J. (2009). Pulsed jet dynamics of squid hatchlings at intermediate Reynolds numbers. *Journal of Experimental Biology*, 212, 1506-1518.

Benjamin, T. (1976). The alliance of practical and analytical insights into the non-linear problems of fluid mechanics. *Application of Methods of Functional Analysis to Problems in Mechanics*, Lecture Notes in Mathematics, 503, 8-29.

Bishop, K.L., Wainwright, P.C., & Holzman, R. (2008). Anterior-to-posterior wave of buccal expansion in suction feeding fishes is critical for optimizing fluid flow velocity profile. *Journal of the Royal Society Interface*, 5, 1309-1316

Dabiri, J. (2009). Optimal vortex formation as a unifying principle in biological propulsion. *Annual Review of Fluid Mechanics*, 41, 17-33.

Dabiri, J., Colin, S., Costello, J., & Gharib, M. (2005). Flow patterns generated by oblate medusan jellyfish: field measurements and laboratory analyses. *Journal of Experimental Biology*, 208, 1257-1265.

Dabiri, J., & Gharib, M. (2004). A revised slug model boundary layer correction for starting jet vorticity flux. *Theoretical and Computational Fluid Dynamics*, 17, 293-295.

Dabiri, J., & Gharib, M. (2005). The role of optimal vortex formation in biological fluid transport. *Proceedings of the Royal Society B*, 272, 1557-1560.

DeMont, M., & Gosline, J. (1998). Mechanics of jet propulsion in the hydromedusan jellyfish, Polyorchis Penicillatus II. Energetics of the jet cycle. *Journal of Experimental Biology*, 134, 333-345.

Didden, N. (1979). On the formation of vortex rings: rolling-up and production of circulation. *Zeitschrift für Angewandte Mathematik und Physik* (ZAMP), 30(1), 101-116.

Gharib, M., Rambod, E., Kheradvar, A., Sahn, D., and Dabiri, J. (2006). Optimal vortex formation as an index of cardiac health. *Proceedings of the National Academy of Sciences*, 103(16), 6305-6308.

Gharib, M., Rambod, E., & Shariff, K. (1998). A universal time scale for vortex ring formation. *Journal of Fluid Mechanics*, 360, 121-140.

Hill, B. (1972). Measurement of local entrainment rate in the initial region of axisymmetric turbulent air jets. *Journal of Fluid Mechanics*, 51(4), 773-779.

Hill, M. (1894). On a spherical vortex. *Proceedings of the Royal Society of London*, 55, 219-224.

James, S., & Madnia, C. (1996). Direct numerical simulation of a laminar vortex ring. *Physics of Fluids*, 8(9), 2400-2414.

Jiang, H., & Grosenbaugh, M. (2006). Numerical simulation of vortex ring formation in the presence of background flow with implications for squid propulsion. *Theoretical and Computational Fluid Dynamics*, 20(2), 103-123.

Joshi, A., & Schreiber, W. (2006). An experimental examination of an impulsively started incompressible turbulent jet. *Experiments in Fluids*, 40, 156-160.

Kambe, T., & Oshima, Y. (1975). Generation of decay of viscous vortex rings. *Journal of the Physical Society of Japan*, 38(1), 271-280.

Kelvin, L. (1880). Vortex statics. *Philosophical Magazine Series 5*, 10(60), 97-109.

Ko, N., & Chan, W., 1978. Similarity in the initial region of annular jets: three configurations. *Journal of Fluid Mechanics*, 84(4), 641-656.

Ko, N., & Lam, K. (1985). Flow structures of a basic annular jet. *AIAA Journal*, 23(8), 1185-1190.

Krueger, P. (2005). An over-pressure correction to the slug model for vortex ring circulation. *Journal of Fluid Mechanics*, 545, 427-443.

Krueger, P., & Gharib, M. (2003). The significance of vortex ring formation to the impulse and thrust of a starting jet. *Physics of Fluids*, 15(5), 1271-1281.

Krueger, P., & Gharib, M. (2005). Thrust augmentation and vortex ring evolution in a fully pulsed jet. *AIAA Journal*, 43(4), 792-801.

Kulman, J. (1987). Variation of entrainment in annular jets. *AIAA Journal*, 35(3), 373-379.

Langhaar, H. (1942). Steady flow in the transition length of a straight tube. *Journal of Applied Mechanics*, 9, 55-58.

Lauder, G.V. (1980). The suction feeding mechanism in sunfishes (Lepomis): an experimental analysis. *Journal of Experimental Biology*, 88, 49-72.

Linden, P., & Turner, J. (2001). The formation of 'optimal' vortex rings, and the efficiency of propulsion devices. *Journal of Fluid Mechanics*, 427, 61-72.

Linden, P., & Turner, J. (2004). 'Optimal' vortex rings and aquatic propulsion mechanisms. *Proceeding of the Royal Society of London B*, 271, 647-653.

Maxworthy, T. (1972). The structure and stability of vortex rings. *Journal of Fluid Mechanics*, 51(1), 15-32.

Mohseni, K., & Gharib, M. (1998). A model for universal time scale of vortex ring formation. *Physics of Fluids*, 10(10), 2436-2438.

Morton, T. (2004). The velocity field within a vortex ring with a large elliptical cross-section. *Journal of Fluid Mechanics*, 503, 247-271.

Muller, M., Osse, J.W., & Verhagen, J.H. (1982). A quantitative hydrodynamical model of suction feeding in fish. *Journal of Theoretical Biology*, 95, 49-79.

Norbury, J. (1973). A family of steady vortex rings. *Journal of Fluid Mechanics*, 57, 417-431.

Obot, N., Trabold, T., Graska, M., & Gandhi, F. (1986). Velocity and temperature fields in turbulent jets issuing from sharp-edged inlet round nozzles. *Industrial & Engineering Chemistry Fundamentals*, 25(3), 425-433.

Pawlak, G., Cruz, C., Bazan, C., & Hrdy, P. (2007). Experimental characterization of starting jet dynamics. *Fluid Dynamics Research*, 39, 711-730.

Riley, N., & Steven, D. (1993). A note on leapfrogging vortex rings. *Fluid Dynamics Research*, 11(5), 235-244.

Rosenfeld, M., Rambod, E., & Gharib, M. (1998). Circulation and formation number of laminar vortex rings. *Journal of Fluid Mechanics*, 376, 297-318.

Sallet, D.W., & Widmayer, R.S. (1974). Experimental investigation of laminar and turbulent vortex rings. *Zeitschrift fur Flugwissenschaften*, 22(6), 207-215.

Satti, R.P., & Agrawal, A.K. (2008). Computational study of buoyancy effects in a laminar starting jet. *International Journal of Heat and Fluid Flow*, 29, 527-539.

Seno, T., Kageyama, S., & Ito, R. (1988). A modeling of vortex rings in an axisymmetric pulsed jet. *Journal of Chemical Engineering of Japan*, 21(1), 1-5.

Shusser, M., & Gharib, M. (1999). A new model for inviscid vortex ring formation. *30th AIAA Fluid Dynamics Conference*, Norfolk, VA.

Shusser, M., & Gharib, M. (2000). Energy and velocity of a forming vortex ring. *Physics of Fluids*, 12(3), 618-621.

Shusser, M., Gharib, M., Rosenfeld, M., & Mohseni, K. (2002). On the effect of Pipe Boundary layer growth on the formation of a laminar vortex ring generated by a piston/cylinder arrangement. *Theoretical and Computational Fluid Dynamics*, 15, 303-316.

Syed, A.H., & Sung, H.J. (2009). Propagation of orifice- and nozzle-generated vortex rings in air. *Journal of Visualization*, 12(2), 139-156.

U.S. Standard Atmosphere. (1976). Washington, DC: U.S. Government Printing Office.

Uyttendaele, M., & Shambaugh, R. (1989). The flow of annular jets at moderate Reynolds numbers. *Industrial & Engineering Chemistry Research*, 28, 1735-1740.

Van Wassenbergh, S., & Aerts, P. (2009). Aquatic suction feeding dynamics: insights from computational modeling. *Journal of the Royal Society Interface*, 6, 149-158.

Yehoshua, T., & Seifert, A. (2006). Active boundary layer tripping using oscillatory vorticity generator. *Aerospace Science and Technology*, 10, 175-180.